The University of Kansas

KU INFORMATION & TELECOMMUNICATION TECHNOLOGY CENTER
The University of Kansas

Technical Report

OFDM-Based Cognitive Radio for

DSA Networks

Rakesh Rajbanshi

ITTC-FY2008-TR-31620-05

September 2007

Abstract

With the advent of new high data rate wireless applications, as well as growth of existing wireless services, demand for additional bandwidth is rapidly increasing. Existing "command-and-control" spectrum allocations defined by government regulatory agencies, such as federal communications commission (FCC), prohibit unlicensed access to licensed spectrum, constraining them instead to several heavily populated, interference-prone frequency bands. However, it has been shown that the spectrum is not utilized efficiently across time and frequency. Therefore, FCC is currently working on the concept of unlicensed users "borrowing" spectrum from incumbent license holders temporarily to improve the spectrum utilization. This concept is called *dynamic spectrum access* (DSA). Cognitive radios offer versatile, powerful, and portable wireless transceivers enabling DSA. This dissertation investigates physical layer techniques to enhance a cognitive radio performance.

Multi-carrier techniques, such as orthogonal frequency division multiplexing (OFDM), support huge data rates that are robust to channel impairments. However, with a growing demand for spectrum access, it may be difficult for any single transmission to obtain a large contiguous frequency spectrum block in DSA environment. This dissertation proposes a novel non-contiguous OFDM (NC-OFDM) technique, where the implementation achieves high data rates via collective usage of a large number of non-contiguous subcarriers while simultaneously avoiding any interference to the existing transmissions by turning off the subcarriers corresponding to these spectrum bands. Moreover, the performance of the proposed NC-OFDM technique is compared with other multi-carrier technique, such as multi-carrier code division multiple access (MC-CDMA).

One of the major drawbacks of an OFDM signal is that it may exhibit large peak-to-average power ratio (PAPR) values resulting in expensive transceivers. This dissertation presents an extensive overview and taxonomy of the PAPR reduction algorithms proposed in the literature. This dissertation presents five novel techniques for reducing PAPR of an OFDM signal viz., subcarrier phase adjustment algorithm, adaptive-mode PAPR reduction algorithm, subcarrier power adjustment algorithm, variable throughput algorithm, and low correlation phase sequences-based algorithm. Due to the non-contiguous nature of the spectrum in DSA environment, the statistical properties of the PAPR of an NC-OFDM signal are different from that of an OFDM signal. Additionally, the conventional PAPR reduction algorithms need to be carefully chosen and modified to be used for reducing the PAPR of an NC-OFDM signal. This dissertation investigates the statistical properties of the PAPR of an NC-OFDM signal and lay out design requirements for the PAPR reduction algorithms for an NC-OFDM signal.

OFDM technique implements fast Fourier transform (FFT) algorithms for modulating and demodulating the OFDM signal. This dissertation proposes an efficient general FFT pruning algorithm for improving the efficiency of the FFT evaluation by reducing the arithmetic operations, when a large number of subcarriers are deactivated. Given that the cognitive radios employing NC-OFDM need to quickly adapt to the changing operating environment, and that the hardware resources of small form factor cognitive radios are limited, such an algorithm would be beneficial.

Acknowledgments

Contents

List of Figures

List of Tables

Glossary

ADSL	Asymmetric Digital Subscribers Line
AWGN	Additive White Gaussian Noise
BER	Bit Error Rate
BPSK	Binary Phase Shift Keying
CCDF	Complementary Cumulative Distribution Function
CDF	Cumulative Distribution Function
CDMA	Code Division Multiple Access
CP	Cyclic Prefix
CR	Cognitive Radio
D/A	Digital-to-Analog
DAB	Digital Audio Broadcasting
DARPA	Defense Advanced Research Projects Agency
DB	Data Bearing
DFT	Discrete Fourier Transform
DIF	Decimation in Frequency
DIMSUMnet	Dynamic Intelligent Management of Spectrum for Ubiquitous Mobile Access Networks
DIT	Decimation in Time
DSAP	Dynamic Spectrum Access Protocol
DSL	Digital Subscriber Line

DSP	Digital Signal Processing
DVB	Digital Video Broadcasting
DVB-T	Digital Video Broadcasting - Terrestrial
FCC	Federal Communications Commission
FDM	Frequency Division Multiplexing
FFT	Fast Fourier Transform
FFTW	Fastest Fourier Transform in the West
FMT	Filtered Multi-Tone
FPGA	Field Programmable Gate Array
HPA	High Power Amplifier
i.i.d.	Indepedent and Identically Distributed
I/Q	In-phase and Quadrature-phase
IBO	Input Backoff
ICI	Inter-Carrier Interference
IDFT	Inverse Discrete Fourier Transform
IFFT	Inverse Fast Fourier Transform
ISI	Inter-Symbol Interference
ISO	Incumbent Spectral Occupancy
LAN	Local Area Network
MAN	Metropolitan Area Network
MC-CDMA	Multi-Carrier Code Division Multiplexing
MCM	Multi-Carrier Modulation
NC-MC-CDMA	Non-Contiguous Multi-Carrier Code Division Multiplexing
NC-OFDM	Non-Contiguous Orthogonal Frequency Division Multiplexing

NDB	Non-Data Bearing
OFDM	Orthogonal Frequency Division Multiplexing
OOB	Out of Band
P/S	Parallel-to-Serial
PA	Power Amplifier
PAPR	Peak-to-Average Power Ratio
PSK	Phase Shift Keying
PTEQ	Per Tone Equalization
PTS	Partial Transmit Sequences
QAM	Quadrature Amplitude Modulation
QPSK	Quadrature Phase Shift Keying
RCC	Radio Control Channel
RF	Radio Frequency
RMS	Root Mean Square
RPU	Random Phase Updating
S/P	Serial-to-Parallel
SDR	Software Defined Radio
SLM	Selective Mapping
SNR	Signal-to-Noise Ratio
SR	Software Radio
UHF	Ultra High Frequency
UWB	Ultra Wide Band
VHF	Very High Frequency

WSSUS	Wide Sense Stationary Uncorrelated Scattering
XG	Next Generation

List of Symbols

$s(n)$	Baseband Transmit Sequence
$r(n)$	Baseband Receive Sequence
$(\Delta f)_c$	Coherence Bandwidth
τ_{max}	Maximum Delay Spread
τ_{rms}	RMS Delay Spread
B	Signal Bandwidth
T_d	Symbol Duration
N	Number of Subcarriers
$N_{\mathrm{ISI,\ sigle\text{-}carrier}}$	Number of Interfering Symbols in a Single-Carrier Modulated System
$N_{\mathrm{ISI,\ multi\text{-}carrier}}$	Number of Interfering Symbols in a Multi-Carrier Modulated System
j	$\sqrt{-1}$
$s(t)$	Baseband OFDM symbol
n_i	Zero-mean Complex Gaussian Independent Random Noise
τ_m	Delay of the mth Path
X_k	Complex Input Symbols on k-th Subcarrier
$X_{m,k}$	Complex Input Symbols on k-th Subcarrier at m-th Time Instant
C_i	i-th Spreading Code
$h(\tau)$	Channel Impulse Response
N_0	Input Noise Power Spectral Density
α	Incumbent Spectral Occupancy
$\Re(.)$	Real part of (.)

$\Im(.)$	Imaginary Part of (.)
$E(.)$	Expectation Operator
$s_{\mathrm{PB}}(t)$	Passband Transmit Signal
$s_I(t)$	In-Phase part of s(t)
$s_Q(t)$	Quadrature-Phase part of s(t)
η	Power Amplifier Efficiency
P_{av}	Average Power of a Signal
R	Absolute Rate Loss in bits-per-subcarrier due to PAPR Reduction Requirements
π_k	Power Level of k-th Subcarrier

Chapter 1

Introduction

1.1 Research Motivation

With the advent of new high data rate wireless applications, as well as growth of existing wireless services, demand for additional bandwidth is rapidly increasing. Government agencies, such as the Federal Communications Commission (FCC), allocate frequency spectrum and impose regulations on its usage, such as control of features, priorities, allocations, and exclusions. Since spectrum management is a sovereign right of nations, spectrum usage policies vary from country to country. Spectrum management is further complicated when considering worldwide operations. Moreover, there might be measurement-based controls on the spectrum usage, such as temporal, spectral, or energy characteristics, that would constrain the availability of the contiguous frequencies [1, 2]. Currently, spectrum allotment operates by providing each new service with its own fixed frequency block. Demand for access to spectrum has been growing dramatically, and is likely to continue to grow in the foreseeable future. New services, such as unlicensed wireless Internet access and satellite digital audio broadcasting (DAB),

are being launched and are quickly reaching hundreds of thousands of consumers. At the same time, most "prime" spectrum has been assigned, and it is becoming increasingly difficult to find spectrum that can be made available for either new services or to expand existing infrastructures. Existing "command-and-control" spectrum allocations defined by government regulatory agencies prohibit unlicensed access to licensed spectrum, constraining them instead to several heavily populated, interference-prone frequency bands. As a result, there exists an apparent scarcity of transmission spectrum that is forcing a critical rethinking of how wireless communications is performed. Additionally, it may be difficult to gain access to a large contiguous block of frequency spectrum, which can be a major limitation for high data rate transmissions.

Even though much of the spectrum has been allocated, preliminary measurements indicate that usage of the frequency spectrum is sparse both spatially and temporally [3]. As the spectrum is underutilized by the primary license holders, there exists 'spectrum holes'[1], that can be used by secondary users, yielding efficient utilization of the spectrum and eliminating the apparent spectrum scarcity. For instance, a survey of spectral usage was conducted during a weekday afternoon from the roof of a 3-storied building located in Lawrence, Kansas, USA. The spectral occupancy from 9 kHz to 1 GHz is shown in Figure 1.1[2]. From this figure, it is clear that a large portion of the frequency spectrum is sparsely occupied. To ensure that existing services can continue to grow and evolve, it is important that efficient access to and use of the radio spectrum should be promoted [1].

To make better use of radio spectrum resources, government regulatory agen-

---

[1]Spectrum band that has been licensed out but not utilized is known as *spectrum hole* or *white space*.

[2]The spectral occupancy measurements may vary depending on population density of the geographical region.
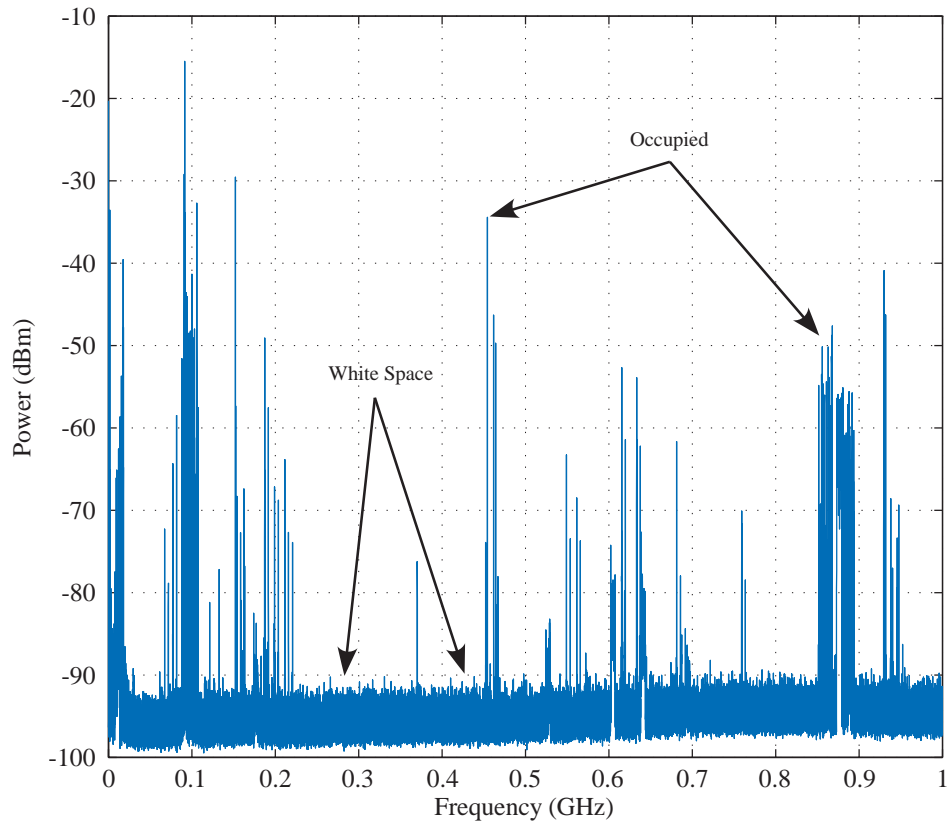
Figure 1.1. Spectrum occupancy measurements from 9 kHz to 1 GHz (8/31/2005, Lawrence, KS, USA).

cies such as the Federal Communications Commission (FCC) are currently working on the concept of unlicensed users "borrowing" spectrum from incumbent license holders. This concept is called *dynamic spectrum access* (DSA) [4, 5]. Wireless communication technology needs to be sufficiently agile in order to perform DSA such that spectrum utilization is improved while not interfering with incumbent user transmissions. In order to guarantee the rights of incumbent users, the unlicensed wireless devices must be sufficiently agile to avoid transmissions

3

over spectrum occupied by the licensed transmissions. Cognitive radios[3] employing adaptive and flexible communication techniques are prime candidates for the DSA networks because of their rapid reconfigurability and adaptability.

Physical layer design is a very important part of the communication system and has a profound impact on the feasibility of the communication processes at the higher layers [7]. Orthogonal frequency division multiplexing (OFDM)-based transmission is a promising candidate for a flexible spectrum pooling system in DSA environment, where the implementation achieves high data rates via collective usage of a large number of subcarrier bands. OFDM is deployed extensively in many modern communication systems, such as IEEE 802.11a, 802.11g, 802.16a/d/e, 802.20, due to its potential to achieve very high data rates. This modulation technique allows digital data to be transmitted over a radio channel by using a large number of narrow bandwidth subcarriers. Usually, these subcarriers are regularly spaced in frequency, forming a contiguous block of spectrum. OFDM offers several advantages over other transmission technologies such as high spectral efficiency, robustness to fading channel, immunity to impulse interference, and capability of handling very strong multi-path fading and frequency selective fading without having to provide powerful channel equalization [8]. Moreover, it is possible to turn off subcarriers corresponding to the spectrum occupied by the incumbent users in order to avoid any interference to existing transmissions, thereby enabling secondary utilization of the unused portions of the spectrum to improve the spectrum utilization efficiency as well as mitigate apparent spectrum scarcity problem.

---

[3]Cognitive radio denotes wireless systems that observe, orient, plan, decide, act, and adapt all the time learning about themselves and their environments in order to be more effective over time [6].

The focus of this dissertation is on OFDM-based communications over dynamic spectrum access (DSA) channels. The growing interest of studying OFDM-based cognitive radios is due to the apparent scarcity of the large spectral bandwidth for high data rate communications. OFDM-based cognitive radios can handle this apparent spectrum scarcity and enable high data rate communications utilizing aggregate non-contiguous bands of spectrum.

1.2 Research Objectives

The main objective of this research is to develop a number of performance-enhancing techniques that are applicable to an OFDM-based cognitive radio. A cognitive radio can enable the secondary usage of the unused portions of the licensed spectrum in order to improve spectrum utilization efficiency as well as improve the efficiency of a radio communication as a whole.

When the available frequency spectrum is sparsely distributed, use of conventional OFDM[4] implementations would be inefficient with respect to peak-to-average power ratio (PAPR) reduction and modulation/ demodulation (IFFT/ FFT algorithms). In this thesis, our objective is to develop novel techniques for a non-contiguous OFDM (NC-OFDM) system employed in a wide-band communication system, which collectively utilizes large number of non-contiguous subcarrier channels for high speed data communications.

Therefore, to reach this main objective, several sub-objectives have been established in this dissertation as follows:

- OFDM has been proposed to be used in the cognitive radios for DSA environ-

---

[4]Conventional OFDM implies the OFDM implementation with a contiguous set of subcarriers.

ment. However, it is important to compare the performance of the OFDM in DSA environment with other multi-carrier techniques. An OFDM-based cognitive radio should have following attributes:

- It should utilize dynamic radio frequency (RF) environment measurements and permit mining of the available spectrum, avoid interference with existing systems, and improve the quality of service.

- It should adjust to government regulations and local spectral usage controls regarding RF emissions.

- It should utilize non-contiguous bands of frequency spectrum collectively for high speed data communications.

• One of the major drawbacks of an OFDM signal is that it may exhibit large PAPR values, which requires large dynamic ranges of the digital-to-analog (D/A) converters and power amplifiers (PA). As a result, PAPR reduction algorithms need to be developed. Several algorithms proposed in the literature are iterative in nature and are suitable for specific scenarios. Thus, it is important to develop the PAPR reduction algorithms which find the solution in as few iterations as possible. Moreover, the algorithms should be able to minimize PAPR in wide range of scenarios.

• When a large number of subcarriers are deactivated in NC-OFDM transmission to avoid any interference to the incumbent user transmissions, the PAPR characteristics of an NC-OFDM signal would be different from that of an OFDM signal. Thus, it is important to study the PAPR characteristics of an NC-OFDM signal as well as specify the design requirements for reducing the PAPR values of an NC-OFDM signal.

- In DSA environment, several subcarriers need to be deactivated to avoid any interference to the primary user[5] transmissions. The information about the deactivated subcarriers can be used for pruning the FFT operations, thereby improving the efficiency of IFFT/FFT computations required for modulation and demodulation of an OFDM signal.

The primary focus of this work is to develop, implement, and validate high performance digital signal processing (DSP) algorithms and components for generation and detection of NC-OFDM signals and use a combination of analysis and simulations to evaluate the performance of NC-OFDM communication system. NC-OFDM communication systems require coordination between the transmitter and receiver. For example, the receiver needs to know the frequency bands used by the transmitter. Moreover, the target transmitter needs to know frequencies used by other transmitters and interferers (existing RF signals) so that they can use available frequency spectrum for transmissions without interfering others. In this work, we assume there already exists mechanisms for the transmitters and receivers to share this knowledge.

Before outlining the contributions of this thesis, it is necessary to outline the current state-of-the-art to reach some of these objectives.

1.3 State-of-the-Art

Dr. Jospeph Mitola III had first coined the term cognitive radio [9], which can be used as an aggressive solution to increase the spectrum utilization and is being promoted in the Spectrum Policy Task Force report of the FCC in 2002 [10]. Since

---

[5]In this thesis, we have used the term primary, incumbent, and licensed user interchangably.

then, several researchers around the world have focused on cognitive radio research and development. The FCC has been working on a concept is called dynamic spectrum access, where unlicensed users can borrow portions of the spectrum from the incumbent license holders enabling its secondary usage [4, 5]. IEEE has formed a working group for IEEE 802.22 for enabling the secondary usage of the unused portions of the TV spectrum [11, 12].

After identifying and selecting an available spectrum segment, a cognitive radio should use modulation schemes that provide the best spectrum utilization and capacity while avoiding interference to any primary user. The desired transmission scheme should be flexible enough to allow assignments of any band to any user, and should be scalable with the number of users and bands. The digital modulation scheme based on orthogonal frequency division multiplexing (OFDM) is natural approach due to inherent frequency sub-banding [13]. OFDM has two key advantages [14]: First a set of subcarriers represented by their corresponding IFFT inputs can be fed with zeroes to avoid any emission of radio power in the bands occupied by primary user transmissions. Second, the FFT operation in the OFDM demodulation process can be used for analysis of the spectral activity of the licensed users. OFDM spectrum access is scalable while keeping users orthogonal and non-interfering provided the users are synchronized. Moreover, OFDM is a proven technique which supports high data rates that are robust to channel impairments due to frequency selective channels. OFDM has been used in several standards, such as IEEE 802.11a, 802.11g, 802.16a/d/e, 802.20.

OFDM based transmissions suffer from large PAPR values requiring large dynamic ranges of the D/A converters and PAs. Several algorithms have been proposed in literature for the PAPR reduction of an OFDM signal. However, most of

8

the algorithms are computationally complex, and useful for only limited scenarios. More information about PAPR reduction can be found in Chapter 4.

In order to keep the cognitive receiver demodulator fairly simple, it has been proposed to restrict a single user transmission to a single frequency band. In this dissertation, we proposed an NC-OFDM framework which allows the single user to utilize multiple frequency bands collectively for high data rate transmissions. In NC-OFDM transceiver, FFT pruning technique can be used to reduce the complexity of the FFT computations.

With respect to OFDM-based cognitive radios, several groups in University of California, Berkeley, Virginia Tech Universtity, University of South Florida, Trinity College, Ireland, are focusing on several research aspects.

1.4 Thesis Contributions

This dissertation presents the following novel contributions in the areas of digital communications, data transmissions, and signal processing for communications:

- An NC-OFDM framework that enables using non-contiguous spectrum collectively for high data rate transmissions in DSA environment. The framework can achieve the agility necessary for secondary usage of a licensed frequency occupied by the primary users. Moreover, the NC-OFDM technique is viable and performs better that another popular multi-carrier technique, viz. multi-carrier code division multiple access (MC-CDMA).

- An extensive survey of PAPR reduction algorithms proposed in literature and a taxonomy of the PAPR reduction algorithms is presented. The theo-

retical background, analysis and characterization of PAPR properties, and theoretical bounds on PAPR are presented.

- A subcarrier phase adjustment technique that computes the subcarrier phase adjustments which reduces the PAPR of an OFDM signal. The proposed algorithm exhibits low computational complexity as well as being non-iterative. Even though the proposed algorithm is suitable only when an OFDM signal exhibit large PAPR values, the technique can be combined with other techniques, such as data randomization technique, to minimize wide range of PAPR values of an OFDM signal.

- Several PAPR reduction algorithms proposed in the literature are suitable for specific scenarios. An adaptive-mode PAPR reduction algorithm which adaptively chooses which PAPR reduction approach or combination thereof to employ based on the current operating conditions, such as instantaneous PAPR.

- A subcarrier power adjustment technique for PAPR reduction, in which subcarrier power levels are altered to minimize PAPR values of an OFDM signal. In the proposed technique, information regarding the power level adjustments does not need to be transmitted to the receiver. Therefore, there is no throughput penalty an no additional processing is required at the receiver side. Moreover, the proposed technique yields the power levels that obey regulatory power requirements.

- An OFDM symbol design technique for PAPR reduction employing non-data bearing subcarriers. It is known that PAPR can be reduced by using non-data bearing subcarriers. However, determining the optimal number of

NDB subcarriers and their values is nontrivial. Therefore, a novel scheme is proposed to determine the values of the fixed or variable number of NDB subcarriers to minimize PAPR values of an OFDM signal. An optimal number of NDB subcarrier necessary for PAPR reduction varies on per frame basis. Therefore, a scheme is also proposed to determine suboptimal number of NDB subcarriers as well.

- A technique for using the low correlation phase sequences for PAPR reduction of an OFDM signal. Low correlation phase sequences such as Schroeder phase can be used to generate the phase adjustment factors for selected mapping (SLM)-based PAPR reduction techniques. In the proposed technique, the phase adjustment procedure can be made as simple as flipping the sign of the symbol of the input sequence for an OFDM signal.

- A PAPR analysis for NC-OFDM signals. Due to the non-contiguous nature of the subcarriers, the PAPR distribution of an NC-OFDM signal would be different from that of an OFDM signal. Moreover, the design requirements of the PAPR reduction techniques for an NC-OFDM signal are elaborated.

- An efficient implementation of NC-OFDM transceivers for cognitive radios. In DSA environment, several subcarriers need to be deactivated to avoid any interference to the primary user transmissions. The information about the deactivated subcarriers can be used to prune the FFT operations, thereby yielding an efficient FFT implementation for the NC-OFDM transceivers.

1.5 Thesis Organization

This dissertation is organized as follows: In Chapter 2, a brief introduction to cognitive wireless transceivers, motivation for using the frequency agile multi-carrier modulation technique in DSA environment, and the basic principles of OFDM-based communication system are presented. The chapter also presents an overview of several spectrum sharing strategies for improving spectrum utilization efficiency as well as mitigate apparent spectrum scarcity problem. Moreover, the chapter outlines a design overview of the NC-OFDM systems using the non-contiguous blocks of spectrum for achieving high data-rates, and analyzes several research topics associated with the development of cognitive NC-OFDM system. Several shortcomings of the OFDM-based transmissions, namely the PAPR problem and efficient modulation techniques, are also elaborated.

In Chapter 3, performance of NC-OFDM system is evaluated and viability of the NC-OFDM technique for DSA network is demonstrated. Moreover, the chapter presents qualitative as well as quantitative comparison of NC-OFDM with other candidate multi-carrier modulation technique, such as multi-carrier code division multiple access (MC-CDMA).

One of the issues with the OFDM-based systems is the large variations in the signal envelopes, which is characterized by large PAPR values. In Chapter 4, we present a detailed overview of PAPR problem for OFDM signals. The chapter outlines the motivation for PAPR reduction as well as theoretical bounds on PAPR of an OFDM signal. Moreover, a detailed survey and a taxonomy of several PAPR reduction techniques proposed in literature are presented.

Large values of PAPR signifies the requirement of large dynamic ranges for

the transceiver components, which is inefficient both in terms of cost and power. In Chapter 5, we develop and analyze five novel PAPR reduction techniques for reducing the PAPR value of an OFDM signal. The chapter also elaborates on the different statistical properties for PAPR of NC-OFDM signal relative to that for OFDM signals. Moreover, the design requirements of PAPR reduction techniques for NC-OFDM signals are described.

Due to the non-contiguous subcarriers, it is possible to optimize the FFT-based modulation and demodulation. In Chapter 6, we present a general FFT pruning algorithm to yield an efficient implementation of FFT algorithm for NC-OFDM system. The proposed algorithm can accept any zero-valued input distribution and prune the FFT to yield an implementation that results in a faster execution time.

In Chapter 7, the research achievements of this work are outlined and future research directions are presented.

Chapter 2

Cognitive Wireless Transceivers[†]

2.1 Introduction

The development of *software-defined radio* (SDR) technology has made modern wireless transceivers more versatile, powerful, and portable, by performing baseband processing, such as modulation/demodulation and equalization, entirely in software and digital logic. With the ease and speed of programming baseband operations, SDR technology is a prime candidate for DSA networks. In addition to the agility of the SDR technology, the radio needs to be spectrally aware as well as autonomous in order to dynamically utilize spectrum. A radio transceiver that can adapt its transmitter parameters based on its interaction with the environment[1] in which it operates in order to improve the quality of radio communication is known as a *cognitive radio* [16]. With recent developments in cognitive radio technology, it is now possible for these systems to simultaneously respect the rights of incumbent license holders while providing additional flexibility and access to

---

[†]Parts of this chapter have been presented as a book chapter in *Cognitive Radio Communications Networks* [15].

[1]These changing environments can be at the physical, network, and/or application layers of the system.

14

spectrum.

Research and development of cognitive radios involves experts from various disciplines, including but not limited to the following categories:

- *Spectrum Sharing Policy*: Regulatory agencies assign radio spectrum to license holders, which maintain exclusive rights to a finite bandwidth. However, since radio transmissions propagate throughout space, it is necessary to define enforceable rules and regulations that guarantees the rights of the incumbent license holders [17]. Simultaneously, it is possible to grant temporary access to the unlicensed users to enable the secondary spectrum utilization.

- *Artificial Intelligence* (AI): The radio should autonomously and dynamically determine the appropriate radio parameters without intervention from the user in order to enable the efficient secondary spectrum utilization [18].

- *Cognitive Network Protocols*: The coordination of cognitive radios require the sharing of information in order to agree upon communication parameters dynamically. Dissemination of control traffic among the users is quite important for effective and efficient spectrum sharing [19].

- *Reconfigurable Hardware*: Adaptation to dynamically changing operating parameters require the cognitive radio hardware to be rapidly reconfigurable. Therefore, software defined radios and FPGA-based techniques are prime candidates to build a cognitive radio [20, 21].

- *Agile Physical Layer Transmission Techniques*: As with any wireless communications system, including cognitive radios, the choice of a physical layer

transmission technique is an important design decision [7]. The primary goal of a transmission technique employed by the cognitive radio unit would be to achieve sufficient agility enabling unlicensed users to transmit in a licensed band while not interfering with the incumbent users.

Therefore, cognitive radio research is highly interdisciplinary and various issues need to be addressed to meet the regulatory requirements before becoming a reality.

In this dissertation, we will focus on the design and implementation of agile physical layer transmission techniques for cognitive radios. To support throughput-intensive applications, multi-carrier modulation (MCM) techniques can be employed due to its ability for handling distortions introduced by frequency selective channels [22–24]. Moreover, cognitive radio transceivers based on MCM can readily enable DSA networks by employing spectrum pooling, where secondary users may temporarily access and utilize spectral resources during the idle periods of licensed users [14].

2.2 Multi-Carrier Modulation

As wireless applications are becoming more sophisticated and are widely used, the demand for high data-rate communications will increase substantially. Therefore, in addition of being frequency agile, a communication system should be able to achieve high data-rates for transmission. The MCM approach can supporting huge data-rates by dividing the stream into several parallel bit streams, each with a lower bit rate, and modulating these sub-streams with different subcarriers. As a result, MCM is robust to frequency selective fading or narrow band interference,

which makes MCM a prime candidate for high data rate transmissions. In a single carrier system, a single fade or interferer can cause the entire link to fail, but in a MCM system only a small percentage of the subcarriers will be affected.

The coherence bandwidth $(\Delta f)_c$ of a channel is the bandwidth over which the signal propagation characteristics are correlated and it can be approximated by the inverse of the maximum path delay spread, $\tau_{\max}$,

$$(\Delta f)_c \approx \frac{1}{\tau_{\max}}. \tag{2.1}$$

The channel is frequency selective if the signal bandwidth, B, is larger than the coherence bandwidth, $(\Delta f)_c$. On the other hand, if B is smaller than $(\Delta f)_c$, the channel can be approximately considered flat. As shown in Figure 2.1, in MCM communications, the subcarrier bandwidth is small compared to the coherence bandwidth of the channel and fading can be considered relatively flat per sub-channel as compared to single carrier system.

The delay spread can cause inter-symbol interference (ISI) when adjacent data symbols overlap and interfere with each other due to different delays on different propagation paths. The symbol duration of the signal, T_d, is equal to the inverse of the subcarrier bandwidth, B. Then, the number of interfering symbols in a single-carrier modulated system is given by:

$$N_{\text{ISI,single carrier}} = \left\lceil \frac{\tau_{\max}}{T_d} \right\rceil. \tag{2.2}$$

For high data rate applications, single carrier-modulated signal will have a very short symbol duration, i.e. $T_d < \tau_{\max}$, and with increased effect of ISI, highly complex equalizers would be required for satisfactory equalization. As a result,
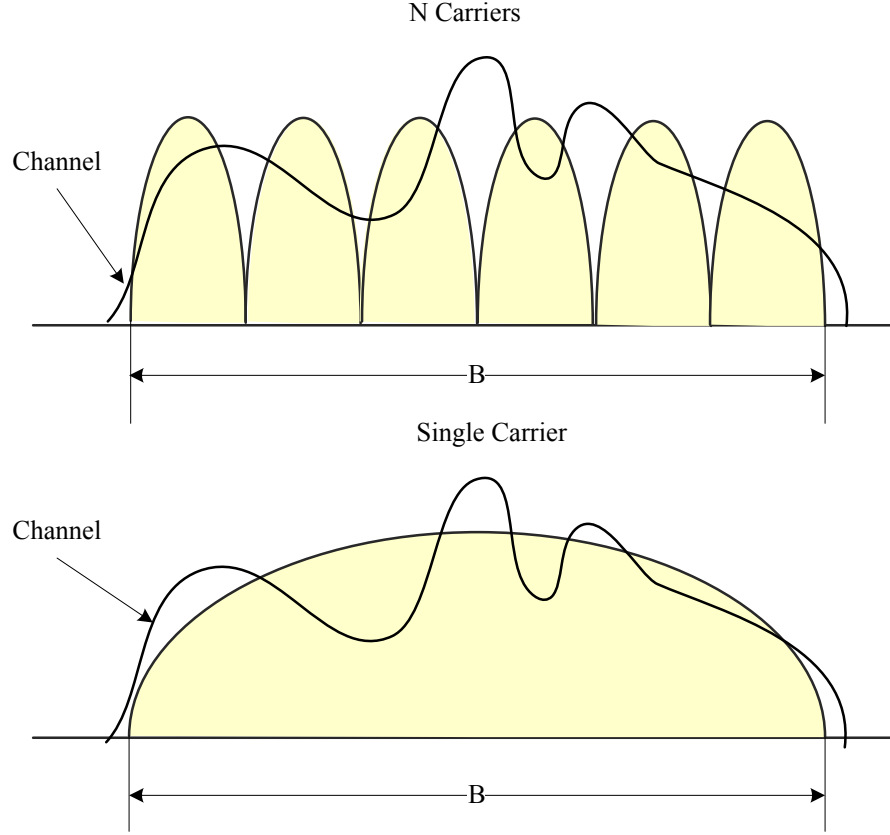
Figure 2.1. Comparison of effect of channel impulse response on single carrier versus multi-carrier communication.

complexity and cost of the receiver can increase significantly.

If the symbol duration is significantly larger than the maximum delay spread $T_d \gg \tau_{\max}$, the channel produces a negligible amount of ISI. This effect is exploited in a multi-carrier system. The subcarrier bandwidth for the multi-carrier modulated signals, with N subcarriers, is B/N. In this case, the symbol duration would be equal to $N \times T_d$, and the number of interfering symbols in a multi-carrier modulated system is given by:

$$N_{\text{ISI,multi-carrier}} = \left\lceil \frac{\tau_{\max}}{N \times T_d} \right\rceil .$$

(2.3)

Therefore, $N_{\text{ISI,multi-carrier}} \ll N_{\text{ISI,single carrier}}$, and low complexity equalizers would suffice to compensate for the channel distortions at the receivers for the multi-carrier transmission systems, thereby reducing the overall cost and complexity of the receiver.

Saltzberg compared the performance of single carrier and multi-tone digital modulation for ADSL applications, as summarized in Table 2.1 [23]. There is little difference in the performance between single carrier and multi-carrier systems, because the MCM can be interpreted as a linear reversible transformation of a single carrier signal. Under ideal channel conditions, both systems are equivalent in terms of throughput and error probability. However, there are many practical differences between these systems. For instance, multi-carrier systems are less susceptible to impulse noise, as the energy of the impulse noise gets distributed over several subchannels at the multi-carrier receiver, thereby reducing its effect. multi-carrier systems can perform adaptive bit loading in a straightforward fashion, which can enhance performance with respect to maximizing throughput or minimizing error probability. However, multi-carrier systems are more sensitive to the effects of narrowband noise, amplitude clipping, frequency offsets, timing jitter, and delay. The FFT algorithms reduce the computational complexity of the multi-carrier systems during modulation and demodulation. Moreover, low complexity equalizers are sufficient for satisfactory equalization in multi-carrier implementation, whereas more complex equalizers are required for satisfactory equalization in a single carrier system. So, the number of multiplications and additions per unit of time is typically larger in the single carrier system.

Multi-carrier modulation schemes can be combined with efficient implementations of spectrum opportunistic algorithms in a cognitive radio in order to achieve

Table 2.1. Relative advantages of single carrier and multitone modulation for ADSL. '$\sqrt{}$' denotes the system with better performance or lower cost (from [23])

Issue	Single-carrier	Multitone	Equivalent
Performance in Gaussian noise			$\sqrt{}$
Sensitivity to impulse noise (uncoded)		$\sqrt{}$	
Sensitivity to narrowband noise (uncoded)	$\sqrt{}$		
Sensitivity to clipping	$\sqrt{}$		
Latency (delay)	$\sqrt{}$		
Need for echo cancellation	$\sqrt{}$		
Computation per unit time		$\sqrt{}$	
Complexity of algorithms	$\sqrt{}$		
Cost and power consumption in analog sections	$\sqrt{}$		
Adaptability of bit rate		$\sqrt{}$	

high data-rate transmissions and develop wireless architectures that searches and finds an appropriate frequency band for transmission instead of operating in a fixed assigned band. In this work, we mainly focus on OFDM-based cognitive radios, which is a MCM technique, and we will describe fundamentals of OFDM transceiver design in next section.

2.3 Fundamentals of OFDM Transceiver Design

2.3.1 System Overview

OFDM is a multi-carrier transmission technique that divides the available spectrum into subcarriers, with each subcarrier containing a low rate data stream. The subcarriers have appropriate spacing and passband filter shape to satisfy orthogonality. As compared to classical parallel data system, frequency division multiplexing (FDM), where a guard band is necessary between the subcarriers which
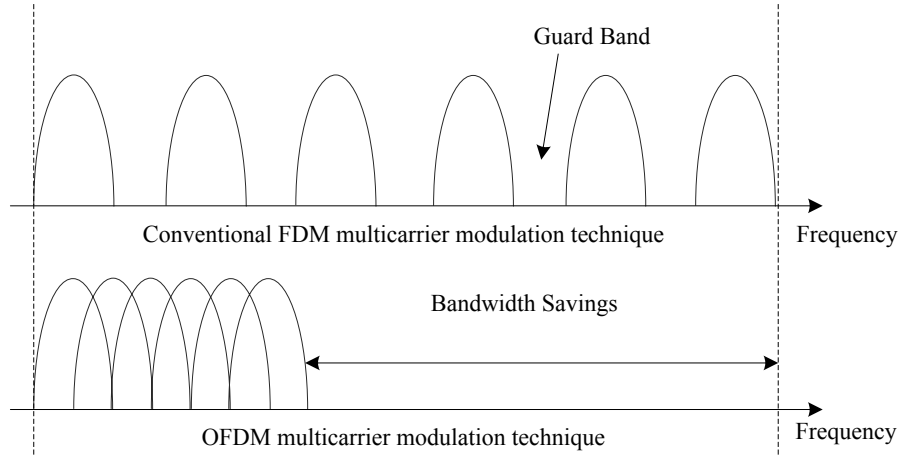
Figure 2.2. Comparing bandwidth utilization between the conventional FDM system and OFDM system (from [25]).

results in an inefficient usage of spectrum, OFDM uses overlapping spectrum of orthogonal subcarriers which leads to effective usage of spectrum, as shown in Figure 2.2 [25]. Therefore, OFDM can be considered as a spectrally efficient version of FDM. As will be explained in next section, OFDM uses inverse discrete Fourier transform (IDFT) for modulation operation, in which the temporal pulse shape of one symbol is rectangular. This results in a *sinc*-shaped[2] Fourier transform of the signals on each subcarrier with large side-lobes due to the frequency response of the filters that characterize subcarrier channels. However, as long as the transceivers are synchronized with each other, the subcarrier channels are orthogonal to each other and the resulting interference is insignificant. The normalized frequency spectrum of 8-tone OFDM signal is shown in Figure 2.3.

Multi-carrier modulation, such as OFDM, is widely deployed in high speed data transceivers, for e.g. xDSL [26], IEEE 802.11a [27], IEEE 802.11g [28], IEEE 802.16a [29], due to its ability to efficiently handle the distortions introduced by

---

[2]A sinc function is defined as $sinc(x) = \frac{\sin(x)}{x}$.
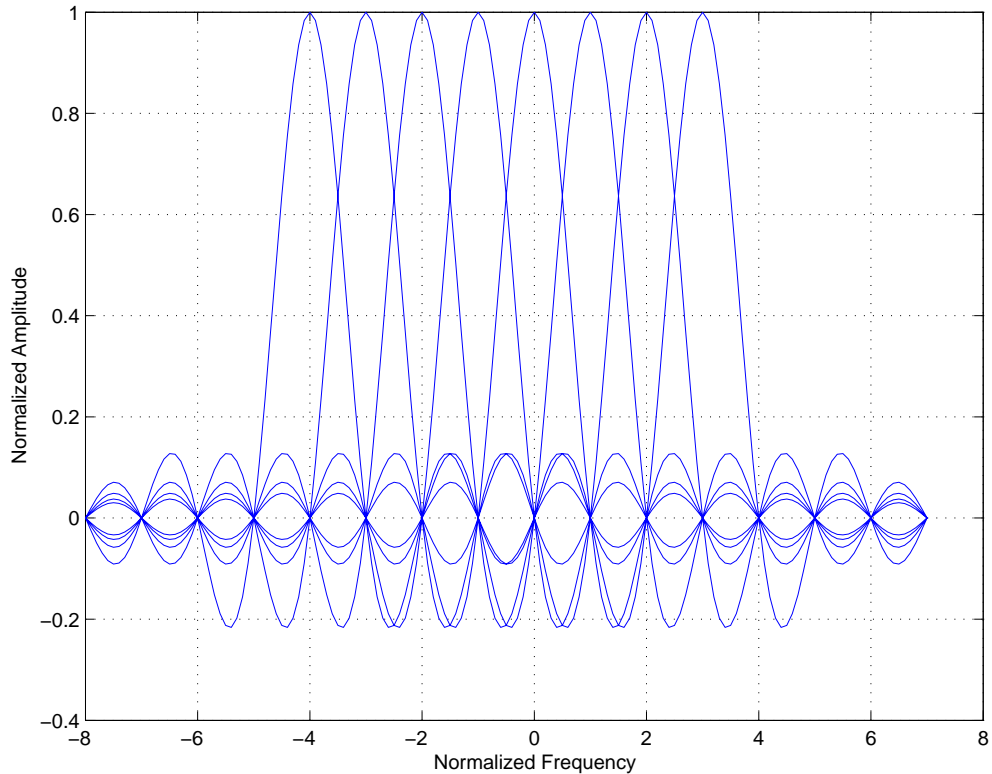
Figure 2.3. Normalized frequency response of the subcarriers in a 8-tone OFDM signal.

frequency selective fading channels [24].

2.3.2 OFDM Signal Generation and Reception

A generic block diagram for a simplex point-to-point OFDM transceiver system is shown in Figure 2.4. The basic principle of OFDM is to split a high-rate data stream from a data source into N lower rate streams. These streams are then individually modulated by using M-ary phase shift keying (PSK) or M-ary quadrature amplitude modulation (QAM). These streams are transmitted simultaneously over N orthogonal subcarriers using a serial-to-parallel (S/P) converter. These data over subcarriers are summed up to yield an OFDM symbol. Mathe-
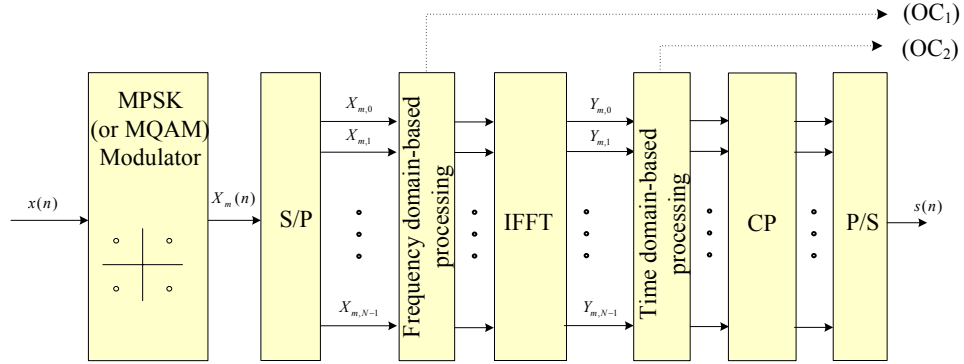
(a) Transmitter.
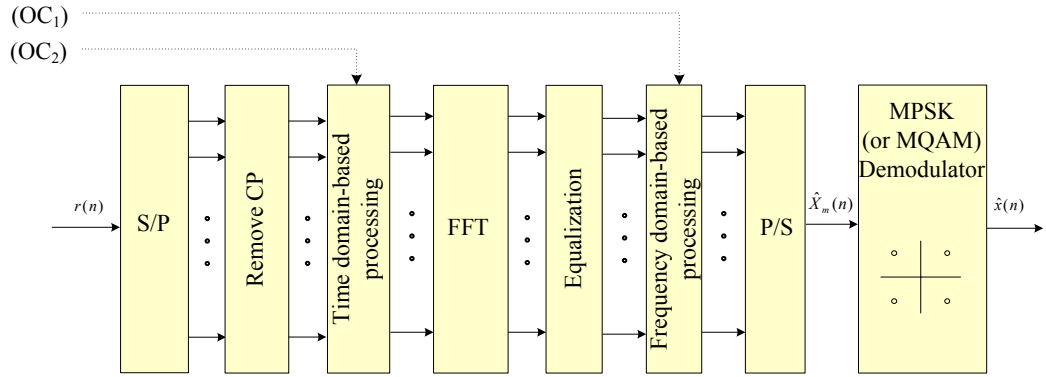
(b) Receiver.

Figure 2.4. General block diagram of an OFDM transceiver.

matically, if $X_{m,k}$, $k = 0, 1, \ldots, N-1$, represents the complex input symbols of the k-th subcarrier at the m-th time instant, N is the number of subcarriers, and T the symbol duration, then one OFDM symbol starting at $t = t_s$ in complex baseband notation can be written as:

$$s_m(t) = \frac{1}{N} \sum_{k=0}^{N-1} X_{m,k} \exp\left(j2\pi\frac{k}{T}(t - t_s)\right) \qquad t_s \leq t \leq t_s + T \qquad (2.4)$$

where, $j = \sqrt{-1}$.

The complex baseband OFDM signal defined in Eq. (2.4) is equivalent to the

inverse Fourier transform of N M-ary PSK (or M-ary QAM) input symbols. The time discrete equivalent is the inverse discrete Fourier transform (IDFT). So, the IDFT and the discrete Fourier transform (DFT) are used for modulating and demodulating the data constellations on the orthogonal subcarriers. These signal processing algorithms replace the bank of in-phase and quadrature-phase (I/Q)-modulators and demodulators that would otherwise be required [30]. The discrete samples of the OFDM symbol is given by:

$$s_m(n) = \frac{1}{N} \sum_{k=0}^{N-1} X_{m,k} \exp\left(j2\pi\frac{kn}{N}\right) \qquad n = 0, 1, \dots, N-1 \qquad (2.5)$$

The guard interval for each OFDM symbol is chosen to be larger than the expected channel delay spread such that multipath components from one symbol cannot interfere with the next symbol. The guard interval need not contain any specific signal, but cyclically extending the OFDM signal in the guard interval ensures that the delayed replicas of the symbol always have an integer number of cycles within the FFT interval. This holds true as long as the delay is smaller than the guard interval (i.e. cyclic prefix (CP)) and the effect of the time-dispersive channel becomes equivalent to a cyclic convolution. Due to the properties of the cyclic convolution, the inter-symbol interference (ISI) is eliminated to a large extent and inter-carrier interference (ICI) becomes manageable with simple equalization. The only drawback of this principle is the reduction in the efficiency of OFDM transmissions. Following the parallel-to-serial (P/S) conversion, the baseband OFDM signal $s(n)$ is upsampled and passed through the digital-to-analog (D/A) converter to convert the digital signal into an analog signal. The baseband OFDM signal is then low pass filtered, upconverted to the desired centering fre-

quency using a mixer and a local oscillator (LO), and amplified for transmission by the power amplifier (PA).

As shown in Figure 2.4, the receiver performs the reverse operation of the transmitter, mixing the RF signal to baseband for processing. Then, the signal is low pass filtered, converted to digital signal using an analog-to-digital (A/D) converter, and downsampled. The serial stream of sampled time signal is converted into parallel streams with a S/P converter and the cyclic prefix is discarded from the received composite signal, $r_{m,n}$. Then, the DFT is used to transform the time domain data into frequency domain:

$$\hat{X}_{m,k} = \sum_{n=0}^{N-1} r_{m,n} \exp\left(j2\pi\frac{kn}{N}\right) \qquad n = 0, 1, \ldots, N-1 \qquad (2.6)$$

These parallel streams are then demodulated to yield digital data and are multiplexed together using the P/S converter to yield the serial bit stream, and delivered to the data sink.

At the receiver, frame detection is an important task. Moreover, frequency and timing synchronization is required before the OFDM symbol can be correctly demodulated. Suitable channel estimation and equalization would also be required depending upon the surroundings and the BER requirements of the communication system. A known preamble is sent before each OFDM frame to allow receiver synchronization and channel estimation, as well as an initial acquisition of the frequency offset.

Due to the summation of the subcarriers at the transmitter, the composite OFDM signal in time domain could exhibit large envelope variations, which is characterized by a large PAPR. When high PAPR occurs, the D/A converter and

PA of the transmitter must have large dynamic ranges to avoid amplitude clipping, thus increasing both power consumption and component cost of the transceiver. It is possible to reduce the PAPR of an OFDM signal by modifying the signal characteristics in time-domain or frequency-domain, which will be explained in Section 4.6. If the OFDM signal is modified in the frequency-domain, the information is transmitted to the receiver via Control Channel (OC_1) (if needed). This information would enable the receiver to reverse the modifications made at the transmitter side for correctly demodulating transmitted information. Similarly, if the OFDM signal is modified in the time-domain, the information is transmitted to the receiver via Control Channel (OC_2) (if needed) as shown in Figure 2.4. Please refer to Chapter 4 and Chapter 5 for details regarding the PAPR.

2.4 Dynamic Spectrum Access Techniques

Spectrum sharing can mitigate the apparent spectrum scarcity problem and improve spectrum efficiency. Several spectrum sharing strategies have been proposed in literature, which can be broadly categorized based on [31]:

1. Network Architecture

    (a) Centralized Approach

    (b) Distributed Approach

2. Spectrum Allocation Behavior

    (a) Cooperative Approach

    (b) Non-cooperative Approach

3. Spectrum Access Technique

    (a) Underlay Approach

    (b) Overlay Approach

The following sections describe these categories in greater detail.

2.4.1 Centralized and Distributed Spectrum Sharing Approaches

In a *centralized spectrum sharing* approach, a centralized entity coordinates with arbitrary wireless technologies and manages access to arbitrary radio spectra by issuing clients temporary leases for parts of the radio spectrum [32]. In this model, a centralized server collects information from a collaborating group of secondary users, which learn about the primary user transmission characteristics, along with primary user cooperation, if possible[3], and manages a database for the spectrum access and availability information. The users communicate with the centralized server using a pre-assigned dedicated radio control channel (RCC). A basic framework for a centralized spectrum sharing model is shown in Figure 2.5(a). In the figure, the dashed RCC link between the primary user and the centralized server implies that the primary user may or may not choose to cooperate, whereas the solid RCC link between the secondary user and the centralized server implies that they must cooperate with each other. This form of spectrum management offers simpler and coordinated spectrum access, which enables efficient spectrum sharing and utilization in wireless environments.

---

[3]Since spectrum sharing techniques generate additional interference to the primary user, and the process of cooperation implies the addition of overhead for the incumbent license holders, primary user cooperation would not be easily anticipated without providing significant benefit to the incumbent users.
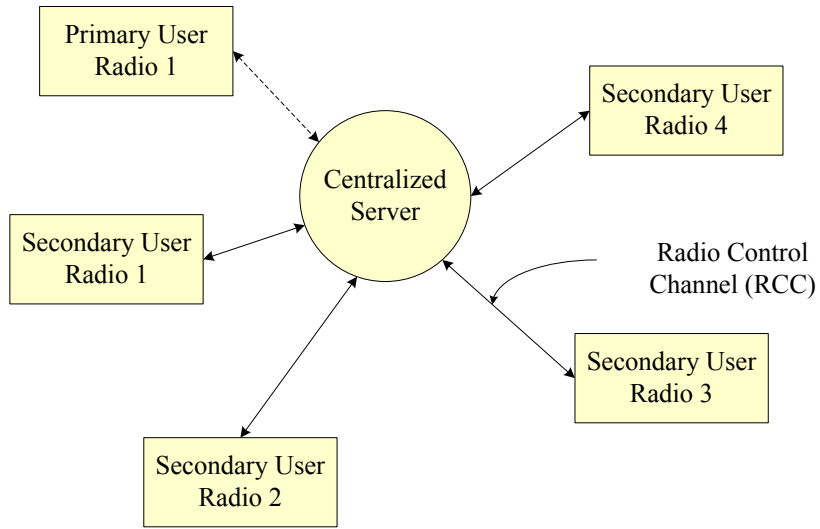
(a) Centralized.
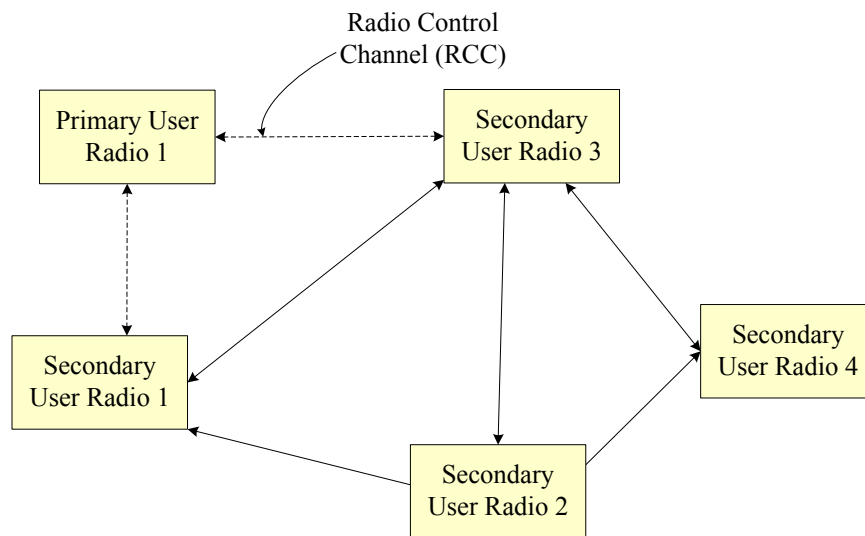
(b) Distributed.

Figure 2.5. Centralized and distributed spectrum sharing.

Even though a centralized server can optimize across network-wide information, there are two serious limitations [33]:

- The spectrum server and all secondary users need to communicate using a pre-assigned dedicated RCC. As the network grows in density, a pre-defined

control channel can limit the bandwidth available for data communication.

- As the number of users grows, the server processing complexity will scale at least polynomially [33]. Therefore, any central spectrum server can quickly become a computational bottleneck in the system.

Several centralized spectrum sharing approaches have been proposed in the literature, including the *dynamic intelligent management of spectrum for ubiquitous mobile access networks* (DIMSUMnet) [34], which can be employed as a regional spectrum broker, and the *dynamic spectrum access protocol* (DSAP) [35], which can be used as a spectrum broker for heavily-used, densely-populated localized areas where lease updates can occur frequently.

In a *distributed spectrum sharing* approach, each node is responsible for its own spectrum allocation and access based on primary user transmissions in its vicinity and policies [36, 37]. In this model, since secondary users can sense and share the local spectrum access information among themselves, primary user contributions need not be enforced. Therefore, this model poses an advantage for the primary license holders, since there would be no overhead involved with the incumbent users. A basic framework for a distributed spectrum sharing model is shown in Figure 2.5(b). In the figure, the dashed RCC link between the primary user and other secondary users implies that the primary user may or may not choose to cooperate, whereas the solid RCC link among the secondary users implies that they must cooperate with each other. Since individual nodes are responsible for maintaining the correct information about current spectrum usage, distributed spectrum sharing results in increased overhead communications among the secondary users. However, cooperative distributed algorithm can produce ef-
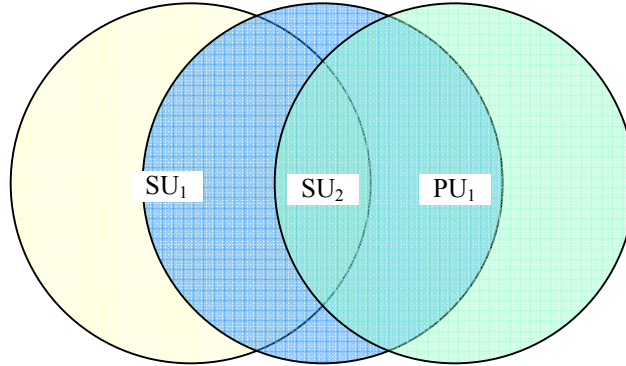
Figure 2.6. An example illustrating a hidden node problem, where the primary user PU_1 is hidden from the secondary user SU_1.

fects similar to global optimization through cooperative local actions distributed throughout the system [33]. One of the serious drawbacks of the distributed spectrum sharing approach is the *hidden node problem*, where the secondary users fail to detect incumbent users[4] and as a result inadvertently interfere with the incumbent user transmissions [38]. For example, in Figure 2.6, the secondary user SU_2 can sense both primary user PU_1 and secondary user SU_1, however, the PU_1 is hidden to SU_1 . Moreover, large amounts of measurement information gathered by the secondary user terminals during the detection cycle need to be transmitted to the other users, which can be a significant overhead in the system.

2.4.2 Cooperative and Non-cooperative Spectrum Sharing Approaches

Spectrum sharing techniques can be classified into *cooperative* and *non-cooperative* spectrum sharing based on the spectrum allocation behavior. In cooperative spectrum sharing, the primary and secondary users can cooperate and share spectrum occupancy information with each other to improve the spectral usage. The model

---

[4]The secondary user may fail to detect incumbent user because of its low power, inactivity, distance, or the poor channel conditions.

can either use centralized server sharing [35], where a centralized entity maintains the database of the spectrum usage and coordinates the spectrum access information among the users, or distributed sharing [36,37], where each user maintains the information about the local spectrum usage and share its knowledge with other nearby users to improve spectrum utilization efficiency. Even though the cooperative approach seems to be the most straightforward method, the primary user must be involved for efficient sharing of spectrum access information among the secondary users, which is often an unwanted burden on the part of the primary users. On the other hand, secondary users may cooperate with each other without any involvement of primary users and share information to detect the presence of a primary user to achieve significant performance enhancements on spectrum utilization and interference avoidance [39].

Cooperative approaches may lead to results that closely approximate the optimal spectrum allocation among the users. However, a cooperative approach model may heavily depend on the communication resources of the DSA networks. As a result, this communication overhead might limit the available spectrum for data communications. Since the ultimate goal of the cooperative approach is to achieve acceptable overall spectrum utilization, the users must be somewhat selfless, occasionally sacrificing local performance to improve overall system utility [40].

In a non-cooperative spectrum sharing approach, information exchange among the users is kept to a minimum, such that the secondary users independently interpret the spectrum usage and availability, while not interacting with the primary users [41, 42]. The non-cooperative approaches result in minimal communication requirements among the nodes at the expense of poor spectrum utilization efficiency. The non-cooperative approaches may act in a selfish, greedy, or rational

way [43].

2.4.3 Underlay and Overlay Spectrum Sharing Approaches

Spectrum sharing techniques can be classified into *underlay* and *overlay* spectrum sharing based on the spectrum access techniques. Underlay systems use ultrawide band (UWB) [44, 45] or spread spectrum techniques, such as code division multiple access (CDMA) [46], to transmit the signal below the noise floor of the spectrum [47]. An example of the time and frequency domain information of an underlay spectrum sharing system is shown in Figure 2.7(a). In this figure, we see that the underlay systems use wide band low power signals for transmissions. However, this technique can increase the overall noise temperature and thereby worsen error robustness of the the primary users as compared to the case without underlay systems. To avoid any interference to the primary users, underlay system can use interference avoidance techniques, such as *notching* [48] and *waveform adaptation* [49].

To improve the spectral efficiency, overlay systems utilize the unused portions of the spectrum. The spectrum holes[5] filled in by secondary transmissions in an overlay system is shown in Figure 2.7(b). As shown in this figure, the overlay systems use the unoccupied portions of the spectrum with a reasonable amount of guard intervals for secondary transmissions keeping the interference to the primary users to a minimum. Since the licensed system has privileged access to the spectrum, it must not be disturbed by any secondary transmissions. This results in two main design goals for an overlay system [51]:

- Minimum interference to licensed transmissions

---

[5]A spectrum hole is an unused portion of the licensed spectrum [50].
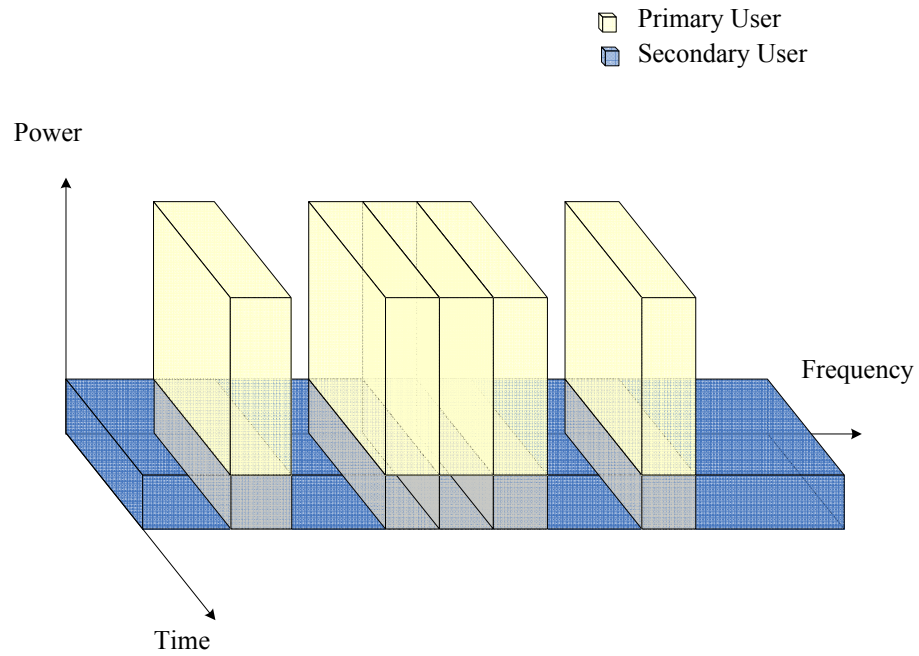
(a) Underlay.
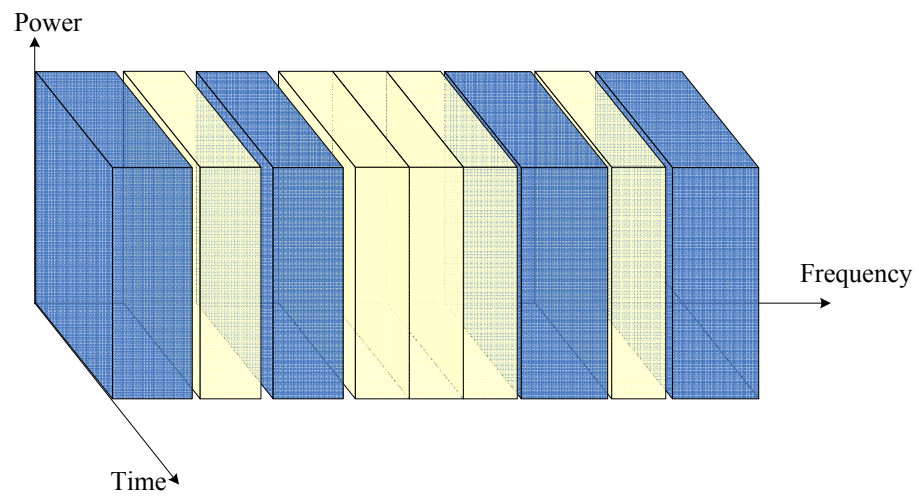
(b) Overlay.

Figure 2.7. Overlay and underlay spectrum sharing.

- Maximum exploitation of the gaps in the time-frequency domain.

In order to achieve these goals, the overlay system needs information about the spectrum allocation of the licensed systems by regularly performing spectrum

measurements. When interference among the users is high, it has been shown that frequency division multiplexing is an optimal technique [43].

To enhance spectral efficiency, an approach called *spectrum pooling* is proposed [14], which enables secondary access to licensed frequency bands by filling in the spectrum holes with secondary user transmissions without requiring any changes to the primary licensed systems. Spectral pooling represents the idea of merging spectral ranges from different spectrum owners (military, trunked radio, etc.) into a common pool, where users may temporarily rent spectral resources during idle periods of licensed users, thereby enabling the secondary utilization of already licensed frequency bands [14]. In spectrum pooling system, a centralized entity can collect measurement information gathered by the secondary user terminals during the detection cycle, and maintain the spectrum usage information. The centralized entity is responsible for making decisions on granting portions of the spectrum to the secondary users. With the use of a centralized entity, the information management of a spectrum access network would be relatively simple. However, this same entity can also easily be a bottleneck for the network, as already explained in Section 2.4.1. Since the overlay systems can readily exploit the unused portions of the spectrum without interfering with the incumbent users and without increasing the noise temperature of the system, we will consider overlay systems from this point forward.

One of the most challenging problems of spectrum sharing systems is their successful co-existence in the same frequency band, i.e. an overlay system should not degrade the performance of systems already working in the target frequency band. For instance, out-of-band radiation has to be reduced in order to enable co-existence. The transmitter spectral mask is a measure of the transmitter spectral

profile in order to verify that the device is not transmitting excessive amounts of energy outside its assigned channel bandwidth. Several approaches have been proposed in literature for suppressing the sidelobe levels, such as the deactivation of subcarriers lying at the borders of an OFDM spectrum [52], windowing [53], subcarrier weighting [54], and insertion of cancellation carriers [55].

2.5 Non-Contiguous Transmission

As mentioned previously, MCM is highly suited for high speed data transmissions, due to its ability to efficiently handle the distortion introduced by frequency selective channels [22]. Moreover, MCM techniques, such as OFDM, can provide the necessary agile spectrum usage, when portions of the target licensed spectrum are occupied by both primary and secondary users. This is achieved by deactivating (i.e. nulling) subcarriers that can potentially interfere with other users. This form of an OFDM, where the implementation achieves the high data rates via collective usage of a large number of non-contiguous subcarriers, is called NC-OFDM. A frequency spectra for 16-subcarrier NC-OFDM with nine active and seven deactivated subcarriers is shown in Figure 2.8, where the subcarriers are orthogonally overlapped. The subcarriers corresponding to the spectrum occupied by incumbent user transmissions, which are determined from the spectrum sensing measurements, are deactivated[6]. In this section, we present a brief overview of the NC-OFDM framework, efficient implementations of NC-OFDM transceivers, and conduct a performance analysis of the system.

---

[6]The deactivated subcarriers implies that no information is transmitted over these subcarriers.
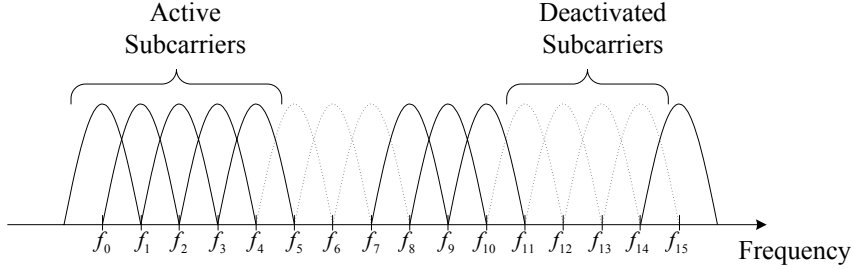
Figure 2.8. Frequency spectra of NC-OFDM subcarriers.

2.5.1 Non-Contiguous OFDM Framework

A general schematic of an NC-OFDM transceiver is shown in Figure 2.9. Without loss of generality, a high speed data stream, $x(n)$, is modulated using either M-ary PSK or M-ary QAM. The modulated data stream is then split into N slower data streams using a S/P converter. Note that the subcarriers in the NC-OFDM transceiver do not need to be all active as in conventional OFDM transmission. Moreover, the active subcarriers are located in the unoccupied spectrum bands, which are determined by dynamic spectrum sensing and channel estimation techniques [43, 56, 57]. The inverse fast Fourier transform (IFFT) is then applied to these streams, modulating them to different subcarrier center frequencies. The complex envelope of a baseband NC-OFDM signal, consisting of all N contiguous subcarriers over a time interval $[0, T]$ at m^{th} time instant, is given by:

$$s_m(t) = \frac{1}{N} \sum_{k=0}^{N-1} X_{m,k} e^{j2\pi kt/T} \tag{2.7}$$

where $X_{m,k}$ is the symbol of the kth subcarrier[7], T is the OFDM symbol duration, and $j = \sqrt{-1}$. The symbol over the kth deactivated subcarrier is $X_{m,k} = 0$. The

---

[7]For example, $X_{m,k} \in \{1, -1\}$ for BPSK signaling and $X_{m,k} \in \{\pm 1, \pm j\}$ for QPSK signaling.

discrete samples of the NC-OFDM signal are given by:

$$s_m(n) = \frac{1}{N} \sum_{k=0}^{N-1} X_{m,k} e^{j2\pi kn/N} \quad n = 0, 1, \ldots, N-1. \tag{2.8}$$

Prior to transmission, a guard interval of length greater than the channel delay spread is added to each NC-OFDM symbol, known as a cyclic prefix (CP). This block is used to mitigate the effects of intersymbol interference (ISI). Following P/S conversion, the baseband NC-OFDM signal, $s(n)$, is then passed through the transmitter radio frequency (RF) chain, which amplifies the signal and upconverts it to the desired center frequency.

The receiver performs the reverse operation of the transmitter, mixing the RF signal to baseband for processing, yielding the signal $r(n)$. Then, the signal is converted into parallel streams using S/P converter, the CP is removed, and the fast Fourier transform (FFT) is applied to transform the time domain data into the frequency domain. After compensating for distortion introduced by the channel using equalization techniques, the data in the active subcarriers is multiplexed using a P/S converter, and demodulated into a reconstructed version of the original high-speed input, $\hat{x}(n)$.

The 'null subcarrier selection' block at the NC-OFDM transmitter periodically collects information about the spectrum occupancy from the spectrum sensing measurements. Then, the subcarriers corresponding to the incumbent user transmissions are deactivated at the transmitter for avoiding any interference to the primary license holders. This information can be transmitted to the receiver via control channel before any data communication process begins so that the data over the active subcarriers are demodulated correctly.

(a) NC-OFDM Transmitter.

(b) NC-OFDM Receiver.
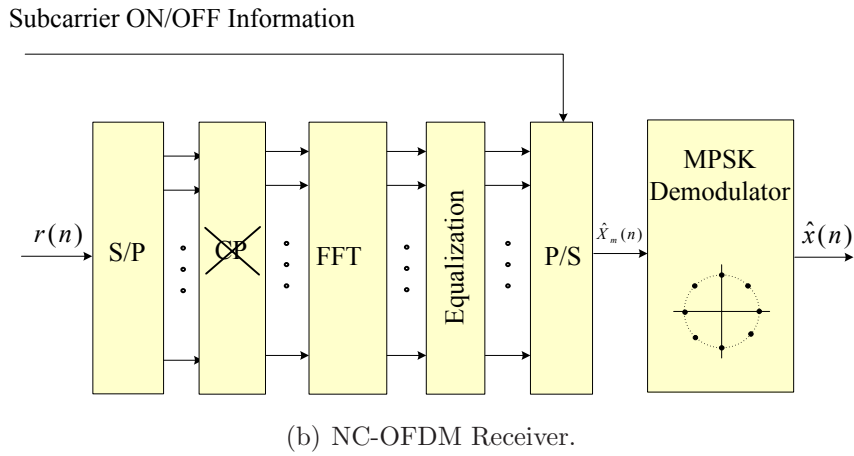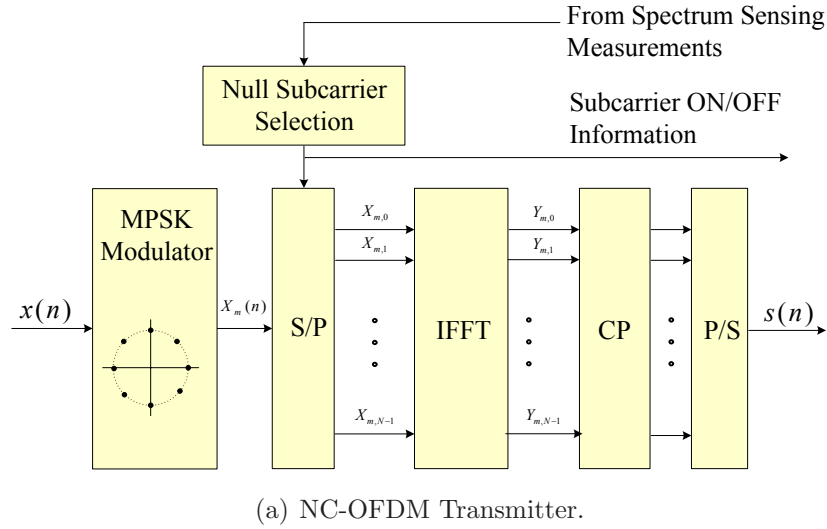
Figure 2.9. Schematic of an NC-OFDM transceiver employing null subcarrier selection block.

Fundamentals of the NC-OFDM signal generation and reception are quite similar to that of the OFDM signal explained in Section 2.3. However, with growing scarcity of the large contiguous frequency spectrum, NC-OFDM techniques offer very important advantage, i.e. it can support efficient and dynamic spectrum pooling for high data rate transmissions. We have identified following research areas to develop and implement NC-OFDM system:

1. *Performance Evaluation*: NC-OFDM is sufficiently agile with respect to spectrum usage, "filling in" the available spectral gaps within a transmission bandwidth partially occupied by other users (incumbent and other unlicensed) while not sacrificing its error robustness [58, 59]. Since power of the nulled subcarriers can be redistributed to the active subcarriers to improve signal-to-noise ratio (SNR) in NC-OFDM systems, their bit error rate (BER) performance can be improved as compared to conventional OFDM.

2. *Peak-to-average power ratio problem*: An OFDM signal consists of a sum of independent signals modulated over several orthogonal subcarriers of equal bandwidth. Therefore, when added up coherently, the OFDM signal may exhibit large peaks, while the mean power remains relatively low. Being a variant of OFDM, NC-OFDM signals also suffer from this same problem. When high PAPR occurs, the digital-to-analog (D/A) converter and power amplifier of the transmitter would require a large dynamic range in order to avoid amplitude clipping, thus increasing both power consumption and component cost of the transceiver. Therefore, it is highly desirable to reduce the PAPR of an OFDM and NC-OFDM signal.

3. *Efficient modulation and demodulation*: As we have seen in the previous section, OFDM-based transceivers employ IFFT and FFT blocks. The FFT algorithm make modulation and demodulation of the subcarriers highly efficient in terms of hardware and computational complexity [30]. However, an NC-OFDM transceiver may have several subcarriers that are deactivated in order to avoid any interference to the incumbent user transmissions. These deactivated subcarriers would result in zero-valued inputs to the IFFT and

FFT blocks. Thus, the hardware resources of the FFT are not fully exploited since the computations involving zeroes are unnecessary. Therefore, an approach is needed to efficiently implement the FFT blocks when several subcarriers are deactivated.

NC-OFDM technique offers a great flexibility of utilizing non-contiguous subcarriers for high data rate communications enabled by the cognitive radios. In this dissertation, NC-OFDM performance will be evaluated in DSA environment and several issues with OFDM-based technique, such as PAPR and efficient modulation and demodulation, are explored in the following chapters.

2.6 Chapter Summary

In this chapter, details regarding the physical layer components of the wireless communication systems and multi-carrier modulation techniques were presented. Moreover, importance of developing NC-OFDM technique and the research areas for developing the NC-OFDM techniques were also outlined.

Brief introduction to the cognitive wireless transceivers as well as multiple disciplines in cognitive radio research were presented in Section 2.1. Section 2.2 elaborated the motivation behind using multi-carrier modulation technique for high speed data transmissions and its superior performance as compared to the single carrier modulation technique is elaborated. The fundamentals of OFDM transceivers, including the methods of OFDM signal generation and reception, were presented in Section 2.3. Section 2.4 provided an overview of several dynamic spectrum sharing strategies to improve spectrum utilization efficiency and mitigate apparent spectrum scarcity. In Section 2.5, basic introduction to the NC-OFDM

technique was presented, where subcarriers corresponding to the incumbent user transmissions are disactivated for avoiding any intereference to primary users. Moreover, three research areas were identified to develop and implement NC-OFDM based cognitive radio.

Chapter 3

NC-OFDM Performance

Evaluation[†]

3.1 Introduction

The choice of a physical layer transmission technique is a very important design decision when implementing a cognitive radio. To achieve the agility necessary for transmission within a licensed frequency band occupied by incumbent users, multi-carrier-based transceivers are an appropriate choice [14, 60]. Besides being able to deactivate, or "null", subcarriers that could potentially interfere with other users, multi-carrier-based transceivers are also capable of providing high data rates at an acceptable level of error robustness [22, 23]. Although there are several multi-carrier-based transceiver implementations available, the two most popular choices are OFDM and multi-carrier CDMA (MC-CDMA) [8]. When an OFDM transceiver deactivates several subcarriers in order to avoid incumbent

[†]Parts of this work were presented at the *1st International Workshop on Technology and Policy for Accessing Spectrum* [58] and *IEEE Consumer Communications and Networking Conference - Workshop on Cognitive Radio Networks* [59].

users, we refer to this transceiver implementation as NC-OFDM [56,60]. The NC-OFDM technique achieves high data rates via collective usage of a large number of non-contiguous subcarriers, while simultaneously avoiding interfering with the incumbent user transmissions by deactivating subcarriers within their vicinity.

In this chapter, we evaluate the viability of NC-OFDM as a transmission technology for high data-rate wireless communications over non-contiguous spectrum. The analytical expressions for the probability of error of an NC-OFDM transceiver is represented and validated using computer simulations. NC-OFDM is then quantitatively compared with another candidate transmission technology for DSA networks, a variant of MC-CDMA, in terms of error robustness.

3.2 NC-OFDM Framework

Refer to Section 2.5.1.

3.3 MC-CDMA Framework

The structure of MC-CDMA was devised in order to overcome the high sampling rates required by direct sequence CDMA (DS-CDMA) transmission, where spreading is performed in the time domain. This high sampling rate makes DS-CDMA very susceptible to performance degradation caused by multipath propagation [8].

Referring to the MC-CDMA schematic in Figure 3.1, we observe that a high data rate input, $x(n)$, is fed into an M-ary PSK modulator[1] prior to S/P conversion into L streams. Each of these streams has a data rate less than $x(n)$ by a factor of

---

[1]Other forms of digital modulation, including M-ary QAM, can also be employed by the transceiver.

L. Following the S/P conversion, each stream is replicated into N parallel copies using the '*copy*' function[2], with copy m of stream i being multiplied by chip m of spreading code C_i, i.e. $C_{i,m}$, for $i = 0, 1, \ldots, L - 1$ and $m = 0, 1, \ldots, N - 1$ [61]. The result is having all the streams being spread in the frequency domain. Note that all the spreading codes used must be orthogonal with each other in order for the MC-CDMA transceiver to work. After the frequency domain spreading, copy m of all the streams are added together, for $m = 0, 1, \ldots, N - 1$, yielding N subcarrier inputs to the IFFT block, which converts these subcarriers into the time domain. The resulting normalized complex envelope of an M-ary PSK-modulated MC-CDMA signal is given as:

$$s(n) = \frac{1}{N} \sum_{i=0}^{L-1} \sum_{m=0}^{N-1} b_i C_{i,m} e^{j2\pi mn/T}, \tag{3.1}$$

where b_i is the M-ary PSK-modulated symbol from stream i, and $C_{i,m}$ is chip m of spreading sequence i. A guard interval, with a length greater than the channel delay spread, is then added to each symbol using the CP block in order to mitigate the effects of ISI. Following the P/S conversion, the baseband MC-CDMA signal, $s(n)$, is then passed through the transmitter RF chain, which amplifies the signal and upconverts it to the desired center frequency.

The receiver performs the reverse operation of the transmitter, where the received baseband signal $r(n)$ undergoes S/P conversion, CP removal, time-to-frequency conversion via FFT, and per subcarrier equalization. Each of the equalizers outputs are then replicated into L parallel copies using the copy function, with each copy allocated to one of L streams, where despreading is performed

---

[2]The data rate of the stream and its copies are identical.
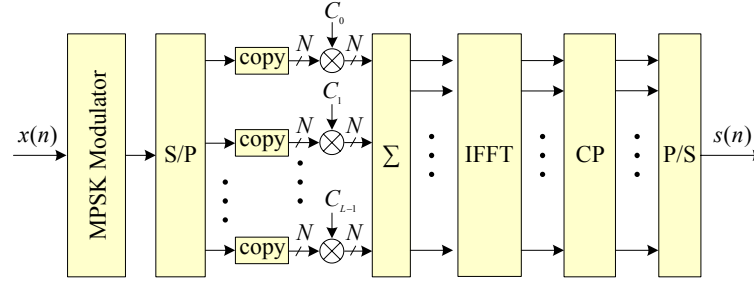
(a) MC-CDMA Transmitter.
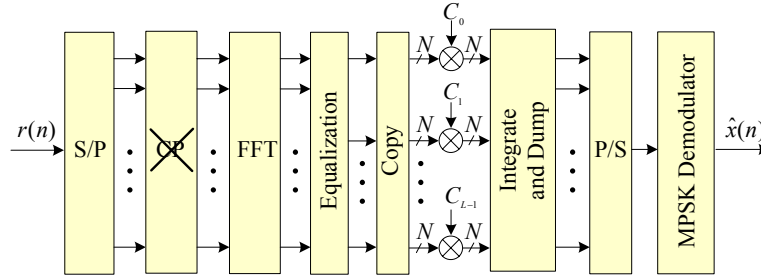
(b) MC-CDMA Receiver.

Figure 3.1. Schematic of an MC-CDMA transceiver.

using C_i, for $i = 0, 1, \ldots, L - 1$. An integrate-and-dump procedure is then performed per stream, followed by P/S conversion and M-ary PSK demodulation. This results in a reconstructed version of the original high data rate input signal, $\hat{x}(n)$.

To implement a non-contiguous version of MC-CDMA[3], subcarriers that interfere with occupied portions of spectrum are deactivated, in much the same way as is done in NC-OFDM. However, in order to compare with NC-OFDM, it is necessary that both implementations employ identical data rates. Therefore, the number of streams, L, must also be reduced. Note that when all of the subcarriers are active, $L = N$.

---

[3]Throughout this chapter, only the non-contiguous version of MC-CDMA is employed.

3.4 Qualitative Comparison

Thus far, we have presented the transceiver frameworks for NC-OFDM and MC-CDMA. To understand the advantages and disadvantages of employing NC-OFDM in a cognitive radio transceiver, we start with a qualitative comparison between this transmission technique and both MC-CDMA (employing non-contiguous subcarriers) and conventional OFDM. A summary of the qualitative comparison is shown in Table 3.1.

Several DFT-based modulation techniques are very sensitive to frequency and timing offsets [8]. However, there exist a number of synchronization techniques that make use of regularly-spaced pilot subcarriers in the frequency domain. Although conventional OFDM can exploit the pilot subcarriers since its transmission bandwidth is contiguous, both NC-OFDM and MC-CDMA cannot use these pilot subcarriers, since they might be located in occupied spectrum and are deactivated [14]. As a result, this solution is unavailable to these two techniques, which must resort to more complex approaches to obtain synchronization.

Both NC-OFDM and MC-CDMA are very agile with respect to spectrum usage, "filling in" the available spectral gaps within a transmission bandwidth partially occupied by other users (incumbent and other unlicensed). All that conventional OFDM can do is transmit in the largest unoccupied portion, if its transmission bandwidth fits in the first place. However, the spectrum agility for NC-OFDM and MC-CDMA comes at the cost of increased transmission overhead, where the activity status of each subcarrier must be shared between the transmitter and receiver. Moreover, if the occupied spectrum changes rapidly, frequent updates are required.

Table 3.1. Qualitative comparison MC-CDMA, OFDM and NC-OFDM system, where '√' denotes the transceiver with best performance.

Characteristics	MC-CDMA	OFDM	NC-OFDM
Synchronization		√	
Spectrum Agility	√		√
Throughput	√		√
Overhead		√	
Error Robustness		N/A	√
PAPR	√		

Since NC-OFDM is based on conventional OFDM, it has a potentially serious problem with large values of PAPR, while this problem is less pronounced in MC-CDMA since it employs frequency domain spreading [61]. Although PAPR is an issue with NC-OFDM, there are several techniques that can be employed to reduce the PAPR of a transceiver.

With respect to the nulling of subcarriers within the vicinity of occupied spectrum, NC-OFDM can accomplish this task without any degradation in its error robustness since the subcarriers are relatively independent of each other given a sufficient CP length and adequate equalization techniques. However, the subcarriers of an MC-CDMA transceiver are not independent due to the spreading in the frequency domain. As a result, the error robustness of an MC-CDMA system decreases as subcarriers are nulled, as we will see in the following section.

3.5 System Performance

3.5.1 Channel Model

For both the NC-OFDM and MC-CDMA systems, we assume the maximum delay of the multipath channel is shorter than the cyclic prefix. Moreover, a

transmitter and a receiver are perfectly synchronized and fading is slow enough for the channel to be considered constant for one symbol period.

With these assumptions, the ith received symbol can be described as follows:

$$Y_i = X_i \cdot H_i + \tilde{n}_i \tag{3.2}$$

where Y_i represents N received data symbols, X_i represents N transmitted data symbols, $H_i = \text{FFT}(h_i)$ is the frequency response of the channel, h_i is the impulse response of the channel padded with zeroes to obtain length of N, and $\tilde{n}_i = \text{FFT}(n_i)$, with n_i representing zero-mean complex Gaussian independent random variables.

We use a general equivalent baseband multipath channel model [62]. The channel consisting of M multipath components has the form of:

$$h(\tau) = \sum_{m=0}^{M-1} \alpha_m \delta(\tau - \tau_m) \tag{3.3}$$

where α_m is a zero-mean complex Gaussian independent random variable and τ_m is the delay of the mth path.

We assume an exponential power delay profile given by:

$$
\begin{aligned}
E[h(\tau)h^*(\tau)] &= E[\alpha_m \alpha_m^*] \\
&= Ce^{-\tau/\tau_{\text{rms}}}, \; 0 < \tau < \tau_{\text{max}}
\end{aligned}
\tag{3.4}
$$

where τ_{rms} is the RMS delay spread, τ_{max} is the maximum delay spread, and C is the normalization constant which makes the total multipath power equal to unity,

i.e.,

$$\sum_{m=0}^{M-1} E[\alpha_m \alpha_m^*] = 1. \tag{3.5}$$

3.5.2 Equalization

For simplicity, frequency domain equalization is employed to compensate for the channel impairments. In freqency domain equalization, the flat fading α_i on the ith subchannel is basically inverted in the receiver [63]. The coefficient sequence $(A_0, A_1, \ldots, A_{N-1})$ which determines the equalizer frequency response is the DFT of a sequence $(\alpha_0, \alpha_1, \ldots, \alpha_{M-1}, 0, \ldots, 0)$, where $(\alpha_0, \alpha_1, \ldots, \alpha_{M-1})$ represents the tap-gain vector of the equivalent M-tap time-domain equalizer.

In frequency domain, equalized data symbols are given by:

$$\hat{X}_n = Y_n/A_n, \ n = 0 \text{ to } N - 1. \tag{3.6}$$

The frequency domain equalization removes the impact of flat fading channel, it enhances the noise. Specifically, the incoming noise signal is also multipled by $1/\alpha_i$, so the noise power becomes $N_0 B/\alpha_i^2$, where N_0 is the input noise power spectral density.

3.5.3 NC-OFDM Signal-to-Noise Ratio Analysis

The SNR is defined as the ratio of the desired signal power to the noise power [62]. The SNR indicates reliability of transmission link between the transmitter and receiver, and is accepted as a standard measure of signal quality.

Assuming a wide sense stationary uncorrelated scattering (WSSUS) channel [64], the mean SNR can be given by the ratio of the mean signal power and

mean noise power as follows [65]:

$$E(\gamma_i^f) = \frac{E(|X_i|^2 \cdot |H_i|^2)}{E(|\tilde{n}_i|^2)} = \frac{E(|X_i|^2) \cdot E(|H_i|^2)}{E(|\tilde{n}_i|^2)} \qquad (3.7)$$

where $E(\cdot)$ denotes an expectation operator and γ_i^f denotes the SNR at i'th sub-channel.

In the following two subsections, we present the SNR analysis for the NC-OFDM system over additive white Gaussian noise (AWGN) and Rayleigh multipath channels.

3.5.4 AWGN Channel

Consider an AWGN channel with noise spectral density N_0 and bandwidth B, the noise power is given by:

$$E(|\tilde{n}_i|^2) = \sigma_N^2 = N_0 B \qquad (3.8)$$

while the SNR is given from Eqs. (3.7) and (3.8) as follows:

$$\gamma_1 = 10 \log_{10} \left(\frac{E(|X_i|^2)}{\sigma_N^2} \right) = 10 \log_{10} \left(\frac{E(|X_i|^2)}{N_0 B} \right). \qquad (3.9)$$

Suppose the incumbent spectral occupancy[4] (ISO) is α, then the total available bandwidth would be $(1 - \alpha)B$. Since the channel response is assumed to be approximately flat, the signal power would remain almost constant, irrespective

---

[4]Incumbent spectral occupancy (ISO) is defined as the fraction of the intended transmission bandwidth occupied by incumbent user transmissions.

of the available bandwidth. However, the effective noise power would be:

$$\sigma_N^2 = N_0(1 - \alpha)B \tag{3.10}$$

then, the SNR is given from Eqs. (3.7) and (3.9) as follows:

$$\gamma_2 = 10 \log_{10}\left(\frac{E(|X_i|^2)}{\sigma_N^2}\right) = 10 \log_{10}\left(\frac{E(|X_i|^2)}{N_0(1 - \alpha)B}\right). \tag{3.11}$$

Then, from Eqs. (3.9) and (3.11), the SNR gain is given by:

$$\text{SNR}_{\text{gain}} = -10 \log_{10}(1 - \alpha). \tag{3.12}$$

However, the total throughput would also reduce to pNR_b, where p corresponds to the unoccupied subcarriers.

3.5.5 Rayleigh Multipath Channel

Suppose we consider a frequency non-selective slow fading channel, i.e. flat channel response, where the channel magnitude response $E(|H_i|^2)$ is flat over the spectrum band. The deactivation of subcarriers due to incumbent users will result in a non-zero ISO. This would also filter out a portion of the channel magnitude response, which results in an increase in the magnitude of $E(|H_i|^2)$. Then, the SNR gain is given by:

$$\begin{aligned}
\text{SNR}_{\text{gain}} &= 10 \log_{10}\left(\frac{E(|X_i|^2) \cdot E(|H_i|^2)/(1 - \alpha)}{N_0(1 - \alpha)B}\right) \\
&\quad - 10 \log_{10}\left(\frac{E(|X_i|^2) \cdot E(|H_i|^2)}{N_0 B}\right) \\
&= -10 \log_{10}(1 - \alpha)^2.
\end{aligned} \tag{3.13}$$

In case of frequency selective multipath channel, the channel magnitude response $E(|H_i|^2)$ is not flat over the spectrum. Thus, deactivating a portion of the spectrum would also flatten a portion of the channel magnitude response, which results in a random increase in the magnitude of $E(|H_i|^2)$. Therefore, the SNR gain would not be linear as in the case with a flat AWGN channel.

3.5.6 Simulation Setup

For the simulations of the NC-OFDM and MC-CDMA transceivers, $N = 128$ BPSK-modulated subcarriers were employed. Comparisons were performed when 0%, 5%, 10%, 15%, 20%, and 25% of the N available subcarriers were deactivated, modeling the effects of incumbent user spectral occupancy within the transmission bandwidth. A three-path Rayleigh channel model with an exponential power delay profile was used [64], where each of the multipath components is an independent and identically distributed (*i.i.d.*) zero-mean complex Gaussian random variable. The CP length for both transceivers was three samples long (2.5% of the symbol). Channel distortion compensation was performed using per tone equalization (PTEQ) for each subcarrier [22]. The transceivers for both systems were assumed to be perfectly synchronized, the channel fading was considered to be quasi-stationary, i.e., does not vary over a long period of time, and no coding was performed for the purpose of straightforward comparison. For each SNR point, the simulations continued until 100 bit errors were recorded, and each BER point was averaged over 100 channel realizations.

3.5.7 BER Performance Analysis[5]

The BER results for an NC-OFDM and an MC-CDMA transceiver operating in
an AWGN channel for different percentages of deactivated subcarriers are shown in
Figure 3.2(a). When 0% of the subcarriers are deactivated, both transceivers have
the exact same performance when operating in the AWGN channel. Moreover,
their curves in this case also match the theoretical BER curve for a single car-
rier BPSK-modulated transceiver operating in an AWGN channel, which is true
for both transceivers. On the other hand, when the percentage of deactivated
subcarriers increases, the performance of the two transceivers begins to differ.
The BER performance of the NC-OFDM transceiver slightly improves relative to
the 0% curve due to fewer contributions of subcarrier noise. The improvement
in BER performance matches theoretical expectations as shown in Figure 3.3(a).
However, the BER performance of the MC-CDMA degrades as the number of
deactivated subcarriers increases. This is due to the fact that the subcarriers are
dependent on each other since the information from the original L streams have
been spreaded across them all. Thus, the deactivation of a subcarrier will result
in the loss of some information, which would have been used at the receiver to
reconstruct the original streams.

Given a three-path Rayleigh multipath channel for $\tau_{rms}/T_s = 0.1$ were studied,
where T_s is the NC-OFDM and MC-CDMA symbol period, the BER results for
an NC-OFDM and an MC-CDMA transceiver for different percentages of deacti-
vated subcarriers are shown in Figure 3.2(b). Generally, the performance of the
NC-OFDM transceiver is better than that of the MC-CDMA transceivers. The

---

[5]The simulation results for MC-CDMA error performance was generated by Qi Chen at the
University of Kansas.
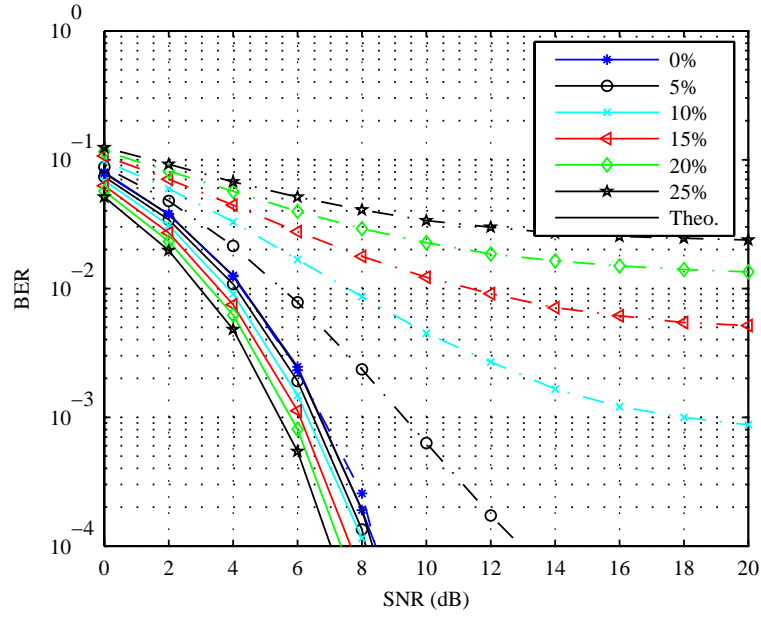
(a) AWGN channel.
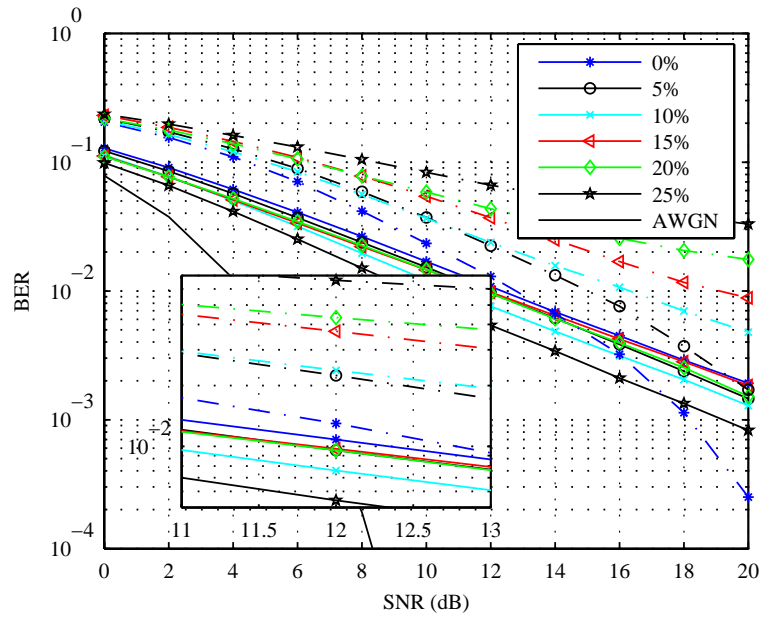
(b) 3-path Rayleigh channel.

Figure 3.2. BER performance of NC-OFDM (solid lines) and MC-CDMA (dashed lines) transceiver for various ISOs.

54

mean BER performance for a frequency selective channel closely follows theoretical expectations as shown in Figure 3.3(b) In particular, as the percentage of deactivated subcarriers increases, the BER performance of the MC-CDMA system worsens while the BER performance of the NC-OFDM transceivers improves slightly.

Total throughput of a N-carrier NC-OFDM system is NR_b, where R_b represents bit rate over an individual subcarrier. In NC-OFDM system, data is not transmitted over subcarriers corresponding to the spectrum occupied by the incumbent users, with prior knowledge of ISO. Therefore, there would be no information loss in NC-OFDM scheme. Moreover, SNR gain for increased ISO would result in improved BER performance of NC-OFDM scheme.

In MC-CDMA system, input symbols are spreaded over the available bandwidth. Therefore, turning off the subcarriers corresponding to incumbent user spectrum would result in fractional loss of information. This partial loss of information may also result in losing orthogonality between the spreading codes. Hence, MC-CDMA BER performance degrades for higher ISO.

3.6 Chapter Summary

In this chapter, we presented NC-OFDM as a viable candidate for cognitive radio transceivers operating in DSA networks. We evaluated its error robustness (both analytically and through simulations) for AWGN and multipath channels and compared it with MC-CDMA. From the SNR analysis, it is observed that BER performance of NC-OFDM is superior to the MC-CDMA system, when available spectrum is non-contiguous.
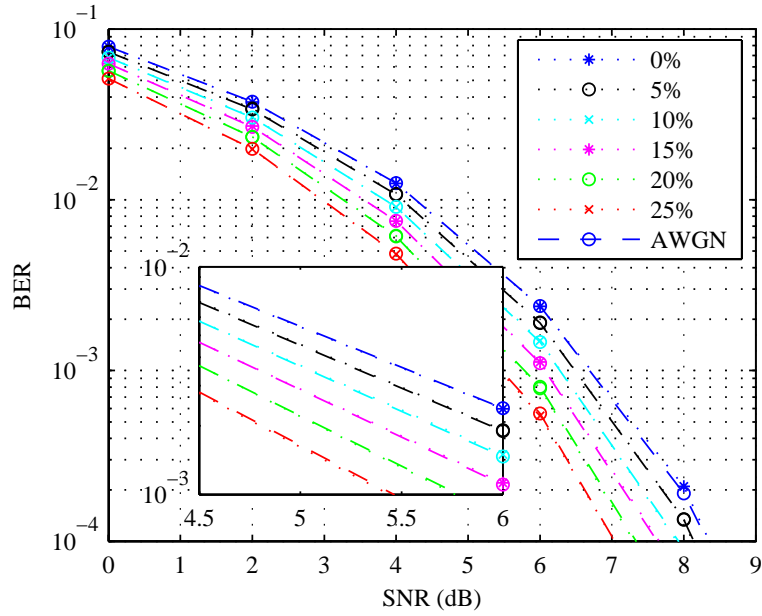
(a) AWGN channel.
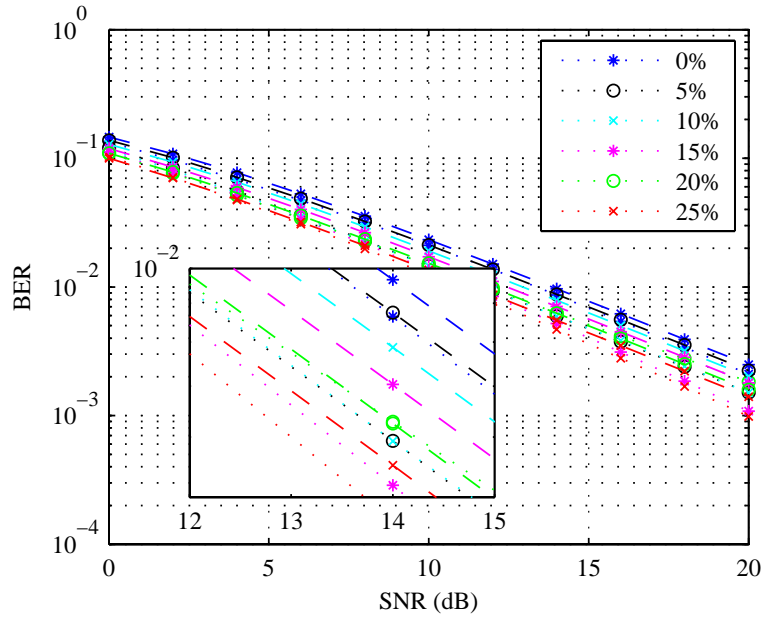
(b) 3-path Rayleigh channel.

Figure 3.3. BER performance of the NC-OFDM transceiver for various ISOs. Note that the dashed lines represent the analytic results while the dotted lines are the results via simulation.

Chapter 4

Peak-to-Average Power Ratio Problem in OFDM†

4.1 Introduction

With the growing demand for existing and new wireless applications, there is a need for transmission technologies that can deliver higher data rates. One such technology is MCM, which is widely deployed in many high data rate applications, e.g. xDSL [26], IEEE 802.11a [27], IEEE 802.11g [28], and IEEE 802.16a [29]. MCM possesses the ability to efficiently handle distortion introduced by frequency selective fading channels [24]. One efficient form of MCM is OFDM, which offers high spectral efficiency, robustness to channel fading, immunity to impulse interference, and the capability to handle frequency-selective fading without resorting to complex channel equalization schemes [22, 23]. As a result, OFDM is often chosen for the high data rate applications.

†Parts of this work have been submitted as a book chapter in *Encyclopedia on Wireless and Mobile Communications* [66] and an article to IEEE Communications Magazine [67].

Due to the summation of subcarriers at the transmitter, the composite MCM signal in the time domain could exhibit large envelope variations when the input sequence is highly correlated [68, 69]. This is often characterized by a large PAPR [70]. When high PAPR occurs, the digital-to-analog (D/A) converter and power amplifier of the transmitter require large dynamic ranges to avoid amplitude clipping, thus increasing both power consumption and component cost of the transceiver. Without sufficient dynamic range, the amplitude clipping would introduce a substantial amount of distortion.

Considering the importance of OFDM and the seriousness of high PAPR, numerous solutions have been proposed in the literature that could be employed by the system. These solutions include *clipping/filtering* [71–73], *error control coding* [74–78], and *constellation shaping techniques* based on phase adjustment [79–81], or power adjustment [82], or both [83–86].

In this chapter, we present an analysis of the PAPR problem in an OFDM framework, including motivations behind reducing PAPR, the statistical properties of PAPR, and the taxonomy of several techniques to reduce PAPR. The rest of this chapter is organized as follows: In Section 4.2, we present a brief introduction of the OFDM framework. Section 4.3 presents the definition of baseband and passband PAPR. In Section 4.4, we present motivations for reducing PAPR, such as reducing the dynamic ranges and improving power efficiency of the transceiver components. In Section 4.5, theoretical bounds on PAPR and its statistical properties are analyzed. In Section 4.6, a taxonomy of the existing PAPR reduction algorithms is presented and criteria for selecting an efficient PAPR reduction algorithm are analyzed in Section 4.7. Finally, Section 4.8 presents several concluding remarks.

4.2 OFDM Framework

A general schematic of an OFDM transceiver is shown in Figure 2.4. For details regarding basic OFDM framework, please refer to Section 2.3.2.

If the data on the subcarriers add up in a constructive manner at the transmitter, the resulting signal could exhibit large PAPR. As a result, the composite transmit signal could be severely clipped by the D/A converters and power amplifiers for their limited dynamic range as shown in Figure 4.1. In this case, the reconstructed output $\hat{x}(n)$ can possess a significant amount of distortion [71, 87]. It is possible to reduce the PAPR of an OFDM signal by modifying the signal characteristics in time-domain or frequency-domain, which will be explained in Section 4.6.

4.3 Definition of Peak-to-Average Power Ratio

An OFDM signal is a sum of several individual signals modulated over a group of orthogonal subcarriers with equal bandwidths. Therefore, when added up coherently, the OFDM signal has large peak, while the mean power remains low. By definition, PAPR[1] is the ratio of the peak power to the average power of a given signal. When signals with same phase are added, the highest possible PAPR occurs. To illustrate an example of the worst-case PAPR, let us consider an BPSK-modulated OFDM system with 16 subcarriers. When input symbols are all ones, the normalized instantaneous power of the OFDM signal in time-domain is shown in Figure 4.2(a). This figure illustrates the envelope power variations of the OFDM signal over time, where the peak power of the signal is unity and

---

[1]Several authors refer to *crest factor* (CF) as a measure of envelope variations in the time domain, where the CF is given by the square root of the PAPR.
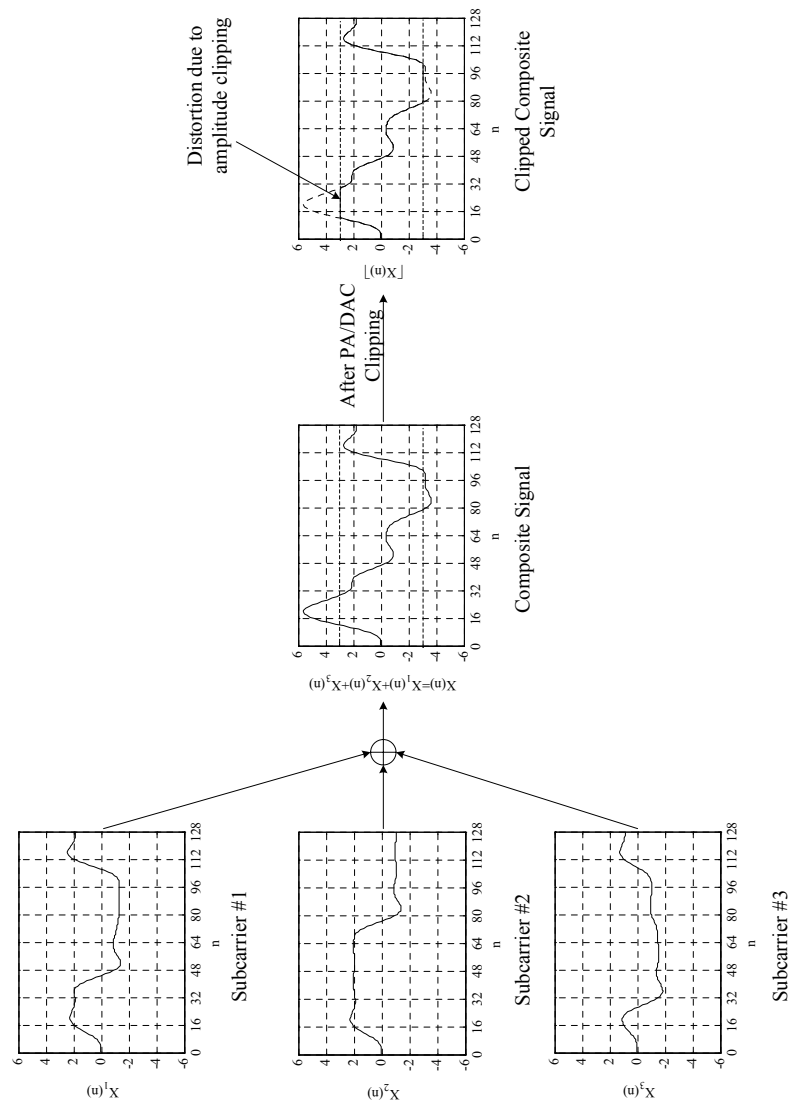
Figure 4.1. An example illustrating effects of clipping.

60

the mean power of the signal is 0.0625. As a result, the PAPR of the signal is 16. Considering a random BPSK-modulated input sequence (e.g. -1-1 1-1 1 1 1-1 1 1 1-1-1-1-1 1), the normalized instantaneous power of the OFDM signal in time-domain is shown in Figure 4.2(b). In this figure, the peak power of the signal is 0.156 and the mean power of the signal is 0.0625. As a result, the PAPR of the signal is 2.496. These figures illustrate that the power envelope variations depend on the input sequence mapped to the subcarriers, even though the total power of the signal remains constant. Moreover, it is clear from the figures that large values of PAPR requires large dynamic ranges of the transceiver components to avoid any amplitude clipping of the signal.

4.3.1 Baseband PAPR

For analyzing the PAPR and developing PAPR reduction techniques, a quantitative definition of the PAPR is important. The definition for the continuous-time and discrete-time baseband PAPR is presented in the rest of this subsection. Note that the D/A converters need to be designed for mitigating the clipping of baseband signals.

Continuous-Time PAPR – The complex envelope of a baseband OFDM signal, consisting of all N contiguous subcarriers over a time interval $[0, T]$, is given by:

$$s(t) = \frac{1}{N} \sum_{k=0}^{N-1} X_k e^{j2\pi kt/T} \tag{4.1}$$

where X_k is the symbol of the kth subcarrier[2], T is the OFDM symbol duration, and $j = \sqrt{-1}$.

---

[2]For example, $X_k \in \{1, -1\}$ for BPSK signaling and $X_k \in \{\pm 1, \pm j\}$ for QPSK signaling.
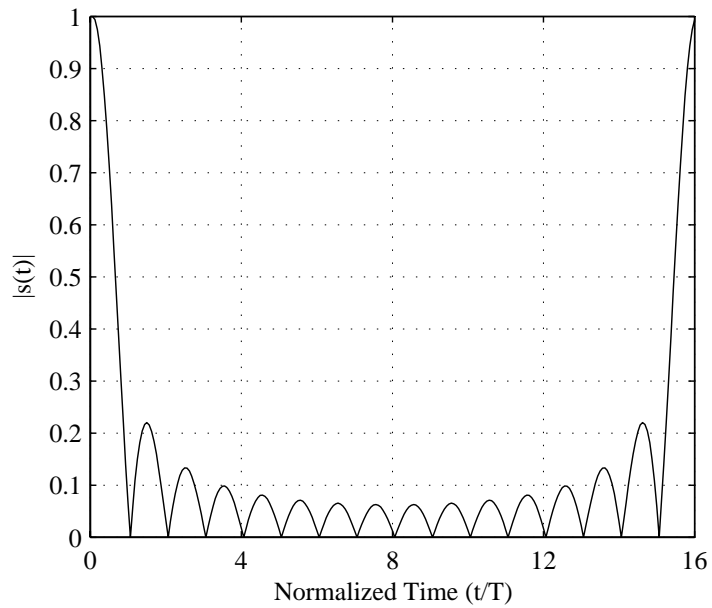
(a) All ones input sequence (e.g. 1 1 1 1 1 1 1 1 1 1 1 1 1 1 1 1).
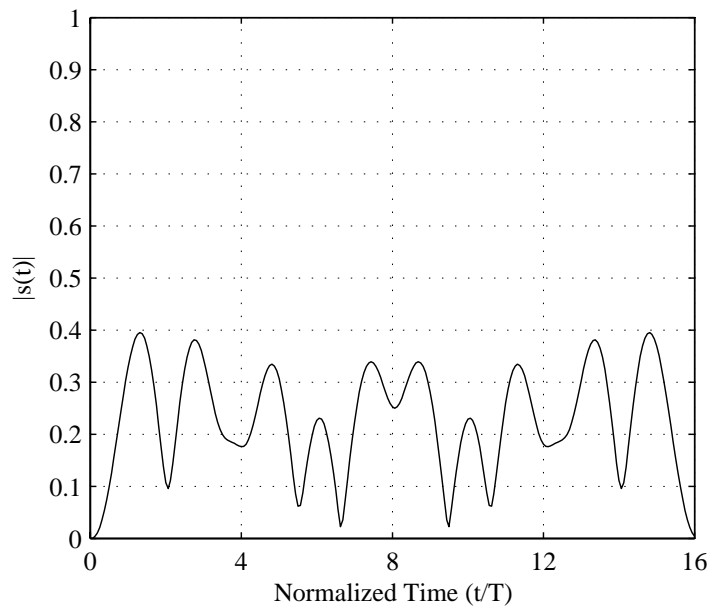
(b) Random input sequence (e.g. -1-1 1-1 1 1 1-1 1 1 1-1-1-1-1 1).

Figure 4.2. Normalized instantaneous power for a 16-subcarrier BPSK-OFDM signal

The PAPR of Eq. (4.1) is defined as the ratio between the maximum instantaneous power and the average power[3], namely:

$$\text{PAPR}(s(t)) = \frac{\max\limits_{0 \leq t \leq T} |s(t)|^2}{E\{|s(t)|^2\}} \tag{4.2}$$

where $E\{.\}$ denotes the expectation operator. Computation of the PAPR for an OFDM signal plays a major role in peak reduction methods. However, computing the continuous-time PAPR is nontrivial. Therefore, the continuous-time PAPR is usually approximated using the discrete-time PAPR, which is obtained from the samples of the OFDM signal.

Discrete Time PAPR − The discrete version of Eq. (4.1), where X_k is the kth modulated data symbol and L is the oversampling factor, is given by:

$$s(n) = \frac{1}{N} \sum_{k=0}^{N-1} A_k e^{j2\pi kn/LN} \quad \text{for } n = 0 \ldots LN - 1. \tag{4.3}$$

The PAPR of the signal is defined as:

$$\text{PAPR}(s(n)) = \frac{\max\limits_{0 \leq n \leq LN-1} \{|s(n)|^2\}}{E\{|s(n)|^2\}} \tag{4.4}$$

where $E\{.\}$ denotes the expectation operator.

Oversampling of an OFDM signal is needed to capture the signal peaks and correctly estimate the PAPR values of the signal. It has been shown that an oversampling factor of four is sufficient to estimate the continuous-time PAPR of a BPSK-OFDM system [88, 89]. In this chapter, PAPR will refer to the discrete-

---

[3]Without loss of generality, we can safely neglect the cyclic extension from the analysis since it does not contribute to the PAPR problem.

time baseband PAPR.

4.3.2 Passband PAPR

Since the power amplifiers operate in RF frequencies, they have to be designed around the PAPR of the passband signal. Therefore, it is desirable to mathematically describe the passband PAPR. Given a passband transmission, the complex baseband multi-carrier signal is modulated onto a carrier frequency, f_c. The real passband signal is shown to be equal to:

$$
\begin{aligned}
s_{PB}(t) &= \Re\{s(t)e^{j2\pi f_c t}\} \\
&= \Re\{s(t)\}\cos(2\pi f_c t) - \Im\{s(t)\}\sin(2\pi f_c t)\} \\
&= \{s_I(t)\}\cos(2\pi f_c t) - \{s_Q(t)\}\sin(2\pi f_c t)\}.
\end{aligned}
\tag{4.5}
$$

Since the carrier frequency is usually much higher than the signal bandwidth, i.e. $f_c \ll N/T$, the maximum of the modulated signal is approximately equal to the maximum of the baseband signal [70], i.e.:

$$
\max|s_{PB}(t)| \approx \max|s(t)|.
\tag{4.6}
$$

Moreover, the average power of the passband signal is given by:

$$
\begin{aligned}
E[|s_{PB}(t)|^2] &= E[|\Re\{s(t)e^{j2\pi f_c t}\}|^2] \\
&= E[|\{s_I(t)\}\cos(2\pi f_c t) - \{s_Q(t)\}\sin(2\pi f_c t)|^2] \\
&= \frac{1}{2}E[\{s_I(t)\}^2 + \{s_Q(t)\}^2] \\
&= \frac{1}{2}E[|s(t)|^2].
\end{aligned}
\tag{4.7}
$$

From Eqs. (4.2), (4.6), and (4.7), the passband PAPR is given by:

$$
\begin{aligned}
\text{PAPR}\{s_{PB}(t)\} &= \frac{\max |s_{PB}(t)|}{E[|s_{PB}(t)|^2]} \\
&\approx \frac{\max |s(t)|}{\frac{1}{2} E[|s(t)|^2]} \\
&\approx 2\,\text{PAPR}\{s(t)\}.
\end{aligned}
\tag{4.8}
$$

Therefore, the passband PAPR is approximately twice the baseband PAPR.

4.4 Motivation for PAPR Reduction

When the PAPR of a given OFDM signal is high, the D/A converters and power amplifiers should have a high dynamic range to avoid clipping of the given signal. Moreover, a high dynamic range implies increased complexity, reduced efficiency, and increased cost of the components, as will be discussed in the following subsections.

4.4.1 Dynamic Range of D/A Converters and Power Amplifiers

Clipping of the composite OFDM signal causes several undesirable outcomes, such as signal distortion and spectral regrowth. For instance, clipping causes in-band noise that results in a degradation of the BER performance [71]. Moreover, higher-order harmonics that spill over into out-of-band spectrum can also result from signal clipping. Although filtering after the high power amplifier (HPA) can be employed to remove this spectral leakage, it is very power-inefficient, so it is an undesirable solution [85]. Therefore, the dynamic range of D/A converters should be large enough to accommodate the large peaks of signals or high PAPR values. A high-precision D/A converter supports high PAPR with a reasonable amount of

quantization noise, but might be very expensive for a given sampling rate of the system. On the other hand, a low-precision D/A converter would be cheaper, but the quantization noise will be significant, which reduces the signal SNR when the dynamic range of D/A converter is increased to support high PAPR. Otherwise, the D/A converter will saturate and clipping will occur [8,70]. The dynamic range of the power amplifiers should also be large enough to accommodate large PAPR values. Otherwise, the power amplifiers may saturate and clipping might occur. The component cost of the D/A converters and power amplifiers increase with the increase in the dynamic range.

It should be noted that the clipping of high signal peaks occurs rarely, resulting in a relatively low occurrence of clipping noise [90]. Thus, the effect of clipping at the transmitter on the error performance of the OFDM system subject to frequency selective fading is minimal [87].

4.4.2 Power Savings

A power amplifier with a high dynamic range exhibits poor power efficiency. In [91], it was claimed that PAPR reduction leads to a significant power savings, where the net power savings is directly proportional to the desired average output power and is highly dependent upon the clipping probability level.

Consider a Class A power amplifier (PA), which is mostly linear and has a maximum efficiency, η, of 50%. Assuming an ideal linear model for PA, where linear amplification is achieved up to the saturation point, we get:

$$\eta = \frac{0.5}{\text{PAPR}}. \tag{4.9}$$

To illustrate the power inefficiency of a PA when dealing with PAPR, let us look at the example considering an QPSK-modulated OFDM signal with 256 subcarriers. In order to guarantee that no more than 1 in 10,000 frames are clipped, we need to apply an input backoff (IBO) equivalent to the PAPR at the 10^{-4} probability level, i.e. PAPR = 12 dB ($\approx$15.85) (refer to Figure 4.3). At this point, the efficiency of the power amplifier becomes $\eta = 0.5/15.85 \approx 3.15\%$. If the PAPR of an OFDM signal is reduced by 3 dB ($\approx$7.94), i.e. PAPR=9 dB, then the efficincy of the power amplifier doubles to $\eta = 0.5/7.94 \approx 6.30\%$. Therefore, by reducing the PAPR value of an OFDM signal, efficiency of PA can be improved. This is a strong motivation for reducing the PAPR of an OFDM signal.

Therefore, we observe from this example that it is highly desirable to reduce the PAPR of an OFDM signal. As a result, several techniques have been proposed in literature in order to minimize the PAPR values, thus improving the efficiency and reducing the cost of the components.

4.5 Theoretical Bounds on PAPR

When analyzing the PAPR reduction requirements of an OFDM signal, it is desirable to know the theoretical upper bound and minimum achievable lower bound of the PAPR. Since M-ary PSK and M-ary QAM are commonly used in OFDM transceivers, the PAPR bounds for these modulation techniques will be derived in this section.

M-ary PSK-OFDM – In an M-ary PSK-modulated OFDM system, signal constellation has same amplitude level, thus the power across all the subcarriers is constant. Consider the OFDM signal in Eq. (4.1). Assume the input data

symbols are chosen from an M-ary PSK constellation so that the power across all the subcarriers is kept constant, $|X_k| = A$. Thus, the peak power of the OFDM signal is given by [70]:

$$\max_{0 \leq n \leq LN-1} |s(n)|^2 = \max_{0 \leq n \leq LN-1} \left| \frac{1}{N} \sum_{k=0}^{N-1} X_k e^{j2\pi kn/LN} \right|^2. \qquad (4.10)$$

Since the highest peak will occur when all the symbols across all the subcarriers are coherently added, the peak power of the OFDM signal is always less than or equal to the highest peak, i.e.:

$$\begin{aligned}
\max_{0 \leq n \leq LN-1} |s(n)|^2 &\leq \left(\frac{1}{N} \sum_{k=0}^{N-1} \max |X_k| \right)^2 \\
&= \left(\frac{AN}{N} \right)^2 \qquad\qquad (4.11) \\
&= A^2.
\end{aligned}$$

Given that Parseval's relationship for the DFT is defined by [92]:

$$\sum_{n=0}^{N-1} |s(n)|^2 = \frac{1}{N} \sum_{k=0}^{N-1} |X_k|^2, \qquad (4.12)$$

we divide both sides by N, such that we get the average power in the time domain:

$$\begin{aligned}
E\{|s(n)|^2\} &= \frac{1}{N}\{E|X_k|^2\} \\
&= A^2/N. \qquad\qquad (4.13)
\end{aligned}$$

Then, the PAPR of the OFDM signal is obtained from Eqs. (4.2), (4.11), and

(4.13) as follows:

$$\begin{aligned}
\text{PAPR}(s(n)) &= \frac{\max_{0 \leq n \leq LN-1} |s(n)|^2}{E\{|s(n)|^2\}} \\
&\leq \frac{A^2}{A^2/N} \\
&\leq N.
\end{aligned} \tag{4.14}$$

Therefore, the PAPR of an M-ary PSK-OFDM signal is always less than or equal to N, where N is the total number of subcarriers [70].

M-ary QAM-OFDM – Given that a square M-ary QAM-modulated OFDM signal constellation has varying signal power levels over different constellation points, worst-case PAPR level would depend upon the choice of the signal points over different subcarriers. The square MQAM signal constellation points are given by $(\pm mA, \pm mA)$, where $m = 1, 3, \ldots, \sqrt{M} - 1$. Assuming that the signal points are equally probable in square M-ary QAM signal constellation, the average transmitted signal power is given by [62]:

$$\begin{aligned}
\sigma_s^2 &= \frac{A^2}{M} \sum_{m=1}^{M} (a_{mc}^2 + a_{ms}^2) \\
&= \frac{2A^2}{M} \sum_{m=1}^{M} (a_{mc}^2) \\
&= \frac{8A^2}{M} \sum_{m=1}^{M/4} (a_{mc}^2) \\
&= \frac{8A^2}{M} \sqrt{\frac{M}{4}} \sum_{m=1}^{\sqrt{M/4}} (2m-1)^2 \\
&= \frac{2A^2(M-1)}{3}.
\end{aligned} \tag{4.15}$$

where the coordinates of the m-th constellation point is (a_{mc}, a_{ms}). Note that: $\sum_{k=1}^{N}(2k-1)^2 = N(2N-1)(2N+1)/3$. Using Parseval's relationship in Eq. (4.12), the ensemble average power is:

$$E\{|s(n)|^2\} = \frac{2A^2(M-1)}{3N}.\tag{4.16}$$

As explained earlier, the worst-case PAPR occurs when all the symbols across all the subcarriers have the same phase. Since the lowest power in the signal constellation is $2A^2$, the worst-case minimal envelope power is:

$$\hat{P}_{\min} = 2A^2,\tag{4.17}$$

which is derived in a similar way as Eq. (4.11). Whereas the highest power in the signal constellation is $2(\sqrt{M}-1)^2 A^2$, the worst-case maximum envelope power is:

$$\hat{P}_{\max} = 2A^2(\sqrt{M}-1)^2,\tag{4.18}$$

which is derived in a similar way as Eq. (4.11). Then, from Eqs. (4.16), (4.17), and (4.18), the range of the worst-case PAPR is derived to be equal to:

$$
\begin{aligned}
\frac{\hat{P}_{\min}}{E\{|s(n)|^2\}} &\leq \mathrm{PAPR}_{\max}(s(n)) \leq \frac{\hat{P}_{\max}}{E\{|s(n)|^2\}} \\
\frac{3N}{M-1} &\leq \mathrm{PAPR}_{\max}(s(n)) \leq \frac{3N(\sqrt{M}-1)^2}{M-1}.
\end{aligned}
\tag{4.19}
$$

Therefore, the worst-case PAPR for M-ary QAM modulated OFDM signal with N subcarriers is proportional to N.

In spite of the fact that the theoretical upper bound of the PAPR in OFDM

signals is proportional to the number of subcarriers, the statistical distribution of the PAPR for an OFDM symbol is not so sensitive to the increase in the number of subcarriers, as shown in Figure 4.3. When an OFDM signal consists of a large number of a particular signal constellation point, a high PAPR value occurs [93]. Assuming equiprobable signal constellation points and a large number of subcarriers, the probability that an OFDM signal consists of a large number of a particular signal constellation point would be small. Therefore, the probability of the theoretically highest PAPR occurrence is small. For instance, there are at most M^2 patterns that yield the highest PAPR for M-ary PSK-OFDM. Thus, the probability of observing such a PAPR is equal to $M^2/M^N = M^{2-N}$ [90]. Moreover, the complementary cumulative distribution function (CCDF) of the PAPR for a large number of subcarriers is less sensitive to the modulation schemes, as shown in Figure 4.4.

Lower Bound − Since the peak power of an OFDM signal cannot be smaller than its mean power, the theoretical minimum value for the PAPR would be unity. Several studies have shown that complex multitone signals with low PAPR close to unity do exist if N is sufficiently large [94]. However, there has been very little effort devoted to finding such signals. The lower bound on the achievable PAPR for $N > 1$ is given by [94]:

$$\text{PAPR}_{\text{min}} = 1 + \frac{2}{N}. \tag{4.20}$$

Several low correlation sequences, such as Newman phases [95], Schroeder phases [96], and Narahashi phases [97], describe the closed-form construction rule allowing the rapid generation of multitone signals with varying N and low PAPR.
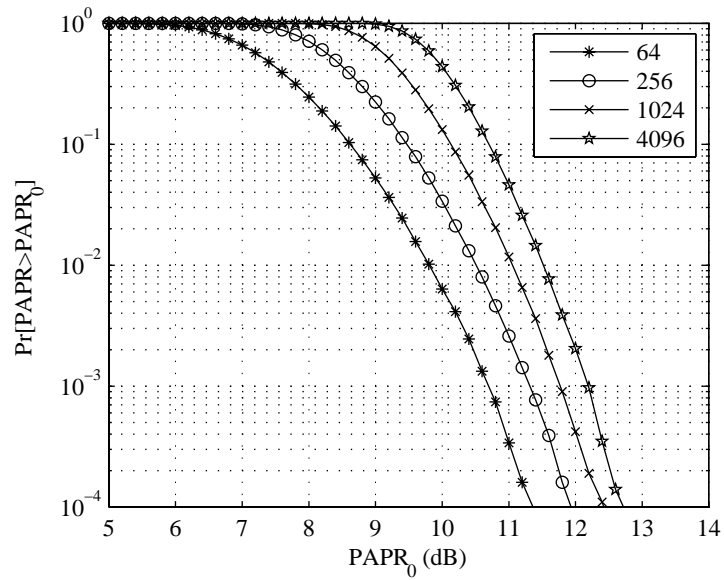
Figure 4.3. PAPR CCDF for a QPSK modulated OFDM system employing N subcarriers.
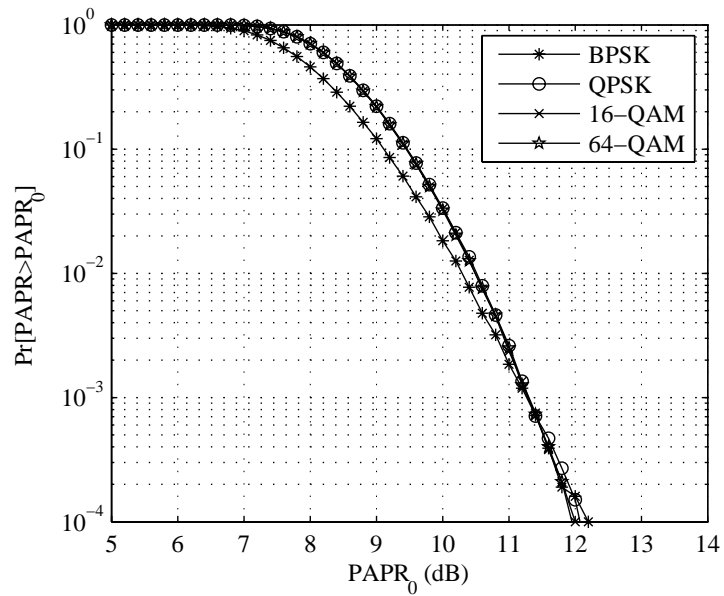
Figure 4.4. PAPR CCDF for a 256-subcarrier OFDM system employing various modulation schemes.

72

However, their PAPR values are not really close to the achievable optimal value. In [94], Friese has proposed several iterative algorithms for generating signals with the PAPR close to the theoretical minimum.

4.5.1 Statistical Properties

Consider the simple case where all the subsymbols are independently and identically distributed (i.i.d.). Then, by the central limit theorem [98], the real and imaginary parts of the N-point IFFT output have mutually independent Gaussian probability distribution function with zero mean and a standard deviation equal to σ i.e. $\mathcal{N}(0, \sigma^2)$. The instantaneous power of a baseband signal, $s(n)$, is defined by:

$$\lambda = \Re\{s(n)\}^2 + \Im\{s(n)\}^2. \tag{4.21}$$

We can characterize the instantaneous power as a Chi-square distribution with two degrees of freedom [98]:

$$f(\lambda) = \frac{1}{\sigma^2} \exp\left(-\frac{\lambda}{\sigma^2}\right), \quad \lambda \geq 0. \tag{4.22}$$

As a result, the cumulative distribution function (CDF) of the PAPR is defined as:

$$
\begin{aligned}
Pr[\lambda < \lambda_0] &= \int_0^{\lambda_0} f(\lambda)d\lambda \\
&= 1 - e^{-\frac{\lambda_0}{\sigma^2}}.
\end{aligned}
\tag{4.23}
$$

Table 4.1. Theoretical approximations to CCDF of PAPR values.

CCDF	Remarks	Reference
$Pr[\lambda > \lambda_0] \approx 1 - \left(1 - e^{-\frac{\lambda_0}{\sigma^2}}\right)^{\alpha N}$	$\alpha = 2.8$ and $N \geq 64$	[99]
$Pr[\lambda > \lambda_0] \approx 1 - \exp\left(-\sqrt{\frac{\pi \lambda_0}{3}} N e^{-\lambda_0}\right)$		[90]
$Pr[\lambda > \lambda_0] \approx 1 - \exp\left(-\sqrt{\frac{\pi \log N}{3}} N e^{-\lambda_0}\right)$		[100]
$Pr[\lambda > \lambda_0] \approx 1 - \exp\left(-\frac{2N}{\sqrt{3}} e^{-\lambda_0/2}\right)$	N and λ_0 are large	[101]

If $E[|s(n)|^2]$ is normalized to unity, then the CCDF of the PAPR is given by:

$$Pr[\lambda > \lambda_0] = 1 - \left(1 - e^{-\frac{\lambda_0}{\sigma^2}}\right)^{N}. \tag{4.24}$$

However, this approximation is not close to the experimental results since the assumption made in deriving CCDF that the samples should be mutually uncorrelated is no longer valid when oversampling is employed [99].

There have been several attempts to determine the closed-form approximations for the distribution of PAPR. Some of the approximations are shown in Table 4.1. While deriving an approximation to the CCDF of the PAPR in [99], OFDM samples are assumed to be Gaussian-distributed and mutually uncorrelated. However, when oversampling is employed, OFDM samples are correlated. To counter this effect, the authors empirically determined a parameter $\alpha = 2.8$. This approximation has shown to be quite accurate when the number of subcarriers N is greater than 64. In [90], the baseband OFDM signal is assumed to be a bandlimited, complex Gaussian process that has statistically uncorrelated signal peaks. In [100], it has been shown that an OFDM signal converges weakly to a Gaussian random process as the number of subcarriers in the system approaches infinity and the approximate CCDF of PAPR is derived. Assuming that

the multi-carrier signal converges weakly to a Gaussian random process, a perfect approximation of the PAPR is derived in [101] for large values of N and PAPR value λ_0. These approximations are valid for circularly-modulated OFDM signals, such as M-ary PSK and square M-ary QAM techniques, since the OFDM symbols converge to a complex Gaussian sequence asymptotically. In [102], it was claimed that non-circularly modulated OFDM symbols, such as BPSK, and 8-QAM, do not converge to a complex Gaussian sequence asymptotically, and the correlation among OFDM symbol powers does not diminish as the number of subcarriers goes to infinity. They concluded that the PAPR cumulative distribution function for non-circular constellation is given by:

$$
Pr[\lambda < \lambda_0] = 1 - \left(1 - 2\exp(-\lambda_0) + \exp\left(-\frac{2}{1+\mu_2^2}\lambda_0\right)\right)^{\frac{N-2}{2}} \cdot
$$
$$
\left\{\int_0^{\sqrt{\lambda_0}} \frac{2}{\sqrt{2\pi}\sigma_r} \exp\left(-\frac{u^2}{2\sigma_r^2}\right) \cdot \left(1 - \mathrm{erfc}\left(\sqrt{\frac{x-u^2}{2\sigma_i^2}}\right)\right) du\right\}^2
$$

$$(4.25)$$

where, μ_2 represents mean power of the symbol constellation, and $\sigma_r^2 = (1+\mu_2)/2$ and $\sigma_i^2 = (1-\mu_2)/2$.

For BPSK, $\mu_2 = 1$, $\sigma_r^2 = 1$, and $\sigma_i^2 = 0$, the PAPR cumulative distribution function is determined to be equal to:

$$
Pr[\lambda < \lambda_0] = 1 - \left(1 - \mathrm{erfc}\left(\sqrt{\lambda_0/2}\right)\right)^2 \left(1 - e^{-\lambda_0}\right)^{\frac{N-2}{2}}. \qquad (4.26)
$$

These approximations were shown to be fairly close to the experimental results, which represent the upper bounds for PAPR values.

4.6 PAPR Reduction Techniques

It is possible for OFDM transceivers to reduce the amount of PAPR in order to keep the cost of the hardware components and power consumption manageable. PAPR reduction techniques can be broadly categorized into *deterministic* and *probabilistic* approaches, as shown in Figure 4.5. Deterministic approaches guarantee that the PAPR of an OFDM signal does not exceed a predefined threshold, whereas the probabilistic approaches minimize the probability that the PAPR of an OFDM signal exceeds a predefined threshold. These categories will be discussed in the following sections.

4.6.1 Deterministic Approach

Deterministic PAPR reduction approaches can be classified into techniques that perform either *time-domain based clipping* or *frequency-domain based coding*.

The simplest approach for PAPR reduction is to deliberately clip the amplitude of the signal to a predefined value before amplification [71]. However, the technique suffers from various drawbacks, such as signal distortion and spectral regrowth. Therefore, clipping alone is not a suitable option for PAPR reduction. Modified clipping techniques exist, which fall under the probabilistic approach explained in the next section.

Coding techniques are applied to OFDM signals in order to map symbols to codes with smaller PAPR values [74]. Each symbol has a choice of two or more codes, where the code yielding the lowest PAPR is selected. However, this technique works well only when the number of subcarriers is small. With the increased number of subcarriers, the search space for finding codes with minimum
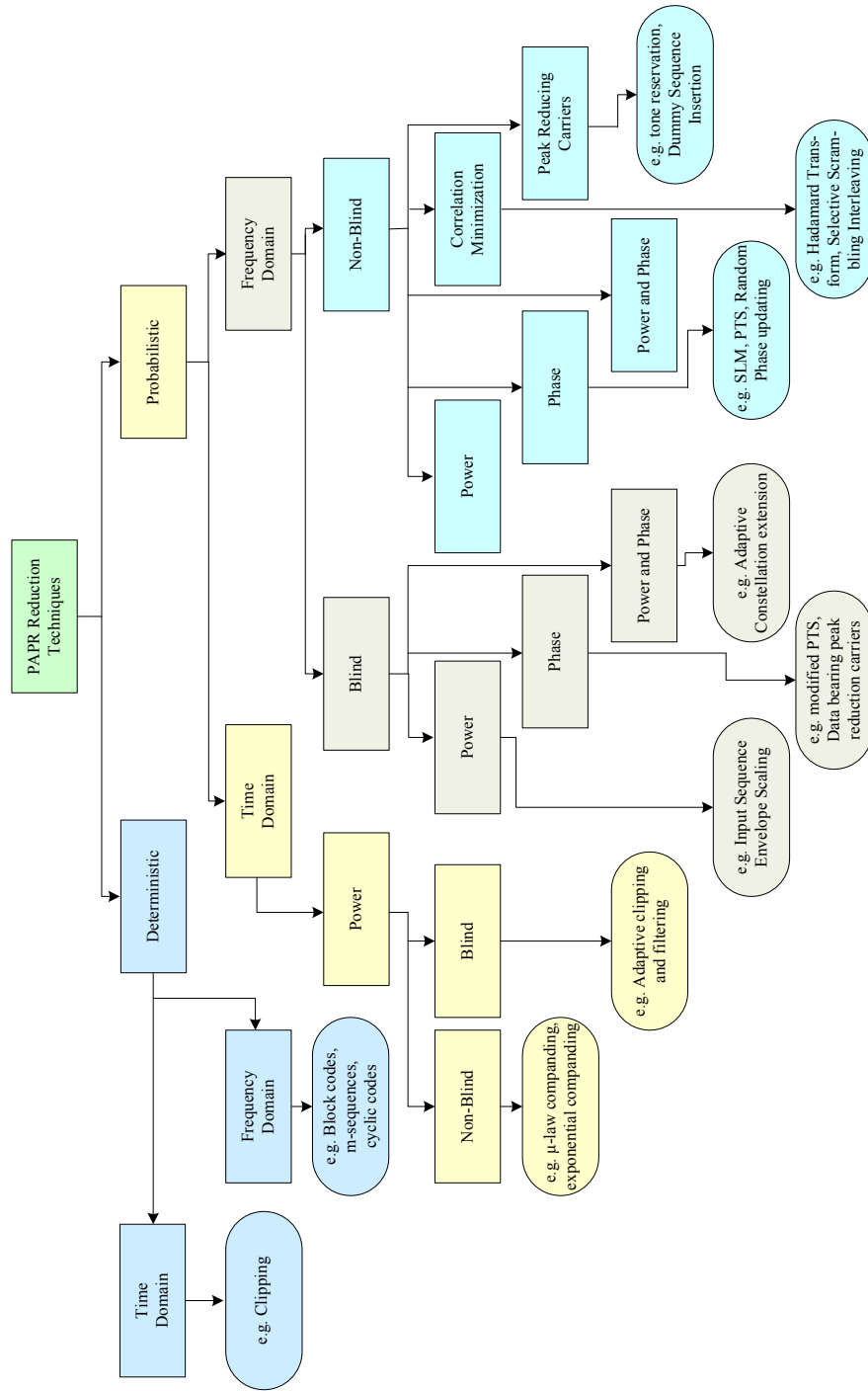
Figure 4.5. Taxonomy of PAPR Reduction techniques.

PAPR increases exponentially and large lookup tables are needed for encoding and decoding.

4.6.2 Probabilistic Approach

Probabilistic approaches attempt to minimize the number of occurrences of OFDM symbols with PAPR values exceeding a predefined threshold, while simultaneously minimizing the signal distortion and spectral growth. Probabilistic approaches can be classified according to whether *time domain processing* or *frequency domain processing* is involved.

4.6.2.1 Time Domain-Based Processing

Time domain-based processing approaches focus on manipulating the power of the signal in the time domain. This approach can be further classified into *blind* and *non-blind* techniques. Blind techniques imply that the receiver is oblivious to the changes made at the transmitter side, whereas non-blind techniques imply that the receiver requires *a priori* knowledge about the modifications made at the transmitter side for correctly demodulating the received signals. Thus, non-blind techniques require additional side information in order to operate, whereas blind techniques might degrade the error performance of the system since the receiver is transparent to the changes made at the transmitter side.

The simplest blind technique for PAPR reduction is to clip the amplitude of the signal to a predefined value and filter the signal to suppress the out-of-band interference [72,73,103,104]. The clipping process might result in spectral regrowth, whereas filtering the signal might result in some peak regrowth. Therefore, clipping may not be an effective technique when reducing the PAPR of the OFDM

signals as long as the transmitted OFDM signal is strictly band-limited. Even though numerous algorithms based on amplitude clipping and filtering have been proposed in the literature, it has been shown that clipping does not improve the reduction of total degradation [105]. Instead, an unclipped system outperforms a clipped system because of the inter-carrier interference (ICI) caused by clipping, and offsets the gain of the PAPR reduction [105]. Another technique called peak windowing can also reduce the PAPR, where large signal peaks are multiplied with a certain narrowband window such as Gaussian, Cosine, Kaiser, and Hamming windows [99].

Among the non-blind techniques, several companding[4] techniques for compressing the large peaks of an OFDM signal in time domain, including μ-law companding [107], and exponential companding [108], have been proposed in literature. By compressing the large peaks of an OFDM signal by companding, the dynamic range of the D/A converters are reduced. However, the receiver needs to expand the compressed signal for correct demodulation.

4.6.2.2 Frequency Domain-Based Processing

Frequency domain-based processing approaches focus on minimizing the correlation of the input signals since it is known that the PAPR of an OFDM signal is high when the input sequences are highly correlated. It has been shown that by altering the phase and/or power of the input sequence, it is possible to lower the correlation of the input sequence, thereby reducing the PAPR of an OFDM signal. However, some approaches also try to directly manipulate the correlation of

---

[4]A companding technique is a method for performing nonuniform quantization where the samples are first passed through a nonlinear element that compressess the large amplitudes to reduce the dynamic range of the signal and at the receiving end, the inverse (expansion) of this nonlinear operation is applied to obtain the sampled value [106].

the input signals. Frequency domain-based processing approaches can be further classified into blind and non-blind techniques.

In blind phase adjustment-based techniques, the phase of the subcarriers are adjusted in order to reduce the coherence between the different subcarriers such that the PAPR value of the OFDM signal is reduced. The phase adjustments should be kept relatively small so as to minimize bit-error-rate (BER) performance degradation. For example, *signal set expansion* technique maps original signal set into an expanded signal set with two or more points, such as binary phase shift keying (BPSK) into quadrature phase shift keying (QPSK), which provides more freedom for phase selection and yields lower PAPR values for the OFDM signal [109].

Blind power-based techniques alter the power level of the subcarriers such that the PAPR of an OFDM signal is reduced. These techniques are suitable only for the MPSK-based OFDM system since the receiver is unaware of the information about the transmit power levels. For example, the *input sequence envelope scaling* technique adjusts the power of the subcarriers so that the power of the individual subcarriers become unequal yielding a minimized PAPR value [82]. Since the phase information of the original signal is unchanged, the receiver can decode the received signal without any side information.

In blind power and phase-based techniques, both the phase and the power of the subcarriers are altered such that the PAPR of an OFDM signal is reduced. If the total transmit power needs to be kept constant, these techniques are suitable only for low order modulation techniques since the error robustness of the higher modulation techniques degrades rapidly with the blind phase and power alterations at the transmitter. When the order of the modulation techniques in-

creases, the complexity (and limitations) of the algorithm increases as well as transmit power level increases. For example, the *active constellation extension* (ACE) [84,110] and *dynamic constellation shaping* [86] techniques allow to change the power and phase of some data symbols without affecting the error probability of the other data symbols. Non-blind power-based techniques, as well as power and phase-based techniques, would be suitable for the higher modulation schemes such as MQAM.

Non-blind phase adjustment-based techniques update phases of the input sequence such that the PAPR of an OFDM signal is reduced. The information about the phase updates is transmitted to the receiver for correct demodulation. Several modified algorithms are proposed in literature, which avoid the requirement of explicit side information. For example, *selective mapping* (SLM) [79], *partial transmit sequences* (PTS) [80], *random phase updating* [81] techniques add random phase factors to each subcarriers in order to reduce PAPR with the information about the phase factors transmitted to the receiver.

The blind techniques reduce the PAPR values at the cost of slight increase in the bit error rate of the system or increased transmit power level since the adjustments would result into increased noise level at the receiver, whereas the non-blind techniques reduce the PAPR values at the cost of a reduced information rate since the information about the adjustments made at the transmitter need to be transmitted to the receiver for the correct demodulation.

Low autocorrelation coefficients of a signal is a sufficient condition for low PAPR. However this is not a necessary condition [68]. Non-blind autocorrelation minimization techniques attempt to minimize the autocorrelation of the input sequence and the information about the changes is transmitted to the receiver

for correct demodulation. For example, the *selective scrambling* [111] and *interleaving* [112] techniques attempt to break the long correlation patterns of the input sequences to reduce the PAPR. However, the techniques perform well only when the OFDM signal has moderate PAPR values since interleaving alone is not effective to break the correlation pattern when the input sequence are highly correlated.

Attempts have been made to develop OFDM signals with a constant envelope to yield unity PAPR values [113]. The constant envelope waveforms have a constant instantaneous power. *Continuous phase modulation* (CPM) is a class of signaling that has very low sidelobe power while maintaining the constant envelope property. However, CPM increases the complexity of the receiver and has a poor performance over frequency selective channels.

4.7 Criteria for Selecting PAPR Reduction Techniques

In selecting the appropriate PAPR reduction technique from the literature, the following criteria can be used in determining the trade-offs between PAPR reduction ability and other design factors [114]:

1. *High PAPR reduction capability*: The PAPR reduction technique should have high PAPR reduction capability, with as few undesirable side effects as possible.

2. *Low computational complexity*: The PAPR reduction technique should be computationally efficient. Both time and hardware requirements for the PAPR reduction should be minimal. Generally, complex techniques exhibit better PAPR reduction as possible.

3. *No loss in throughput*: The loss in throughput due to side information should be avoided or at least be kept minimal. Usually, there exists a tradeoff between the loss in throughput and distortion of the signal. Non-blind techniques suffers from reduced throughput without distorting the signal, whereas blind techniques suffer from distorted signal without reducing throughput. Signal distortion eventually results in degraded BER performance.

4. *No BER performance degradation*: The blind techniques suffer from BER performance degradation, when the transmit power is held constant. Moreover, in the non-blind techniques, error in the side information might result in a whole erroneous data frame. However, attempts should be made to keep BER performance degradation to a minimum.

5. *No spectral spillage*: Spectral spillage is very important aspect of the PAPR reduction technique since it must be avoided. For this reason, clipping techniques are not preferred, even if they exhibit significant PAPR reduction.

6. *No power increase in transmit signal*: For wireless communications, power of the transmit signal should be kept constant. So the techniques such as ACE might not be suitable for wireless communications.

7. *High efficiency and cost savings*: The efficiency of the PAPR reduction technique and the cost savings offered by it in terms of additional hardware requirements and saving in the cost of D/A converters and power amplifiers are also very important factors while choosing the PAPR reduction technique. The efficient PAPR need not be the lowest achievable PAPR.

Among several PAPR reduction algorithms proposed in the literature, it is not sufficient to achieve large reduction in PAPR values alone, it is equally important to ensure that other overall system requirements are not violated. However, it may not feasible to fulfill all the requirements of an ideal PAPR reduction algorithm for a given scenario and a balance between PAPR reduction and other factors, such as overall cost, error performance, complexity, and efficiency, should be found.

PAPR reduction can be achieved by modifying OFDM signal characteristics in time or frequency domain at the transmitter. If information about these changes is transmitted to the receiver, it can reverse the operation, and demodulate the data correctly. Otherwise, these modifications in OFDM characteristics would appear as signal distortion and result in degraded error performance for the overall communication system. Therefore, there always exists a tradeoff between error performance degradation and throughput loss, complexity increase, or information overhead. Depending upon error robustness for a given system, blind or non-blind technique can be chosen for PAPR reduction. For example, if a system has high tolerance to error performance, such as voice communications, blind techniques are preferable, whereas for a system with low tolerance to error performance, non-blind techniques would be suitable.

Another important factor to be considered for choosing an appropriate algorithm is PAPR reduction requirements. In case of non-blind technique, higher PAPR reduction requirements may lead to a system with high computational complexity or large information overhead, whereas in case of blind techniques, it may lead to a large error performance degradation due to significant changes in OFDM signal characteristics for minimizing PAPR. Moreover, in non-blind techniques, error on overhead information can significantly degrade error performance

84

of the overall system.

With PAPR reduction, it is possible to reduce dynamic ranges for PAs and D/A converters, which would result in cost savings on these components. However, it is also important to consider additional cost of the components needed for PAPR reduction, such as companders, filters, or components for the overhead information management. Therefore, there also exists a tradeoff between cost of the additional RF components versus cost savings in PAs and D/A converters by reducing their dynamic ranges.

To make a fair comparison among PAPR reduction techniques, average transmit power should not be increased. Moreover, a practical transmit power constraint needs to be enforced for fulfilling the regulatory requirements. Therefore, depending upon the requirements, certain techniques may not be applicable, which would otherwise be useful for wireline communication, such as DSL.

Another important factor is the increase in the power of out-of-band (OOB) interference, which also needs to be considered before deciding upon the PAPR reduction algorithm. In several scenarios, including NC-OFDM system, spectral spillage can be a serious problem, since the bandwidth under consideration might be non-contiguous. In such cases, techniques yielding higher level of OOB interference, such as time-domain based techniques, may not be used.

4.7.1 Definition of Efficient PAPR in OFDM

PAPR reduction techniques minimize the PAPR at the cost of BER performance degradation or reduction in the system throughput. Assuming that the net data rate must be constant, a decrease in the number of information-carrying subcarriers means less power is devoted to the information bits yielding an increase

in the BER. It has been shown that there exists a PAPR for which the BER of the information bits reaches the minimum value. An efficient PAPR is the PAPR level for which the BER reaches a minimal value, which need not necessarily be the lowest possible value of PAPR [115].

4.7.2 Achievable Information Rate with Peak-Power-Limited OFDM

Absolute rate loss R in bits per subcarrier due to PAPR reduction requirements is given by [116]:

$$R \approx -\log_2\left(1 - e^{-\alpha\lambda_0}\right) \tag{4.27}$$

where λ_0 is the target PAPR and $\alpha = P_{av,subset}/P_{av}$, P_{av} is the average power of the signal, and $P_{av,subset}$ is the average power of a subset of the signals yielding PAPR smaller than λ_0.

The achievable channel capacity of the OFDM signals clipped by an envelope limiter is considerably limited, even for high channel SNR. However, if a powerful channel coding technique is applied to the system with a constellation of relatively low order, such as QPSK, the SNR degradation may be small. In such a system, clipping may not be a major source of performance degradation [117].

4.7.3 Fitness function-based approach for determining an appropriate algorithm

In order to determine an appropriate PAPR reduction algorithm for a given system, it is desirable to consider all above-listed requirements. The number and nature of these requirements may vary depending upon the system (or user) under consideration. For a given scenario and requirements, we propose to use the fitness value or appropriateness value of the algorithm, which is defined as the weighted

sum of the relative changes in the above-listed factors. The appropriateness value provides a single metric for determining the appropriateness of a PAPR reduction algorithm.

Suppose X_1 be the relative degradation in BER performance at certain SNR level, for given channel conditions, AWGN or multipath, given by:

$$X_1 = -10 \log_{10}(\text{BER}_{\text{after}}/\text{BER}_{\text{before}}) \tag{4.28}$$

Let X_2 be the relative increase in system complexity given by:

$$X_2 = -10 \log_{10}(\text{Complexity}_{\text{after}}/\text{Complexity}_{\text{before}}) \tag{4.29}$$

Let X_3 be the relative PAPR reduction given by:

$$X_3 = -10 \log_{10}(\text{PAPR}_{\text{after}}/\text{PAPR}_{\text{before}}) \tag{4.30}$$

Let X_4 be the relative cost savings given by:

$$X_4 = -10 \log_{10}(\text{Cost}_{\text{after}}/\text{Cost}_{\text{before}}) \tag{4.31}$$

Let X_5 be the relative increase in transmit power given by:

$$X_5 = -10 \log_{10}(\text{Transmit Power}_{\text{after}}/\text{Transmit Power}_{\text{before}}) \tag{4.32}$$

Let X_6 be the relative increase in spectral spillage given by:

$$X_6 = -10 \log_{10}(\text{OOB}_{\text{after}}/\text{OOB}_{\text{before}}) \tag{4.33}$$

Let X_7 be the relative reduction in goodput[5] given by:

$$X_7 = -10 \log_{10}(\text{Goodput}_{\text{after}}/\text{Goodput}_{\text{before}}) \tag{4.34}$$

The aggregate fitness value of the PAPR reduction algorithm can be computed as the weighted sum of these factors, where the weights correspond to their relative importance levels. These weights can be determined as per the system or user requirements. Therefore, the fitness value of the algorithm is given by:

$$\Gamma = \sum_{k=1}^{7} \alpha_k \cdot X_k \tag{4.35}$$

where,

$$\sum_{k=1}^{7} \alpha_k = 1 \tag{4.36}$$

Based on these fitness values, an appropriate algorithm can be chosen in order to achieve large reduction in PAPR values as well as satisfy other system requirements.

4.8 Chapter Summary

Multi-carrier transmission techniques, such as OFDM, is a very attractive technique for communications over frequency selective channels. One serious problem with multi-carrier systems is that the composite transmit signal can exhibit a very high PAPR value when the input sequences are highly correlated. In this chapter, we presented the definition of baseband and passband PAPR, motivation

---

[5]We define *goodput* as the total information bits per unit of time transmitted to the receiver minus overhead information bits per unit of time.

for PAPR reduction, as well as theoretical bounds on PAPR for both M-ary PSK and M-ary QAM modulated OFDM signals, and its statistical characteristics. It is possible to reduce the PAPR of an OFDM signal by modifying the transmit signal characteristics in time or frequency domain. Moreover, this chapter presented a survey and taxonomy of PAPR reduction algorithms proposed in the literature and outlined the criteria for selecting PAPR reduction algorithm for different scenarios.

Chapter 5

PAPR Reduction Techniques

5.1 Introduction

To reduce PAPR in OFDM transceivers, there are several solutions proposed in the literature that could be employed by the system. These solutions include the use of error control coding [74–78] and constellation shaping techniques [79–81]. With respect to the latter, one constellation parameter that could be adjusted on a per-subcarrier basis is the subcarrier phase information. However, most of these algorithms possess a high computational complexity, especially for a large number of subcarriers. Moreover, several non-iterative phasing algorithms, based on Newman phases [118], Schroeder phases [96], or Narahashi and Nojima phases [97], compute phase adjustments independent of the input data sequence. As a result, PAPR reduction is not guaranteed in all cases. Furthermore, since the resulting phase adjustments can be any value within $[0, 2\pi)$, the overhead of communicating this information to the receiver would be substantial[1].

Data randomization, such as interleaving, can be employed to disrupt the

---

[1] This is also true of partial transmit sequence [80] and selective mapping [79] techniques, which also use phase adjustments for reducing PAPR.

long correlation patterns of a frame, hence reducing the PAPR of an OFDM signal [112]. However, interleaving is effective only when the data frames have moderate PAPR values. It was proposed that interleaving can be combined with selective mapping (SLM) techniques or partial transmit sequences (PTS) techniques for achieving greater reduction in PAPR [112]. However, combining interleaving with these techniques will substantially increase their computational complexity.

In this chapter, we present five novel PAPR reduction algorithms for OFDM systems. The chapter is organized as follows: In Section 5.2, we present a novel subcarrier phase adjusting PAPR reduction algorithm. In Section 5.3, we present a novel adaptive mode PAPR reduction algorithm. In Section 5.4, a novel subcarrier power adjustment algorithm is presented. A novel variable data throughput approach for PAPR reduction is presented in Section 5.5. In Section 5.6, we present a technique of using low correlation phase sequences for PAPR reduction. Section 5.7 presents the PAPR analysis for NC-OFDM signals.

5.2 Subcarrier Phase Adjusting PAPR Reduction Algorithm

In this section, we propose a novel linear search algorithm for computing subcarrier phase adjustments that leads to the coherent cancellation of subcarriers, thus reducing the PAPR with low computational complexity. Moreover, the computed phase adjustments consist of a discrete set of values in $[0, 2\pi)$, resulting in lower transmission overhead.
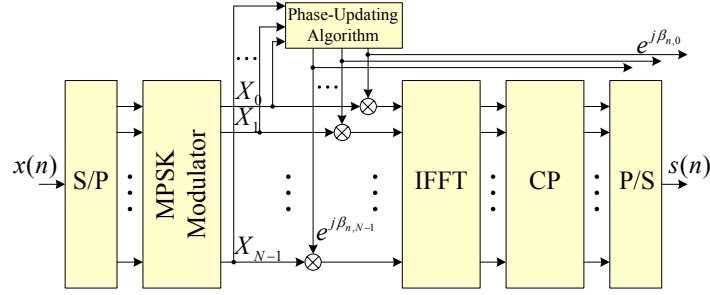
(a) Transmitter with phase updating algorithm.
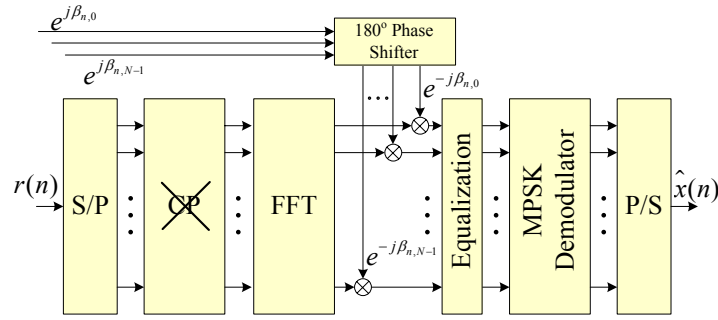
(b) Receiver with phase updating information.

Figure 5.1. Schematic of an OFDM transceiver employing PAPR reduction via phase updating.

5.2.1 OFDM Transceiver

A general schematic of an OFDM transceiver employing the proposed phase adjustment algorithm for PAPR reduction is shown in Figure 5.1. For the basic principle of OFDM, please refer to Section 2.3. As shown in Figure 5.1, the proposed phase-updating algorithm computes the phase adjustments for the input data sequence to reduce the PAPR of an OFDM signal. The information about the phase adjustments need to be transmitted to the receiver for the correct demodulation of the received sequence.

Figure 5.2.   Phase adjustment algorithm for PAPR reduction.

5.2.2 Proposed Subcarrier Phase Adjustment Algorithm

Our main objective is to minimize the PAPR. Knowing that the PAPR is large when the subcarriers sum together coherently, it is possible to reduce the PAPR by adjusting the phase of subcarrier k at time instant n by adding a phase offset $\beta_{n,k}$. Therefore, the proposed algorithm checks the level of the PAPR for an OFDM transmission. If the PAPR exceeds a maximum threshold, i.e., the maximum dynamic range of the PA and D/A converter, the algorithm then searches for the subcarrier phase adjustments that would reduce the PAPR. Once the phase adjustment is performed, the algorithm ends. The phase adjustment algorithm for the PAPR reduction is shown in Figure 5.2.

Therefore, the phase-adjusted version of Eq. (4.3) is

$$
\begin{aligned}
Y(n) &= \frac{1}{N} \sum_{k=0}^{N-1} e^{j\beta_{n,k}} e^{j\alpha_k} e^{j2\pi kn/N} \\
&= \frac{1}{N} \sum_{k=0}^{N-1} (\cos(\gamma_{n,k}) + j\sin(\gamma_{n,k})),
\end{aligned}
\tag{5.1}
$$

where

$$
\gamma_{n,k} = \alpha_k + \beta_{n,k} + n\theta_k
\tag{5.2}
$$

and $\theta_k = 2\pi k/N$.

Using trigonometric manipulation, the expression for the power of Eq. (5.1) can be derived as

$$
\begin{aligned}
|Y(n)|^2 &= \left| \frac{1}{N} \sum_{k=0}^{N-1} (\cos(\gamma_{n,k}) + j\sin(\gamma_{n,k})) \right|^2 \\
&= \frac{1}{N} + \frac{2}{N^2} \sum_{i=0}^{N-2} \sum_{j=i+1}^{N-1} \cos(\gamma_{n,i} - \gamma_{n,j}).
\end{aligned}
\tag{5.3}
$$

Referring to Eq. (4.4) for the definition of PAPR, the smallest value that can be obtained from this ratio is unity, i.e., $\mathrm{PAPR}(Y) = 1$, since the maximum value for the power can never be less than the average power level. Thus, given that the desired PAPR is equal to unity, and applying Eq. (4.4), we obtain the relationship

$$
\max\{|Y(n)|^2\} = E\{|Y(n)|^2\}.
\tag{5.4}
$$

Therefore, it is necessary to find a set of solutions for $\beta_{n,k}$, $k, n = 0, \ldots, N-1$, such that Eq. (5.4) is satisfied. Observing both sides of the expression closer, one solution which presents itself is when the sum of cosines are equal to zero. Therefore, the argument for each cosine becomes

$$
\pi m = (\gamma_{n,i} - \gamma_{n,j}), \ m \in \mathbb{Z},
\tag{5.5}
$$

which can be rearranged to yield

$$
\pi \left(m - \frac{2(i-j)n}{N} \right) = (\alpha_i + \beta_{n,i}) - (\alpha_j + \beta_{n,j}).
\tag{5.6}
$$

Since α_i and α_j are random variables that take on one of M possible phase values

in an M-ary PSK signal constellation, both $\beta_{n,i}$ and $\beta_{n,j}$ must be chosen in order to satisfy Eq. (5.6).

Thus, the objective function for PAPR minimization is

$$f(\gamma_{n,i} - \gamma_{n,j}) = \sum_{i=0}^{N-2} \sum_{j=i+1}^{N-1} \cos(\gamma_{n,i} - \gamma_{n,j}), \qquad (5.7)$$

which is achieved by choosing the appropriate values for $\beta_{n,i}$ and $\beta_{n,j}$.

From Eq. (5.7), the phase correction would vary across both the time and frequency domains, i.e., the values for α_i and α_j would be different for each OFDM symbol. Therefore, to minimize Eq. (5.7) would be very difficult to achieve theoretically since it would result in an extremely large optimization problem. To make our optimization problem tractable, we assume the phase correction depends only on frequency. We then choose $\bar{\gamma}_k$ instead of $\gamma_{n,k}$, and $\bar{\beta}_k$ instead of $\beta_{n,k}$, where $\bar{\gamma}_k = E\{\gamma_{n,k}\}$ and $\bar{\beta}_k = E\{\beta_{n,k}\}$. The resulting simplified objective function would be defined as

$$Q = f(\bar{\gamma}) = \sum_{i=0}^{N-2} \sum_{j=i+1}^{N-1} \cos(\bar{\gamma}_i - \bar{\gamma}_j) = 0, \ \forall n. \qquad (5.8)$$

Finding the roots of Eq. (5.8) is a nontrivial problem since the cosine function is periodic, yielding an infinite number of possible solutions. We present a linear search algorithm for finding the roots of Eq. (5.8) in the following subsection.

5.2.2.1 Linear Search Algorithm

Since the cosine terms assume both positive and negative values, we can choose the values of $\bar{\gamma}_i$ such that approximately half of them yield $\bar{\gamma}_i - \bar{\gamma}_j = \pi \ \forall i, j$ while

1: No of subcarriers: $N = 2^n$
2: Initialize: $\psi = N/2$
3: Define $\bar{\gamma}_i \ \forall i$:
   $\bar{\gamma}_i = \pi$ for $\forall i = 0 \ to \ \psi - 1$
   $\bar{\gamma}_i = 0$ for $\forall i = \psi \ to \ N - 1$
4: Compute Q_1: $Q_1 = f(\gamma)$
5: **while** $(Q_1 > 0)$ **do**
6:     Increment ψ: $\psi = \psi + 1$
7:     Redefine $\bar{\gamma}_i \ \forall i$:
   $\bar{\gamma}_i = \pi$ for $\forall i = 0 \ to \ \psi - 1$
   $\bar{\gamma}_i = 0$ for $\forall i = \psi \ to \ N - 1$
8: **end while**
9: Decrement ψ: $\psi = \psi - 1$
10: Redefine $\bar{\gamma}_i \ \forall i$:
   $\bar{\gamma}_i = \pi$ for $\forall i = 0 \ to \ \psi - 1$
   $\bar{\gamma}_i = 0$ for $\forall i = \psi \ to \ N - 1$
11: Compute Q_2: $Q_2 = f(\gamma)$
12: **if** $(Q_2 < 0)$ **then**
13:     $Q_1 = Q_2$
14:     Go to Step 9
15: **end if**
16: **if** $(|Q_1| < |Q_2|)$ **then**
17:     Increment ψ: $\psi = \psi + 1$
18: **end if**
19: **return** ψ

Figure 5.3. Linear search algorithm for determining $\bar{\gamma}_i$ terms.

the remainder yield $\bar{\gamma}_i - \bar{\gamma}_j = 0 \ \forall i, j$. Thus, the sum of cosine terms will be close to zero[2].

Suppose the solution to Eq. (5.8) is $\bar{\gamma}_k$, then the phase correction terms, $\bar{\beta}_k$, can be calculated from Eq. (5.2) as follows:

$$\bar{\gamma}_k = \alpha_k + \bar{\beta}_k + \frac{N}{2}\theta_k \tag{5.9}$$

---

[2]Although it might not always be possible to find a perfect solution using this technique, it does help making the sum of cosines equal to a value close to zero.

$$\bar{\beta}_k = \bar{\gamma}_k - \frac{N}{2} \times \frac{2\pi k}{N} - \alpha_k$$
$$= \bar{\gamma}_k - \pi k - \alpha_k. \tag{5.10}$$

In Figure 5.3, the proposed linear search algorithm for finding the roots of Eq. (5.8) is presented. The algorithm starts by assuming half of the $\bar{\gamma}_i$ terms equal to π and the other half terms equal to 0. The number of π terms are increased if the sum of the cosine terms, Q, is positive and decreased if Q is negative. The procedure is continued until the value of Q closest to zero has been found. Using this technique, phase adjustments reducing the PAPR of an OFDM signal are found[3].

5.2.2.2 Proposed Phase Grouping Technique

If all the individual subcarrier phase adjustments are sent to the receiver, the overhead will be significant[4]. One solution to this problem is to have a single phase adjustment term per group of subcarriers.

Since the sequences giving high PAPR tend to have a large number of a particular subcarrier signal constellation point, subcarrier phase grouping would help reduce the overhead without affecting the PAPR reduction. The mean or mode[5] of the phase adjustments can be used for grouping. Taking the mean of the phase adjustments would result in an increase in quantization levels. For example, considering a BPSK system, transmitting the individual subcarrier phase information

---

[3]It is clear from Eq. (5.8) that the value of Q does not depend on the location of π and 0. Therefore, the solution for the equation can be found by the one dimensional linear search, instead of N dimensional search.

[4]Since $\exp(j(n\pi + \phi)) = (-1)^n \exp(j\phi)$, $\forall n$, the phase updates calculated by Eq. (5.10) can only take on a discrete set of values used in the input signal constellation.

[5]By definition, the *mode* represents the most common value in the set of observations.

to the receiver would yield a goodput[6] equal to half of the total throughput. Using the mean of eight phase adjustments would result in nine quantization levels, which would require four bits to represent it. In this case, the goodput would become $1 - 4/(4 + 8) = 2/3$. By using the mode of the phase adjustment groupings, the number of quantization levels of the phase adjustments would not change and thus results in a further increase in goodput. For example, if the phase updates are grouped over eight subcarriers, the goodput would become to $1 - 1/9 = 8/9$. However, there is a trade-off between grouping size and PAPR reduction.

Note that assigning phase adjustment terms to a grouping of alternating subcarriers i.e. adjacent subcarriers are not included in a grouping, for a highly correlated sequence would be closer to individual phases as compared to grouping of contiguous blocks of the subcarrier phase updating terms[7]. Method of grouping phase adjustments over four subcarriers for 16-subcarrier OFDM system is shown in Figure 5.4.

5.2.3 Simulation Results

We consider a BPSK system with input data symbols, $X_k = 1\angle 0 \ \forall k$ (or, $X_k = 1\angle \pi \ \forall k$), which represents the case with the highest PAPR. In this case, the phase updates for the kth subcarrier is given by

$$\bar{\beta}_k = \bar{\gamma}_k - \pi k. \tag{5.11}$$

---

[6]We define *goodput* as the total information bits per unit of time transmitted to the receiver minus overhead information bits per unit of time.

[7]Referring to Eq. (5.10), alternating phase adjustment terms for a highly correlated input sequence would be very similar since they have the equivalent $k\pi$ term, as well as very similar α_k terms.
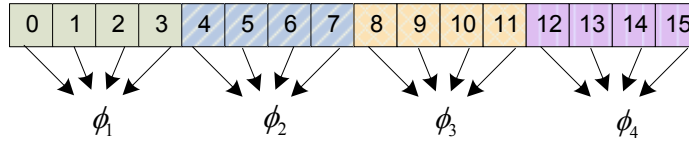
(a) Sequential grouping method
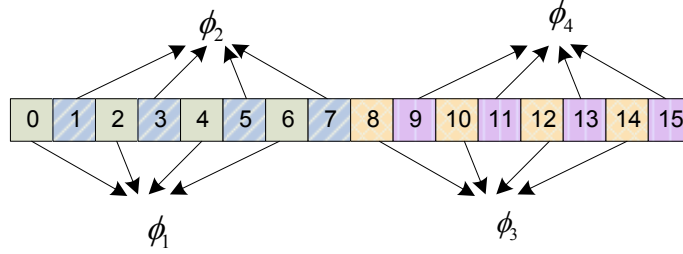
(b) Proposed grouping method

Figure 5.4. Grouping phase adjustments over 4 subcarriers for an OFDM signal with $N = 16$.

The proposed algorithm is compared with the *random phase updating* (RPU) algorithm for reducing the PAPR of an OFDM signal proposed by Nikookar and Lidshein [81]. It is assumed that the receiver has the complete knowledge about the phase adjustments made at the transmitter.

The PAPR value of the modified OFDM symbol is calculated from 16 to 4096 subcarriers and plotted in Figure 5.5. It is observed that the maximum PAPR reduction when the OFDM system is employing the proposed algorithm is around 4 dB (about a 60% reduction).

PAPR reduction using the RPU algorithm for several iterations is shown in Figure 5.5 for comparison. The PAPR value in the plot represents the mean of 100 trials per simulation point. From the figure, it is clear that the RPU algorithm achieves approximately a logarithmic reduction in the PAPR as the number of iterations increases. However, every iteration involves the calculation of power variance of the input signal (or IFFT operation), which is computationally in-
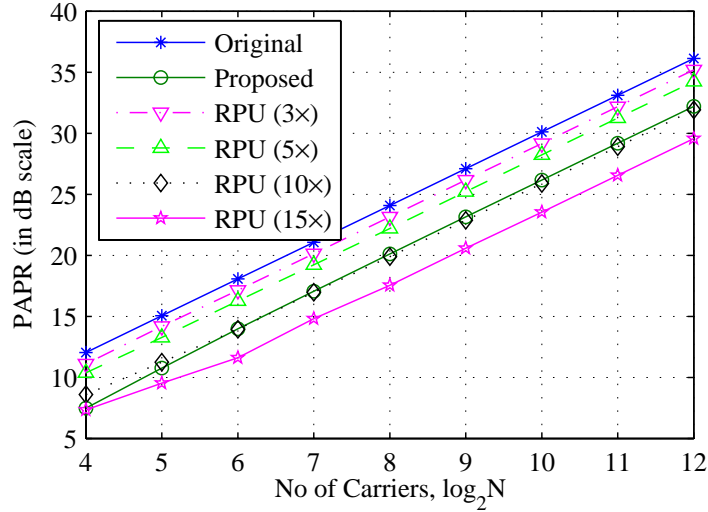
Figure 5.5.   Comparison: Maximum PAPR reduction when the receiver has the complete information about the phase update

tensive. With respect to the non-iterative proposed algorithm, which achieves a 4 dB reduction in the worst-case PAPR, the RPU algorithm requires 10 iterations to achieve the same reduction, making this approach more computationally expensive.

Now, we consider a BPSK system with input data symbols, $X_k \in \{-1, 1\}$ $\forall k$, with the probability of occurrence of "1", $p = 0.9$, to represent a highly correlated input sequence. Phase adjustment for each subcarrier for a random input sequence is given by Eq. (5.10). The PAPR value of the modified OFDM symbol is calculated from 16 to 4096 subcarriers with and without grouping the phase adjustments over several subcarriers, for different number of subcarrier per group. The results are also compared with the RPU algorithm and plotted in Figure 5.6. Simulation results show that increasing the number of subcarriers per group results in a lower reduction of the PAPR, when employing the RPU algorithm. This result is expected because of the reduced resolution of the phase adjustments at
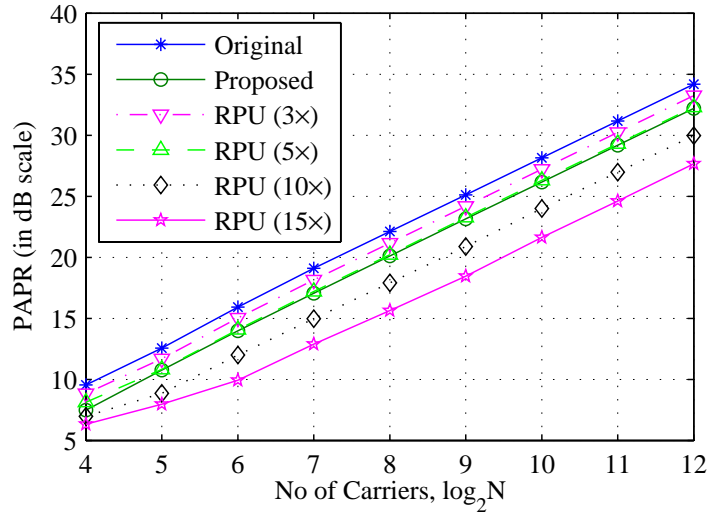
(a) No Grouping.
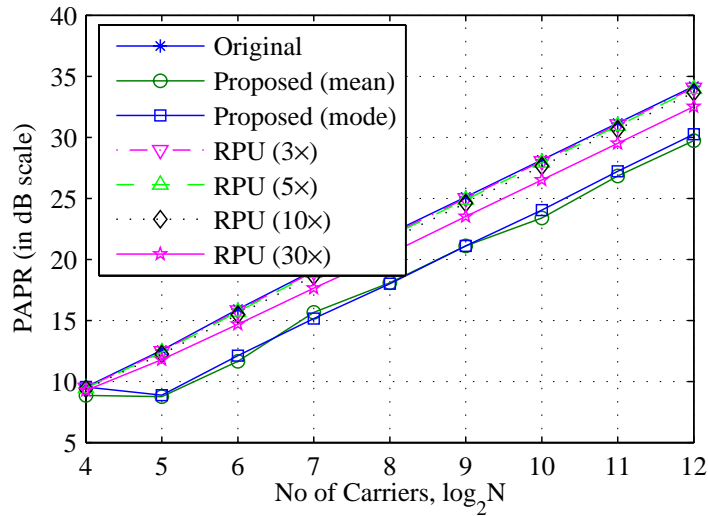
(b) Number of subcarriers per group = 8.

Figure 5.6. PAPR reduction with grouping the phase updates over several subcarriers (Probability of 1, $p = 0.90$).

the transmitter. However, the grouping phase adjustments significantly increases the throughput of the system. Simulation results show that the proposed grouping technique is robust for large number of subcarriers per group. Moreover, taking mean or mode of the phase adjustments for grouping yields similar results.

The proposed algorithm can reduce the PAPR of an OFDM signal with large PAPR values. The proposed phase adjustment technique can be incorporated along with data randomization techniques, such as interleaving technique [112], for developing a PAPR reduction technique which can minimize the PAPR over a wide range of scenarios.

5.3 Adaptive Mode PAPR Reduction Algorithm[8]

In this Section, we propose a novel low complexity algorithm that adaptively chooses which PAPR reduction approach, or combination thereof, to employ based on the current operating conditions, such as instantaneous PAPR. The PAPR reduction approaches employed by the proposed algorithm in this work are: (1) interleaving, and (2) per-subcarrier phase adjustments. The proposed algorithm is then evaluated within the framework of cognitive radio transceiver employing NC-OFDM.

5.3.1 NC-OFDM Transceiver

A general schematic of an NC-OFDM transceiver employing the proposed PAPR reduction algorithm is shown in Figure 5.7. For the basic principle of NC-OFDM technique, please refer to Section 2.5. As shown in Figure 5.7(a), the proposed adaptive-mode PAPR reduction algorithm decides upon computing phase adjustments, interleaving the data sequence, or a combination of both to reduce PAPR of an OFDM signal. The PAPR reduction information is also transmitted to the receiver for correct demodulation of the received sequence.

---

[8]The work was presented at the *64th IEEE Vehicular Technology Converence* [119].
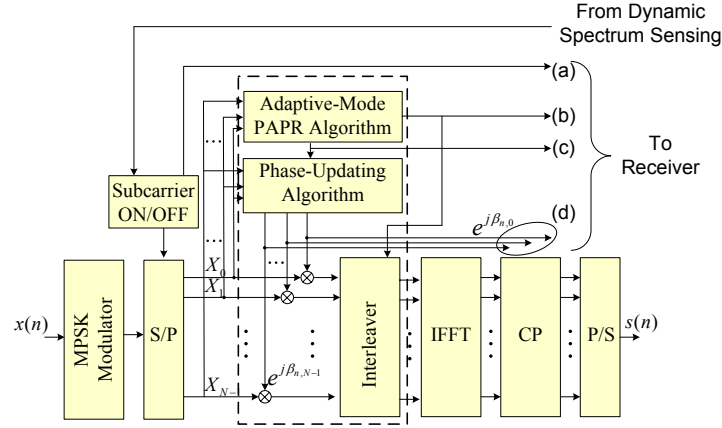
(a) Transmitter with proposed adaptive mode PAPR reduction algorithm.
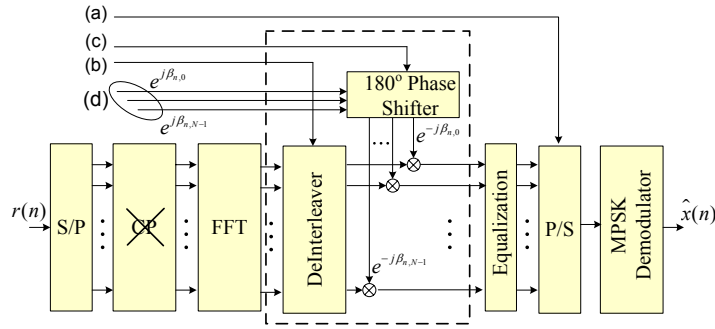
(b) Receiver with PAPR reduction information.

Figure 5.7. Schematic of an NC-OFDM transceiver employing adaptive-mode PAPR reduction algorithm.

5.3.2 Proposed Adaptive-Mode PAPR Reduction Algorithm

Although there has been much research conducted in the area of PAPR reduction, most of these solutions are suited for specific cases, depending on the similarity between the subcarrier information. Thus, a PAPR reduction approach that is effective for one scenario may not be suitable for another scenario. However, the proposed algorithm can choose the PAPR reduction approach best suited for a particular situation.

The objective of the proposed PAPR reduction algorithm is to choose the

PAPR reduction mode that is capable of achieving a substantial decrease in PAPR. For instance, interleaving techniques can substantially decrease the PAPR, when the PAPR is moderate [112]. This is due to the fact that interleaving can be used to randomize the input sequence and disrupt the long correlation pattern of the input sequence. On the other hand, for very high PAPR values, phase-adjusting algorithms have shown to be the best choice for PAPR reduction [81,97,118]. This follows from the fact that binary or polyphase sequences with large out-of-phase aperiodic correlation values can result in signals with large PAPR values[9]. Thus, the resulting PAPR could be very high when the input sequence is highly biased. Although the probability of highly biased data frames is low over a long period of time, it is possible to have scenarios where data is biased for relatively short periods of time[10]. Thus, the proposed *adaptive mode* PAPR reduction algorithm chooses the mode best suited for different transmission conditions in order to achieve a substantial reduction in PAPR for most scenarios.

Referring to the flow diagram of Figure 5.8 and the transceiver schematic of Figure 5.7(a), the proposed algorithm commences by computing the instantaneous PAPR of an OFDM signal without any phase updating or interleaving using the values of X_k. If the resulting PAPR value is less than a pre-defined threshold $\text{PAPR}_{\text{Th}_1}$, then the signal can be transmitted without any modification and the algorithm ends, i.e., neither the phase-updating algorithm block or interleaver block in Figure 5.7(a) are employed. However, if the PAPR value is above the set threshold $\text{PAPR}_{\text{Th}_1}$, the algorithm must choose a PAPR reduction algorithm and lower this value. If the PAPR value is less than a set threshold $\text{PAPR}_{\text{Th}_2}$,

---

[9]It follows from the fact that low out-of-phase aperiodic correlation values of binary or polyphase sequences results in a small value of the PAPR of the signal [68,69].

[10]For example, transmitting uncoded image data from a webcam, when the room is dimly lit, can result in data being highly biased.

M subcarrier OFDM symbol

Calculate PAPR of the OFDM Symbol

Is $PAPR < PAPR_{Th_1}$? — Yes

No

Is $PAPR < PAPR_{Th_2}$? — Yes

No

Calculate M phase increments

Use K Interleavers

END
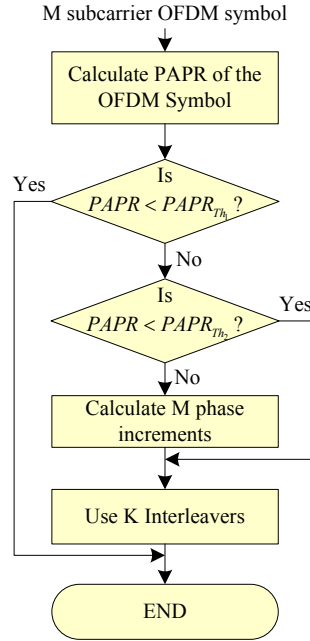
Figure 5.8. Adaptive mode PAPR reduction algorithm.

the proposed algorithm choose the "interleaver" mode, i.e., the interleaver block in Figure 5.7(a), where an interleaver is applied to the data sequence. Since the algorithm has K interleavers available, the interleaver yielding the greatest decrease in PAPR is chosen. If the instantaneous PAPR is greater than $PAPR_{Th_2}$, the algorithm enters the "phase adjustment" mode, i.e., the phase-updating block in Figure 5.7(a), where the subcarrier phases are adjusted to achieve a reduction in PAPR. The algorithm will also employ one of the K interleavers to the phase-updated subcarriers to achieve a larger PAPR reduction.

5.3.3 Simulation Results

We now consider an NC-OFDM transceiver employing 512 BPSK-modulated subcarriers with 0% of the subcarriers being deactivated[11]. The percentage of

---

[11]With all the subcarriers are active, this would yield the worst case PAPR scenario.

subcarriers transmitting the same BPSK symbol, e.g., "1", varies from 50%, i.e., unbiased scenario, to 99%, i.e., highly biased scenario. For each scenario, 100,000 BPSK-modulated NC-OFDM symbols were evaluated and the resulting PAPR values averaged. When generating the CCDF plots of the PAPR for an NC-OFDM transceiver, 100,000 BPSK-modulated NC-OFDM symbols were employed for a given PAPR value. Finally, results for the two modes of operation of the proposed adaptive mode PAPR reduction algorithm are shown: (1) interleavers-only mode, and (2) phase adjustment with interleavers[12].

The mean and standard deviation of the PAPR for an NC-OFDM transceiver, employing only the best of the K interleavers, are plotted in Figure 5.9. We observe that when the percentage of subcarriers employing the same BPSK symbol is around 50%, the interleaver approach appears to limit the PAPR to about 8 dB. However, as the percentage increases beyond 60%, the effectiveness of the interleavers to reduce the PAPR diminishes. Also notice how as the number of available interleavers increases, the PAPR can be reduced by as much as 0.5 dB for $K = 16$ interleavers. In Figure 5.10, the mean and standard deviation of the PAPR for an NC-OFDM signal employing a phase updating algorithm and four interleavers are shown. We observe that with the combination of the phase updating algorithm and the interleavers, the mean PAPR does not exceed 7.5 dB when the percentage of subcarriers employing the same BPSK symbol ranges from 50% to 100%. However, we know from other simulation results that the phase updating approach is ineffective at low percentages. Thus, to save computational and hardware complexity, the proposed algorithm can choose an interleaver-only mode when the percentage of identical subcarrier transmissions is below 60%, and

---

[12]In this work, we employ the random interleaver approach used by Jayalath and Tellambura [112], and the phase updating approach proposed in Section 5.2
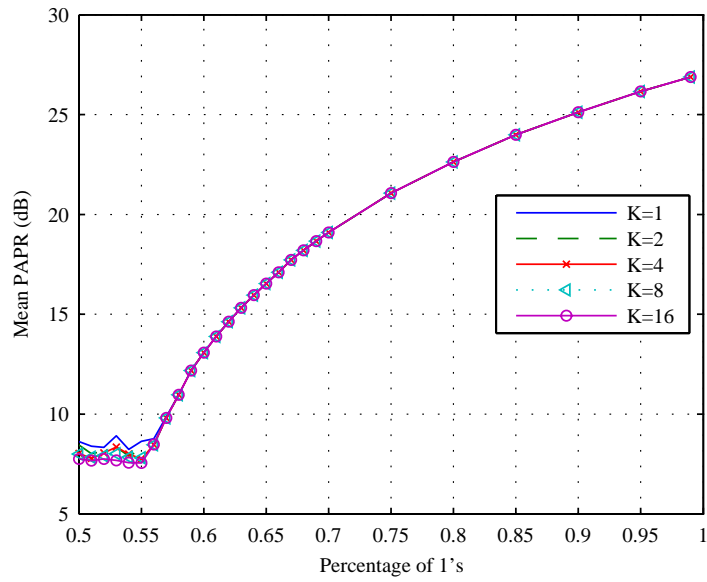
(a) N=512.
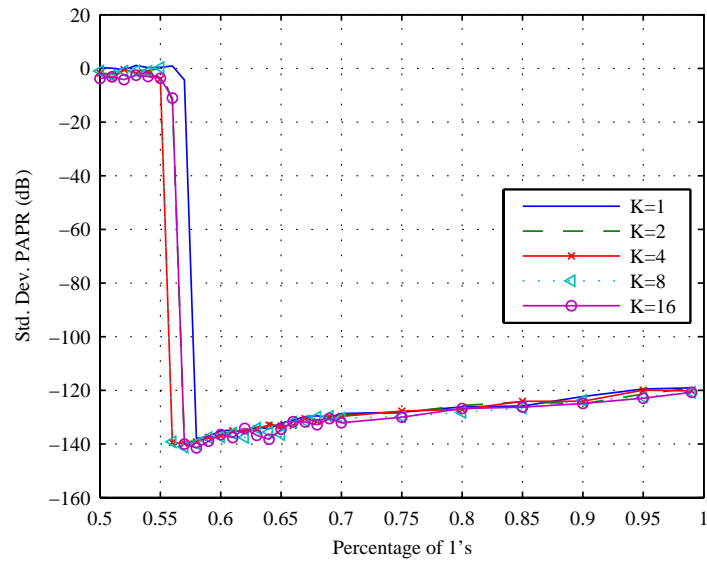
(b) N=512.

Figure 5.9. PAPR statistics for BPSK modulated NC-OFDM signals with $N = 512$ subcarriers and K interleavers

a combined mode when it is above 60%.

To reduce the amount of overhead information required to perform phase adjustment PAPR reduction, the phase updates can be grouped together to reduce the information overhead to the receiver. In this case, as the subcarrier group size, N_{grp}, increases in the number of subcarriers, the PAPR reduction on slightly degrades due to the loss in flexibility. Finally, notice how for percentages less than 60% that the PAPR values are the same as those in Figure 5.9. This implies that at percentages around 50%, phase adjustments do not have any significant impact on the reduction of the PAPR. Therefore, the proposed adaptive mode PAPR reduction algorithm would reduce the computational complexity by choosing only interleavers in this case.

The CCDF of the PAPR for an NC-OFDM transmission is plotted in Figure 5.11, where the only PAPR technique being employed by the transceiver is only $K = 4$ interleavers. It is evident from these results that the PAPR statistics improve with an increasing number of available random interleavers, relative to the case when no PAPR reduction is performed. Moreover, combining the phase adjustment approach and $K = 4$ interleavers results in even better PAPR performance, relative to only employing interleavers. However, as the subcarrier group size, N_{grp}, increases in the number of subcarriers, the PAPR reduction performance of the combined approach begins to deteriorate. Figure 5.12 shows the PAPR CCDF when the number of available interleaver varies from $K = 4$ to $K = 16$. The observed trend is that as K increases, the PAPR performance of the transceiver improves, with the probability that the PAPR which exceeds 8.6 dB is less than 0.1% when $K = 16$ interleavers.
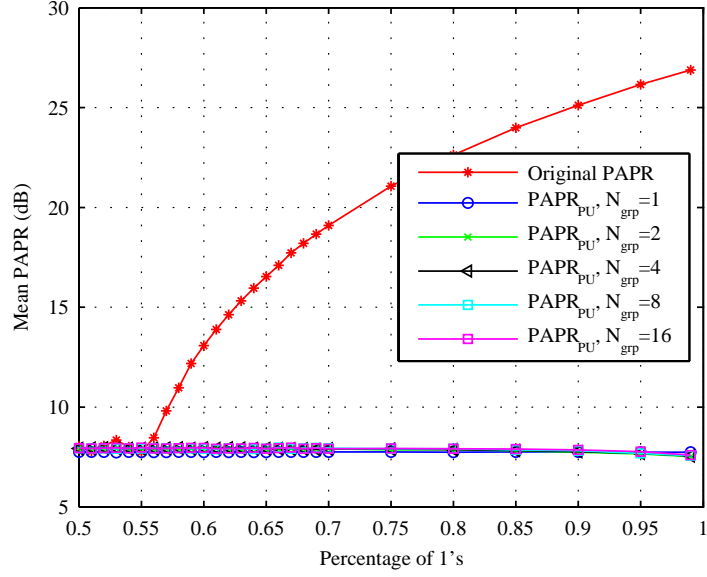
(a) N=512

(b) N=512

Figure 5.10. PAPR statistics for BPSK modulated NC-OFDM signals with $N = 512$ subcarriers and $K = 4$ interleavers

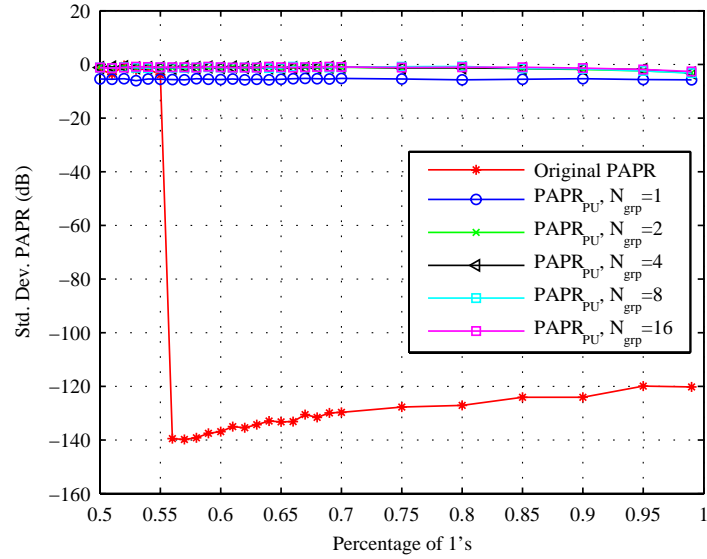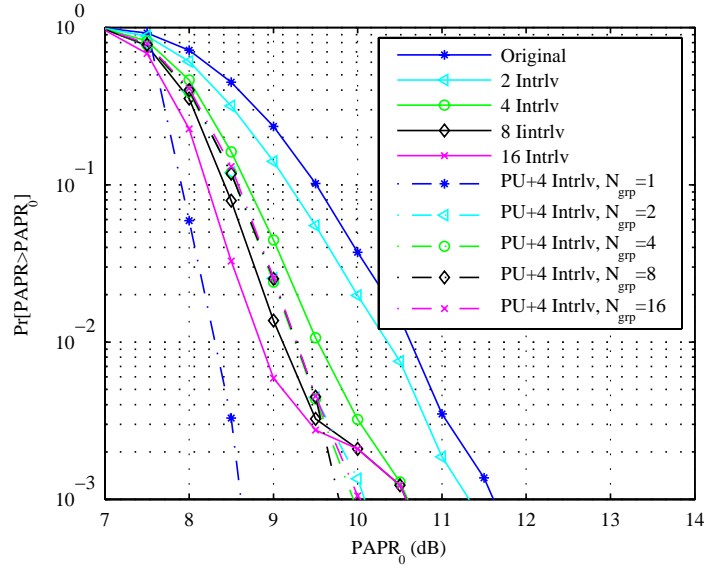**Figure 5.11.** CCDF of BPSK NC-OFDM signal PAPR with phase updating and random interleavers
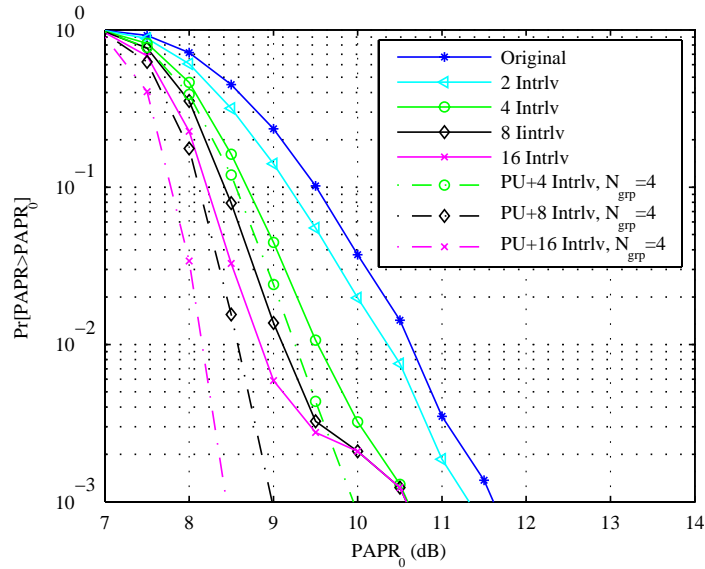
Figure 5.12. CCDF of BPSK NC-OFDM signal PAPR with phase updating and random interleavers

5.4 Subcarrier Power Adjustment PAPR Reduction Algorithm[13]

In this section, we propose a novel subcarrier power adjusting PAPR reduction algorithm for M-ary PSK modulated OFDM signal, in which subcarrier power levels are altered to minimize PAPR. Information regarding the power level adjustments do not need to be transmitted to the receiver. Therefore, there is no throughput penalty. Moreover, the power adjustments obey a subband power constraint. Therefore, the system would not violate regulatory power requirements. However, the PAPR reduction comes at the cost of slight BER performance degradation.

5.4.1 System Framework

A schematic of an OFDM transceiver employing the proposed PAPR reduction algorithm is shown in Figure 5.13. For the basic principle of OFDM, please refer to Section 2.3. As shown in the Figure 5.13, the proposed subcarrier power adjustment algorithm assigns the subcarrier power levels to minimize the PAPR of an OFDM signal.

5.4.2 Subcarrier Power Adjustment

In a multicarrier transmission system, *power loading* is a powerful technique for enhancing system performance when the system operates in a frequency selective fading channel. In power loading, the power distribution across all the subcarriers vary according to the estimated channel conditions in order to minimize the overall

---

[13]The work was presented at the *IEEE Military Communications Conference* [120].
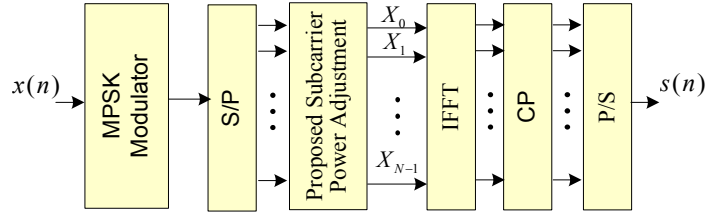
(a) OFDM Transmitter.
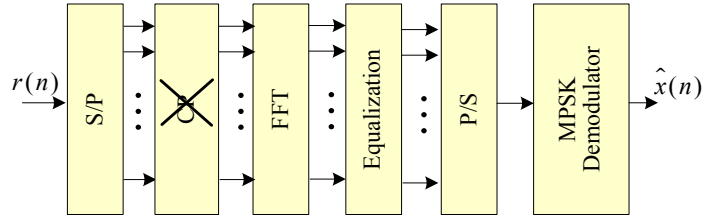
(b) OFDM Receiver.

Figure 5.13. OFDM Transceiver employing subcarrier power adjustment for PAPR reduction.

error probability [121]. It has been shown in the literature that PAPR can be minimized by adjusting subcarrier power levels [82, 84, 122–124]. In this section, we focus on the following two power adjustment approaches that will be employed by the proposed PAPR reduction:

1. Total power constraint [125, 126]

2. Window power constraint [121, 127]

In the following two subsections, these approaches will be described in detail.

5.4.2.1 Total Power Constraint

Total power-constrained power adjustment implies that if power of any subcarrier is reduced or turned off, the excess power allocated to it can be transferred to remaining active subcarriers. Let π_k be the transmitted power of the k-th sub-

carrier ($k = 0, 1, \ldots, N - 1$). If the total number of subcarriers is N, the power constraint is given by:

$$\sum_{k=0}^{N-1} \pi_k = \pi_{\text{total}}. \tag{5.12}$$

The aggregate bit rate is approximately maximized if the bit error rates in all the sub-bands are equal, whereas BER performance is optimized when all the subcarriers have equal power [22]. Without power adjustment, π_k is assumed to be equal for all subcarriers. In case of total power-constrained power adjustment, it is possible that all the power could be concentrated to a single subcarrier. However, such an allocation could potentially violate the spectrum regulations requirements. The following power constraint is designed to avoid these violations.

5.4.2.2 Window Power Constraint

If the power level of certain subcarrier is lowered, in window power-constrained power adjustment the excess power can be transferred to the active subcarriers within certain predefined sliding window. The total power for every grouping of M subcarriers needs to be below the regulatory requirement, say π_{max}. Then, the subcarrier power constraints would be [121]:

$$\sum_{k=l}^{l+M-1} \pi_k \leq \pi_{\text{max}}, \quad \forall l \tag{5.13}$$

and

$$\sum_{k=0}^{N-1} \pi_k \leq \pi_{\text{total}}. \tag{5.14}$$

For example, consecutive windows of subcarriers are shown in Figure 5.14. If the power level of a subcarrier in 'Window 1' is lowered, the power can only be

113
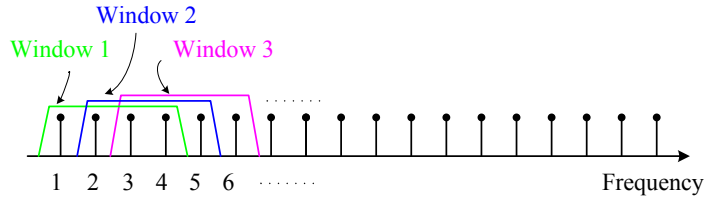
Figure 5.14. Subcarrier power window.

transferred to the other active subcarriers within 'Window 1'. When the power level of a subcarrier (say 'Subcarrier 3') is adjusted, subcarrier power level must satisfy the window power constraints for all the member sliding windows ('Window 1', 'Window 2', 'Window 3').

A practical transmit power constraint is usually enforced to limit the total power across a frequency window of a specified width. For instance, FCC has imposed requirements based on the amount of transmit power across a specified bandwidth in the UNII band [127]. These requirements are imposed since these bands are usually unlicensed and the users are non-cooperative.

5.4.3 Proposed Algorithm

To ensure the system transmissions do not violate regulatory requirements, we propose a subcarrier power adjustment PAPR reduction algorithm employing a window power constraint approach. The proposed subcarrier power adjustment algorithm for reducing PAPR is presented in Figure 5.15. First, the algorithm begins with choosing the subcarrier power adjustment factors with a given distribution, $f(x)$. Second, either L different sets of power adjustment factors are generated or the power adjustment factors are interleaved using L interleavers. Third, the subcarrier power adjustment vectors are then window power-constrained using the algorithm presented in Figure 5.16. Fourth, the input subcarriers are multiplied

1: Initialize $\pi(0 : N - 1) = Z \sim f(x)$
2: Generate L different power adjustment factors, $\{\pi_i\}_{i=0}^{L-1}$, or interleave π using L random interleavers (or other interleavers)
3: Check the FCC power constraint for each (interleaved) subcarrier power window π_i, using the sliding window algorithm presented in Figure 5.16.
4: Modified symbols, $X_{\mathrm{mod}} = X \cdot \sqrt{\pi_i}$
5: Choose π_i, which yields lowest PAPR

Figure 5.15. Proposed PAPR Reduction Algorithm.

element-by-element with the subcarrier power adjustments. Finally, among the subcarrier power adjustment vectors, one yielding minimum PAPR is chosen.

The sliding window algorithm to maintain the power constraint over the window is presented in Figure 5.16. First, the algorithm determines if the total power of the subcarriers in the k-th window, $\sum_{l=0}^{M-1} \pi(l)$, exceeds the practical power constraint, where M represents the total number of subcarriers per window. If the total power of the subcarriers in a given window crosses allowable power level, the subcarrier power levels are scaled down to meet the power requirement. Second, the algorithm determines whether the power level of the l-th subcarrier, $\pi(l)$, is lower than the predefined threshold, π_{min}, in which case, the power level is restored to π_{min}. This minimum power level requirement would ensure that the BER performance would not degrade below certain level. The algorithm is repeated until both requirements are met by all the subcarriers.

The primary advantage of the proposed algorithm is that subcarrier power information need not to be transmitted to the receiver[14]. Therefore, there would not be any throughput loss and no modification would be necessary in receiver structure. Additionally, the subcarrier power levels can be quantized or set to

---

[14]In M-ary PSK modulated OFDM system, inverting the subcarrier power adjustment at the receiver would weight noise power as well, which keeps SNR unchanged.

```
 1: for $k = 0$ to $(N - M + 1)$ do
 2:    for $l = k$ to $(k + M - 1)$ do
 3:       if $\pi(l) < \pi_{\min}$ then
 4:          $\pi(l) = \pi_{\min}$
 5:       end if
 6:    end for
 7:    $S = \sum_{l=k}^{k+M-1} \pi(l)$
 8:    if $S > \pi_{\max}$ then
 9:       $\pi(k : k + M - 1) = \pi(k : k + M - 1) * \pi_{\max}/S$
10:    end if
11: end for
12: return  $\pi$
```

Figure 5.16. Sliding Window Power Constraint.

the one digit decimal to reduce the complexity (or hardware requirements) of multiplication operations.

5.4.4 Simulation Results

5.4.4.1 Simulation Setup

For simulation purposes, OFDM transceiver employing 256 QPSK-modulated subcarriers is considered. To obtain each CCDF plots, 10^4 random OFDM symbols are generated and PAPR is computed for each symbol. The number of subcarriers per sliding window is assumed to be four. In this section, we consider the following three subcarrier power level distributions:

1. Uniform: $f(x) = U(x), \quad x \geq 0$

2. Exponential: $f(x) = -\log(U(x)), \quad x \geq 0$

3. Truncated Gaussian: $f(x) = \mathcal{N}(1, \sigma^2), \quad x \geq 0$

116

For all distributions, mean power is kept unity for fair comparison. We use $L = 16$ random interleavers to generate different sets of power adjustment factors.

5.4.4.2 PAPR Results

For uniform, exponential, and truncated Gaussian subcarrier power distributions, CCDF of the PAPR obtained through simulations are presented in Figure 5.17. The CCDF of PAPR is evaluated for each case with minimum subcarrier amplitude level, i.e. $\sqrt{\pi_{\min}}$ equal to 60%, 70%, 80%, and 90%, and compared with original case. From Figure 5.17, it is observed that PAPR gets reduced when the minimum subcarrier power level $\pi_{\min}$ is reduced. This is because of the higher range of variantion among the subcarrier power levels. There is about 1.5 dB PAPR reduction at 10^{-3} CCDF achieved when the subcarrier power distribution is exponential or truncated Gaussian, whereas there is about 0.5 dB PAPR reduction at 10^{-3} CCDF achieved when the subcarrier power distribution is uniform.

Assuming AWGN channel, BER performance degradation due to subcarrier power adjustments for uniform, exponential, and truncated Gaussian subcarrier power distributions are presented in Figure 5.18. BER performance of the OFDM system is evaluated for each case with minimum subcarrier amplitude level, i.e. $\sqrt{\pi_{\min}}$ equal to 60%, 70%, 80%, and 90%, and compared with original case. The results corroborate the fact that the BER performance of the system degrades as the minimum subcarrier power level gets reduced. However, the BER performance degradation is relatively indifferent to the subcarrier power distributions.

From the results, it is ensured that there exists a trade-off between the PAPR reduction and BER performance degradation. Higher PAPR reduction can be achieved when the minimum subcarrier amplitude level is reduced, but BER per-
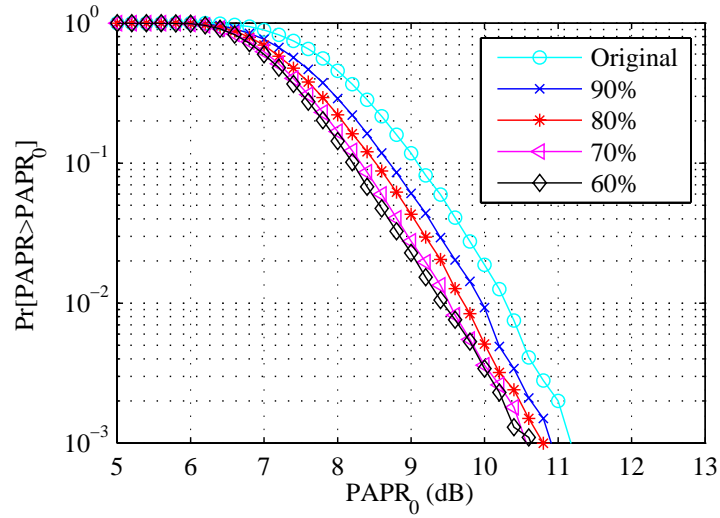
(a) Uniform Distribution.
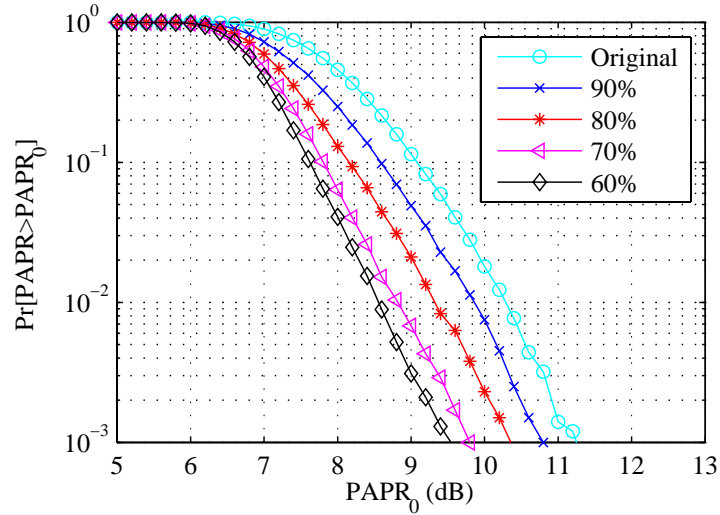
(b) Exponential Distribution.

Figure 5.17. Complementary cumulative distribution function of PAPR for BPSK modulated OFDM with 256 subcarriers.
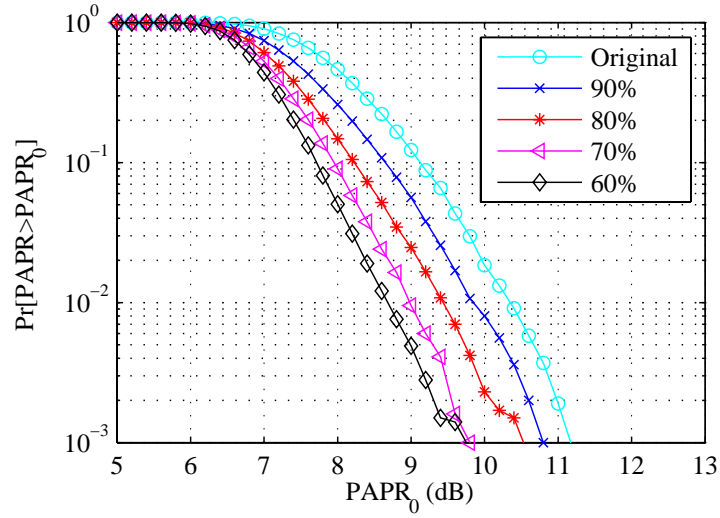
(c) Truncated Gaussian Distribution.

Figure 5.17. Complementary cumulative distribution function of PAPR for BPSK modulated OFDM with 256 subcarriers (contd.).
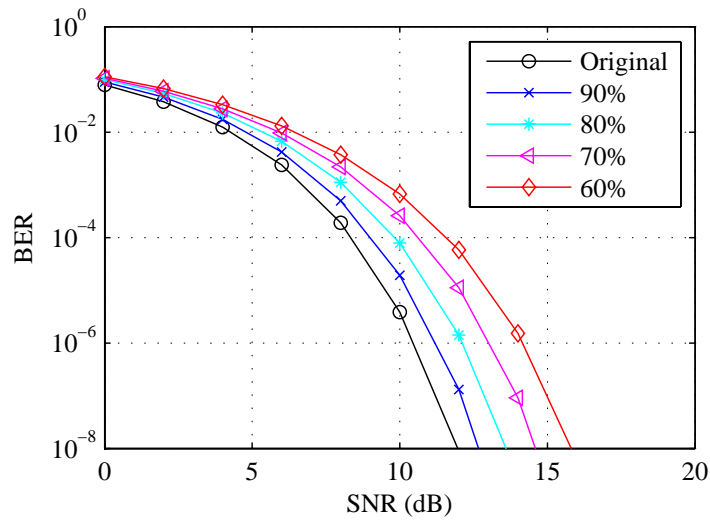
(a) Uniform Distribution.

Figure 5.18. Aggregate BER performance of BPSK modulated OFDM with 256 subcarriers over AWGN channel.
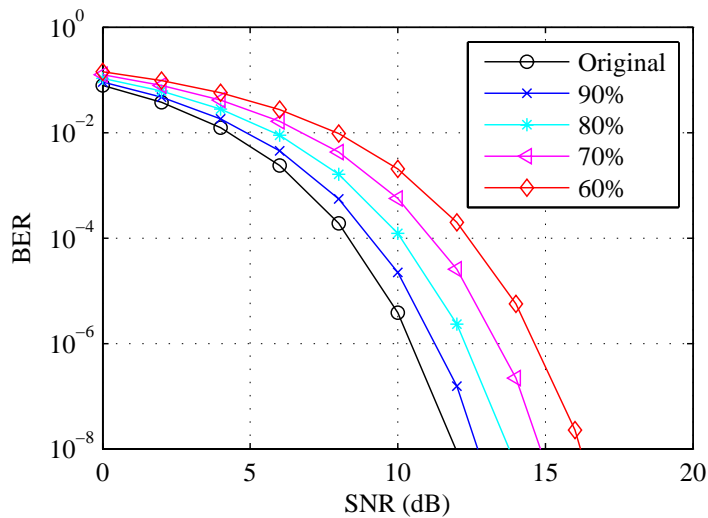
(b) Exponential Distribution.
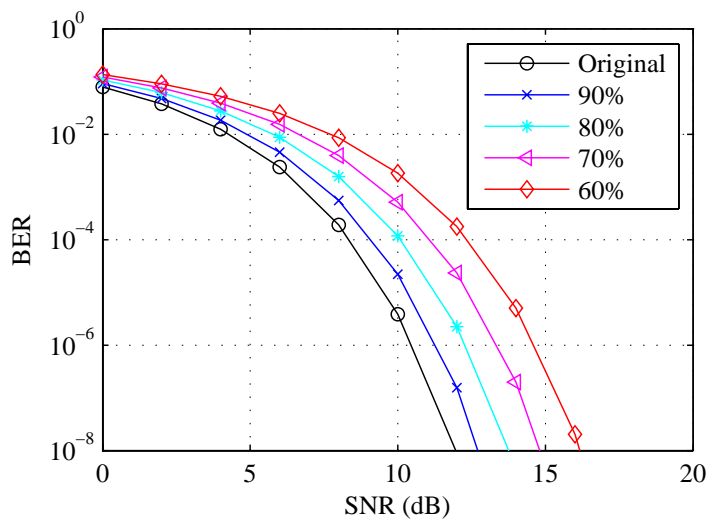
(c) Truncated Gaussian Distribution.

Figure 5.18. Aggregate BER performance of BPSK modulated OFDM with 256 subcarriers over AWGN channel (contd.).

120

formance also degrades side-by-side. If slight degradation in BER performance is acceptable, significant PAPR reduction can be achieved by the proposed algorithm without increasing the complexity of the OFDM receivers.

5.5 Variable Data Throughput Approach for PAPR Reduction[15]

A non-data bearing subcarrier approach for PAPR reduction had been proposed in literature [129], where for a fixed number of subcarriers, several are selected to be data-bearing, while the others are non-data bearing (NDB). The NDB subcarriers are located in fixed locations, and would not always effectively break the long correlation patterns, thereby limiting their ability for PAPR minimization. In the literature, several tone reservation techniques for reducing the PAPR of an OFDM symbol have been proposed [83], in which several subcarriers are reserved for carrying symbols to reduce PAPR. The main drawback of these techniques is that the convergence to absolute minimum peak power is likely to be slower and exhibit large computational complexity [110]. Moreover, a fixed number of NDB subcarriers, regardless of PAPR minimization requirements, would result in a steady data throughput loss. Since the PAPR of an OFDM signal depends on the distribution of input symbols, a fixed number of NDB subcarriers could potentially be too many or too few to sufficiently affect the PAPR.

In this section, we first propose a novel algorithm to determine the number of NDB subcarriers, which can be dynamically adapted based on the PAPR reduction requirements to minimize unnecessary data throughput loss. Second, we

---

[15]The work has been submitted to *66th IEEE Vehicular Technology Converence* [128].

propose a novel PAPR reduction algorithm that adaptively determines symbols over fixed or adaptively determined number of NDB subcarriers. The proposed algorithm, in tandem with data randomization techniques such as interleaving, can effectively break the long correlation patterns and achieve significant PAPR reduction. Moreover, the proposed algorithm is simple, non-iterative, and effective for both moderate to high PAPR values.

5.5.1 Multicarrier System Framework

A general schematic of an OFDM transceiver employing the proposed PAPR reduction algorithm is shown in Figure 5.19. For the basic principle of OFDM, please refer to Section 2.3. The proposed algorithm determines symbols $\{D_i\}_{i=0}^{i=M-1}$ over M NDB subcarriers in order to reduce the PAPR. The number of NDB subcarriers, M, can either be fixed or dynamically adapted by the proposed algorithm based on the PAPR reduction requirements. The data bearing subcarriers, having amplitude levels $\{X_i\}_{i=0}^{i=N-M-1}$, are combined with NDB subcarriers $\{D_i\}_{i=0}^{i=M-1}$ and then converted into N parallel streams using an serial-to-parallel (S/P) converter. Then an interleaver randomizes the input data sequence to break long correlation patterns of the input data sequence. At the receiver, the sequence is deinterleaved and the symbols over NDB subcarriers are discarded, as they do not possess any information.

5.5.2 Proposed NDB Subcarrier Insertion Algorithm

The proposed approach determines the number of NDB subcarriers, M, and symbols over these subcarriers, $\{D_i\}_{i=0}^{i=M-1}$, to balance distribution of subcarrier signal constellation $\{X_i\}_{i=0}^{i=N-M-1}$ in the data frames, where the total number of

(a) OFDM Transmitter.

(b) OFDM Receiver.
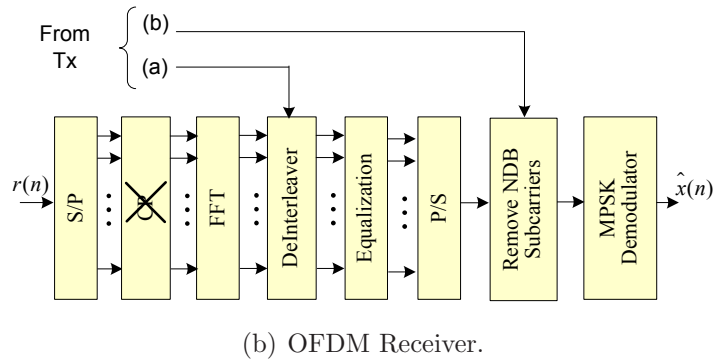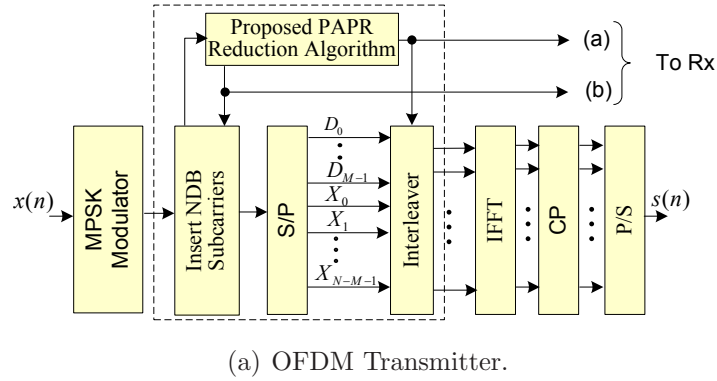
Figure 5.19. OFDM transceiver employing adaptive NDB subcarrier approach with interleaving for PAPR reduction.
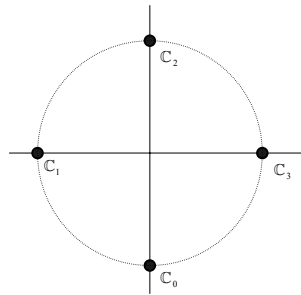
Figure 5.20. Constellation diagram for QPSK symbols.

subcarriers, N, is fixed. When the number of NDB subcarriers increases, the number of data bearing subcarriers, $N - M$, decreases keeping the total number of subcarriers, N, constant.

The number of NDB subcarriers can be fixed to a predefined value to reduce

complexity of the algorithm. However, it comes at the cost of reduced flexibility on PAPR reduction and a steady loss in throughput, regardless of PAPR reduction requirements of an individual data frame. To improve the transmission efficiency, an appropriate number of NDB subcarriers can be determined according to the PAPR minimization requirement for an individual data frame. Based on the information, the number of NDB subcarriers can be determined using the algorithm in Figure 5.21 (see Section 5.5.2.1 for explanation). Once the number of NDB subcarriers is determined, the symbols transmitted over these subcarriers are determined using the algorithm Figure 5.22 (see Section 5.5.2.2 for explanation).

5.5.2.1 Variable Number of NDB Subcarriers

As shown in our previous work, sequences having a high number of a particular subcarrier signal constellation yields symbols with high PAPR [119]. However, different input sequences have different PAPR values. Therefore, the number of NDB subcarriers, to balance the signal distribution in a given data frame, would be different for an individual input data frame.

The algorithm begins with reading $N/2$ data bearing symbols and calculating the symbol distribution in the frame. Suppose C_i represents the count of i-th symbol constellation point, $\mathbb{C}_i$, in the frame, as shown in Figure 5.20. Assume the symbol constellation is bipolar. Then the number n_i represents unbalance between the i-th and $(i+c/2)$-th constellation point, is given by, $n_i = C_i - C_{i+c/2}$, where c is the total number of the constellation points. For example, $c = 2$ for BPSK symbol constellation. The term S, which is the sum of the absolute values of the n_i, represents the number of NDB symbols required to balance the symbol distribution in the given frame. If the sum S is greater than $N/4$, more than $N/4$

1: Let $l = 0$ and $m = N/2 - 1$
2: Let $S_{\text{th}} = N/4 - 1$ and $M_{\text{th}} = \lceil 0.03N \rceil$
3: Let $X = [x_l, x_{l+1}, ..., x_m], x_k \in \{\pm 1, \pm j\}$
4: $M = N - m$
5: $\{C_i\}_{i=0}^{c-1} = \text{Categorize}(X)$
    c - No. of constellation points
6: $\{n_i\}_{i=0}^{c/2-1} = C_i - C_{i+c/2}$
7: $S = \sum_{i=0}^{c/2-1} |n_i|$
8: **while** $(|S| < S_{\text{th}}$ and $M > 0)$ **do**
9:      $l = m + 1$
10:     $m = l + l/2 - 1$
11:     $M = N - m$
12:     **if** $M < M_{\text{th}}$ **then**
13:         $M = 0$
14:         $m = N - 1$
15:     **end if**
16:     $X = [x_0, \dots, x_{l-1}, x_l, x_{l+1}, ..., x_m]$
17:     $\{C_i\}_{i=0}^{c-1} = \text{Categorize}(X)$
18:     $\{n_i\}_{i=0}^{c/2-1} = C_i - C_{i+c/2}$
19:     $S = \sum_{i=0}^{c/2-1} |n_i|$
20:     $S_{\text{th}} = N - (m+1)/2$
21: **end while**
22: **return**

Figure 5.21. Algorithm for determining number of NDB subcarriers for a QPSK modulated OFDM transmitter.

NDB subcarriers would be needed to balance symbol distribution, so number of NDB subcarriers, M, is chosen to be $N/2$. Otherwise, another $N/4$ data bearing symbols are read and total sum is calculated. If the sum is greater than $N/8$, number of NDB subcarriers, M. is chosen to be $N/4$, else another $N/8$ data bearing symbols are read. The procedure continues until the number of NDB subcarriers is less than the predefined threshold M_{th}. In our previous work, we have shown that if the unbalance between BPSK symbols over 512 subcarriers is less than 5% of the total number of subcarriers, mean increase in PAPR due to

125

1: $X = [x_0, x_1, ..., x_{N-1}], \ x_k \in \{\pm 1, \pm j\}$
2: $S = \sum_{i=0}^{c/2-1} n_i$
3: **if** $M > 0$ **then**
4:     **if** $S \neq M$ **then**
5:         **for** $i = 0$ to $c/2 - 1$ **do**
6:             $n_i = \lfloor n_i \cdot M/S \rfloor$
7:         **end for**
8:     **end if**
9:     **for** $i = 0$ to $c/2 - 1$ **do**
10:         **if** $n_i < 0$ **then**
11:             $d_i^k = \mathbb{C}_i \ k = 1, 2, \ldots, |n_i|$
12:         **else if** $n_i > 0$ **then**
13:             $d_i^k = \mathbb{C}_{i+c/2} \ k = 1, 2, \ldots, |n_i|$
14:         **end if**
15:     **end for**
16:     $d = [d_0, d_1, \ldots, d_{c/2-1}]$
17:     Modified frame, $X = [x, d]$
18: **end if**
19: **return**

Figure 5.22. Algorithm for determining symbols over NDB subcarriers for a QPSK modulated OFDM transmitter.

the unbalance is not significant [119].

5.5.2.2 Defining Symbols per NDB Subcarriers

As explained earlier, sequences giving high PAPR tend to have a highly biased signal distribution. Proposed algorithm determines the symbols over NDB subcarriers to balance the subcarrier signal constellation distribution.

If the number of NDB subcarriers, M, is greater than zero, then the algorithm determines the symbols over the subcarriers to balance the symbol distribution over the frame. Since n_i represents the balance of i-th constellation point. The sum S is the total number of NDB subcarriers which will be needed to perfectly

balance the symbol distribution. If the sum is greater than available number of NDB subcarriers, M, the values of the n_i are scaled down, so as to use only M NDB subcarriers. Positive n_i implies that there are more $\mathbb{C}_i$ than $\mathbb{C}_{i+m/2}$, so the values of $|n_i|$ $\mathbb{C}_{i+m/2}$ need to be added to the frame in order to balance the symbol distribution and vice-versa. The NDB subcarriers are appended to the data bearing subcarriers, so that the receiver only needs to know the number of NDB subcarriers for correct demodulation. The proposed algorithm is combined with an interleaving technique to randomize the input data sequence and break long correlation patterns.

Symbols over NDB subcarriers are used only for PAPR reduction and do not carry any information. Therefore, symbols over NDB subcarriers can be discarded after FFT stage at the receiver, unlike the conventional PTS and SLM methods. Therefore, the proposed method can greatly reduce the receiver system complexity and is independent of the error on symbols over NDB subcarriers. Moreover, number of NDB subcarriers can be adapted to the PAPR reduction requirements and unnecessary overhead on data transmission can be minimized.

5.5.3 Simulation Results

For simulation purposes, we considered QPSK modulated OFDM system with 256 subcarriers. To obtain CCDF plots of the PAPR, $100,000$ random OFDM samples were generated. First, we consider a fixed number of NDB subcarriers to minimize the PAPR.

When number of NDB subcarriers is assumed to be 8 out of total 256 subcarriers, the CCDF of the PAPR for OFDM signals obtained through simulations are presented in Figure 5.23. It is evident from Figure 5.23 that when the PAPR of
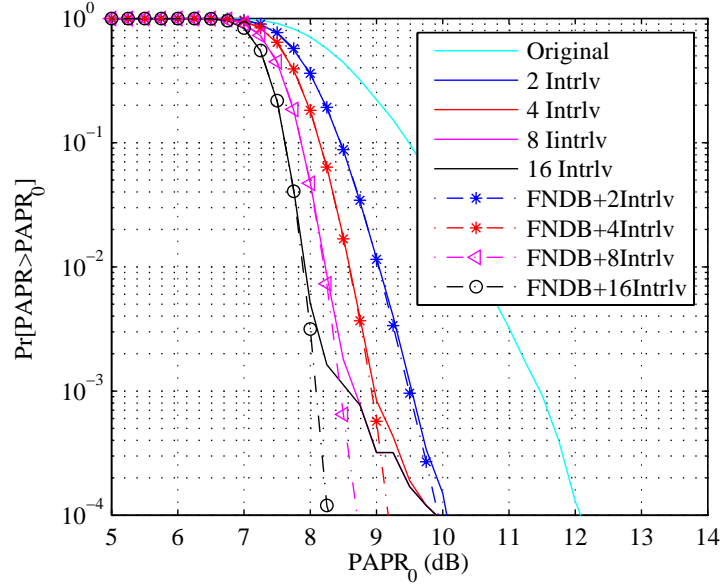
Figure 5.23. CCDF of QPSK-OFDM signal PAPR with 8 fixed NDB (FNDB) subcarriers out of 256 total subcarriers.

the input frame is high, the PAPR reduction with interleavers alone starts to saturate. However, the NDB subcarriers do contribute to the reduction of the PAPR and overcome the saturation point in the case of the interleavers alone. The NDB subcarriers do not contribute when the PAPR of the input sequence is small. In the case of a fixed number of NDB subcarriers, the throughput loss is constant even if these subcarriers are not used for PAPR reduction. On the other hand, if a small number of NDB subcarriers is chosen to minimize throughput loss, it would not be able to minimize the high PAPR values, since there would not be a sufficient number of NDB subcarriers to balance symbol distribution. Therefore, we employ the proposed algorithm for determining the number of NDB subcarriers on per frame basis to overcome the problem of unnecessary overhead.

When a variable number of NDB subcarriers is used, the CCDF of the PAPR of OFDM signals obtained through simulations are presented in Figure 5.24. It is

evident from the results that the PAPR reduction achieved with the proposed algorithm closely follows the reduction achieved with the interleavers alone for small values of PAPR. Moreover, the proposed algorithm is capable of overcoming the saturation in PAPR reduction and is able to reduce the PAPR when interleavers alone start to fail to reduce PAPR.

From simulation results, we observe the number of NDB subcarriers ranges from 0 to 25%, with a mean of approximately 6% and a standard deviation of approximately 7% of the total number of subcarriers. Therefore, throughput loss due to NDB subcarriers for PAPR reduction is kept to a minimum required for PAPR reduction. As the number of NDB subcarriers can be varied, the algorithm is capable of reducing moderate to high levels of PAPR. Moreover, the proposed algorithm is simple, non-iterative, and can be extended to any modulation scheme. Since the number of NDB subcarriers is variable, the reduction in throughput can be tailored according to the PAPR reduction requirements.

Even though, the PAPR minimization by using fixed or variable number of NDB subcarriers are not significantly different in the simulation results, it is intuitive that the PAPR minimization would be limited in case of fixed number of NDB subcarriers, whereas variable number of NDB subcarriers will always be able to reduce the PAPR of even highly correlated input data frame.
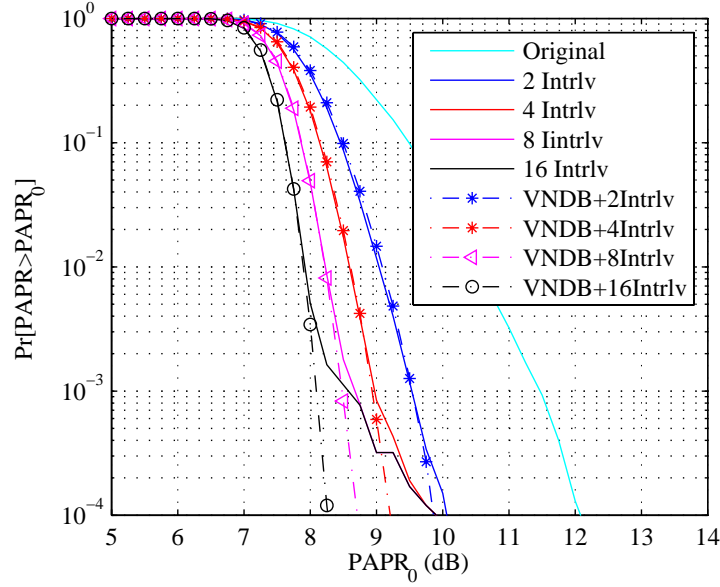
Figure 5.24. CCDF of QPSK-OFDM signal PAPR with variable NDB (VNDB) subcarriers.

5.6 Low Correlation Phase Sequences for PAPR Reduction[16]

A technique has been proposed in the literature for determining suboptimum phase adjustment factors using Newman phase sequences in order to reduce the PAPR of an OFDM signal by the SLM-based technique [131]. However, in this approach, each phase adjustment involves a complex multiplication, which can be a bottleneck for the SLM-based technique. In this section, we present a novel technique for finding the suboptimal phase sequences in order to reduce the PAPR using low correlation Schroeder phase sequences [96]. In the proposed algorithm, the phase adjustments can be carried out without any multiplications. The main concept is to generate several phase adjustment factors based on low correlation phase sequences for randomly generated data sequences and use the phase adjust-

---

[16]The work has been submitted to *IEEE Communication Letters* [130].
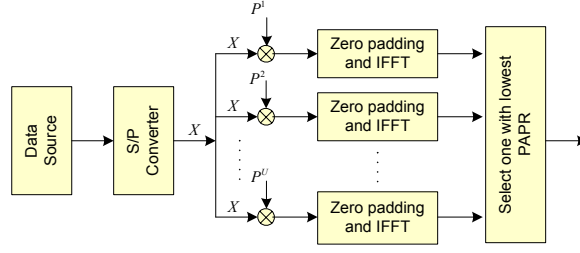
Figure 5.25. Schematic of OFDM transmitter with proposed PAPR reduction technique.

ment factors to update an OFDM signal in order to minimize its PAPR value.

5.6.1 OFDM System and Peak to Average Power Ratio

A block diagram of an OFDM transmitter with an SLM-based PAPR reduction technique is shown in Fig. 5.25. First, a serial data stream from the data source is converted into N parallel data streams using a serial-to-parallel (S/P) converter. Following the S/P conversion, the parallel data stream X is replicated into U copies. Then, U sets of phase adjustment terms $\mathbf{P}^u$, $u = 1, 2, \ldots, U$ are applied to the data and the inverse fast Fourier transform (IFFT) is calculated. The OFDM symbol having the lowest PAPR value is chosen for transmission. Moreover, the information about the corresponding phase adjustment factors is transmitted to the receiver for correct demodulation of the OFDM symbol.

5.6.2 Selected Mapping Technique

In an SLM approach, U sets of statistically independent phase adjustment terms $\mathbf{P}^u = [P_0^u, P_1^u, \ldots, P_{N-1}^u]^T$ with $P_n^u = e^{j\phi_n^u} \in [0, 2\pi)$, $n = 0, 1, \ldots, N-1$, $u = 1, 2, \ldots, U$ are generated. These phase adjustments are applied to a data sequence $\mathbf{X}$ and the resulting sequence with the lowest PAPR is chosen for transmission. If the phase adjustment factors are restricted to W terms, an optimal phase sequence

could be found from W^{N-1} different combinations. Several iterative techniques have been proposed in literature for finding the phase sequence restricted to $\{0, \pi\}$, also known as 'sign flipping method' [48,132]. In the following section, we propose a novel technique for finding the phase adjustment factors in order to reduce the PAPR of an OFDM signal.

5.6.3 Proposed Algorithm

Binary or polyphase sequences with large out-of-phase aperiodic correlation values can result in signals with large PAPR values[17]. Therefore, sequences giving high PAPR tend to have a high number of a particular subcarrier signal constellation. In SLM based techniques, the phases of the sequences are adjusted so as to break the long correlation patterns and reduce the PAPR of the signal.

5.6.3.1 Low Correlation Phase Sequences

We consider following low correlation Schroeder phase sequences to use in the SLM-based PAPR reduction technique:

Schroeder phase Schroeder phase sequence is expressed as [96]:

$$\phi_k = \frac{\pi k^2}{N} \quad \text{where, } k = 0, 1, \ldots, N-1 \tag{5.15}$$

The PAPR of the above sequence is 2.56 dB for $N = 256$.

Restricted Schroeder phase When the phase angles are restricted to 0 and π, it yields the binary sequence with low autocorrelation, and the phase sequence

---

[17]It follows from the fact that low out-of-phase aperiodic correlation values of binary or polyphase sequences results in a small value of the PAPR of the signal [68,69].

can be expressed as [96]:

$$\phi_k = \pi \left\lfloor \frac{k^2}{2N} \right\rfloor_{\text{mod } 2} \qquad \text{where, } k = 0, 1, \ldots, N-1 \qquad (5.16)$$

where 'mod 2' represents the 'modulo 2' operation. The PAPR of the above sequence is 4.89 dB for $N = 256$.

5.6.3.2 Proposed Phase Sequences for SLM Technique

In the proposed scheme, the main idea is to generate the phase adjustment terms such that the transmit sequence phase distribution are as close as possible to Schroeder phase sequence. As a result, the transmit sequence would exhibit low PAPR values. Suppose a random input data sequence is expressed as:

$$A_k = |A_k|\angle\alpha_k = |A_k| \cdot e^{j\alpha_k} \qquad (5.17)$$

then, the phase adjustment factors required to yield the Schroeder phase is given by:

$$\gamma_k = \phi_k - \alpha_k \qquad (5.18)$$

and the u-th phase adjustment vector is given by $P_k^{(u)} = \gamma_k \quad \forall k$.

Using Scroeder phase sequence, U sets of phase adjustment factors, P^u, $u = 1, 2, \ldots, U$, are precomputed for randomly generated data vectors. These sets of phase adjustment factors are applied to input data vectors and the set yielding minimum PAPR is selected. The information about the used phase adjustment factors is transmitted to the receiver for correct demodulation.

The phase adjustment factors can be generated using Schroeder phase se-

quences, which take values $[0, 2\pi)$. Therefore, each phase adjustment would require a complex multiplication. To avoid this complex multiplication, we propose to use Schroeder phase angles which are restricted to 0 and π. If the random input data sequence A_k in Eq. (5.17) is chosen from the symbol constellation used by the system, the phase adjustment factors would rotate the symbol yielding another symbol in the constellation. So, the phase adjustments can be carried out simply by mapping the symbol to corresponding updated symbol from the same constellation. Since the phase adjustments do not require any multiplications, the savings in SLM computations can be significant for large values of U, given that the phase adjustments need to be made for each OFDM symbol.

If Schroeder phase angles are restricted to 0 and π and the random input data sequence A_k in Eq. (5.17) is considered to consists of BPSK symbols, the resulting phase adjustment factors would also be restricted to 0 and π. These phase adjustment factors can be represented by the binary sequence consisting of ± 1. In this case, the phase adjustments can simply be implemented by flipping the sign of a symbol, which is similar to the sign-selection technique [132].

Moreover, the sign information can be embedded with the data so that side information would not be required and receiver can just discard the sign information, since it does not convey any information. However, this would reduce the throughput of the system by 1-bit per symbol i.e. by a factor 1/(M+1) for a M-ary PSK or QAM modulated system.

5.6.4 Simulation Results

For simulation purposes, an OFDM system with 256 subcarriers is used and $100,000$ QPSK modulated random OFDM samples were generated. A CCDF of

the PAPR of OFDM signals without phase updating and with phase updating, for different number of phase sequences, is presented in Fig. 5.26(a). From the figure, we observe the greater reduction in PAPR for larger number of phase sequences. However, the reduction is achieved at the cost of increased complexity, since the given data sequence needs to be updated with large number of phase sequences, PAPR needs to be computed, and the phase sequence yielding lowest PAPR needs to be chosen.

When the Schroeder phases are restricted to 0 and π, CCDF of PAPR is shown in Fig. 5.26(b). The PAPR minimization with the restricted Schroeder phases are slightly less as compared to that with original Schroeder phase factors. However, in this case, the phase adjustments can be made without any multiplications.

When both of the Schroeder phases and the phase adjustment factors are restricted to 0 and π, CCDF of PAPR is shown in Fig. 5.26(c). In this case, PAPR minimization is equivalent to the ones achieved with restricted Schroeder phase factors. Moreover, the complexity of the procedure is highly minimized since the phase adjustment can be implemented as flipping the sign of an signal.

5.7 PAPR Analysis for NC-OFDM signals[18]

Being a variant of OFDM, NC-OFDM also suffer from high PAPR problem. When the number of deactivated subcarriers is large compared to the number of active subcarriers, the common assumption of the input symbols being identically and independently distributed (i.i.d.) do not hold. This results in different statistical properties for the PAPR of NC-OFDM signals relative to that for OFDM signals. The conventional OFDM systems inherently assume a contiguous set of

---

[18]The work has been submitted to *66th IEEE Vehicular Technology Converence* [133].
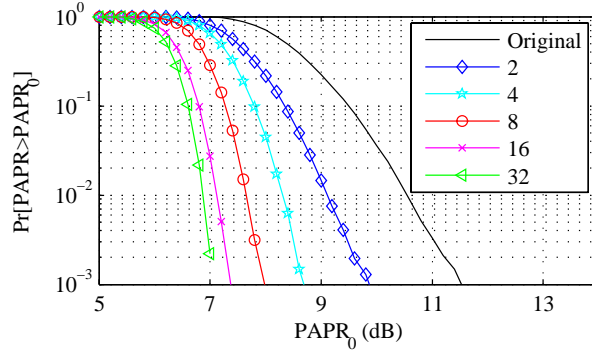
(a) Schroeder phase $[0, 2\pi)$.
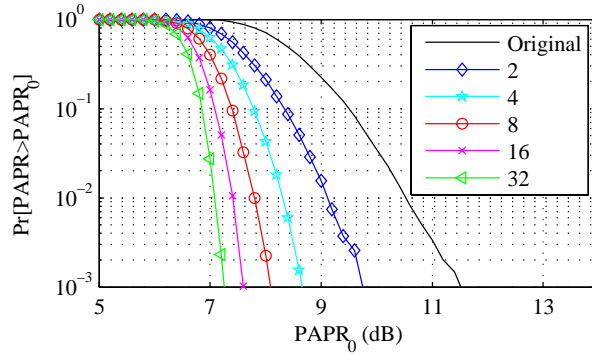
(b) Schroeder phase restricted to 0 and π.
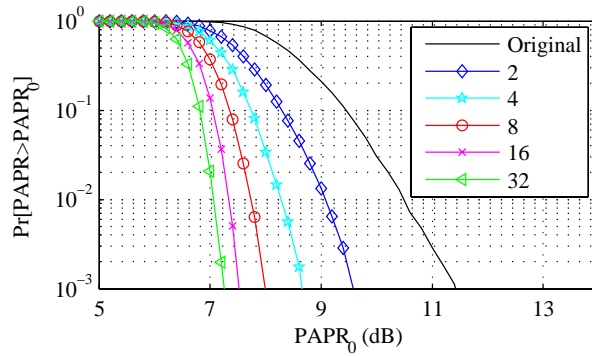
(c) Phase adjustment factors restricted to 0 and π.

Figure 5.26. CCDF of QPSK-OFDM signal PAPR with proposed SLM technique using U phase sequences.

subcarriers, whereas in NC-OFDM system, the active subcarriers are co-located with the occupied subcarriers. Thus, the PAPR reduction techniques proposed for the OFDM systems may need to be modified in order to avoid interfering with existing user transmissions. Moreover, the design requirements for PAPR reduction techniques would be different from that of conventional OFDM systems. In this section, we present statistical analysis of PAPR for NC-OFDM signals and elaborate the design requirements of the PAPR reduction techniques for the NC-OFDM signals.

5.7.1 Statistical Properties of PAPR

The *complementary cumulative distribution function* (CCDF) of the PAPR denotes the probability of an OFDM signal exceeds a given threshold [70]. It is the most frequently used parameter to characterize PAPR and also as performance measures for PAPR reduction techniques. In this section, we present the analysis of PAPR distribution of NC-OFDM signals, and the design requirements for the PAPR reduction techniques.

5.7.1.1 PAPR Distribution of an NC-OFDM Signal

Assume the total number of subcarriers, N, is large. Then, applying the central limit theorem (CLT), $s(n)$ can be modeled as a zero mean Gaussian distributed random variable with variance, $\sigma^2 = N_u \sigma_D^2 / N$, where N_u is number of active subcarriers and σ_D^2 is the variance of the input sequence [134]. Assuming the symbols are i.i.d., then by CLT, the real and imaginary parts of the N-point IFFT output have mutually independent Gaussian probability distribution function, $\mathcal{N}(0, \sigma^2)$.

The instantaneous power of baseband signal, $s(n)$, is given by:

$$\lambda = \Re\{s(n)\}^2 + \Im\{s(n)\}^2. \tag{5.19}$$

Therefore, the instantaneous power can be characterized as Chi-square distribution with two degrees of freedom [98]:

$$f(\lambda) = \frac{1}{\sigma^2} \exp\left(-\frac{\lambda}{\sigma^2}\right), \quad \lambda \geq 0. \tag{5.20}$$

So, the cumulative distribution function (CDF) is given by [98]:

$$Pr[\lambda < \lambda_0] = \int_0^{\lambda_0} f(\lambda) d\lambda \tag{5.21}$$
$$= 1 - e^{-\frac{\lambda_0}{\sigma^2}}.$$

If $E\{|x(n)|^2\}$ is normalized to unity, then the CCDF of the PAPR is given by:

$$Pr[\lambda > \lambda_0] = 1 - \left(1 - e^{-\frac{\lambda_0}{\sigma^2}}\right)^N. \tag{5.22}$$

However, this expression is not close to experimental results because the assumption made in deriving CCDF that the samples should be mutually uncorrelated is not true anymore when oversampling is used [99].

There has been several attempts to more accurately determine the distribution of the PAPR for OFDM signals. In [99], it was claimed that the approximated CCDF for large N is given by:

$$Pr[\lambda > \lambda_0] \approx 1 - \left(1 - e^{-\frac{\lambda_0}{\sigma^2}}\right)^{\alpha N} \tag{5.23}$$

where $\alpha = 2.8$. This approximation is fairly close to the experimental results when the number of active subcarrier is large i.e. $N \geq 64$.

In the following paragraphs, the PAPR analysis for the NC-OFDM system, with three different location distributions of the active subcarriers, are presented.

Contiguously-spaced Active Subcarriers – When the active subcarriers are contiguously spaced along with deactivated subcarriers as shown in Fig. 5.27(a), the data over the active subcarriers is given by:

$$
A_k = \begin{cases} 0 & \text{for } k = 0, 1, \ldots, n_1 \\ x_k & \text{for } k = n_1, n_1 + 1, \ldots, n_2 \\ 0 & \text{for } k = n_2, n_2 + 1, \ldots, N \end{cases} \tag{5.24}
$$

where x_k represents a data symbol, for example, $x_k \in \{\pm 1, \pm j\}$ for QPSK signalling, and subcarriers through n_1 to n_2 are active. The effect of the deactivated subcarriers is equivalent to zero padding i.e. it improves the time resolution of the original OFDM signal. Due to the locations of the zeroes, the NC-OFDM subcarriers would appear as the frequency-shifted version of the original OFDM subcarriers which would result in phase-shifted NC-OFDM signal in time-domain. However, the PAPR remains unchanged [92].

Regularly-spaced Active Subcarriers – When the active subcarriers are regularly spaced as shown in Fig. 5.27(b), the data over the active subcarriers is given by:

$$
A_k = \begin{cases} x_k & \text{for } k = 0, m, \ldots, N \\ 0 & \text{otherwise} \end{cases} \tag{5.25}
$$

139

(a) Contiguous Active Subcarriers.

(b) Regularly Spaced Active Subcarriers.
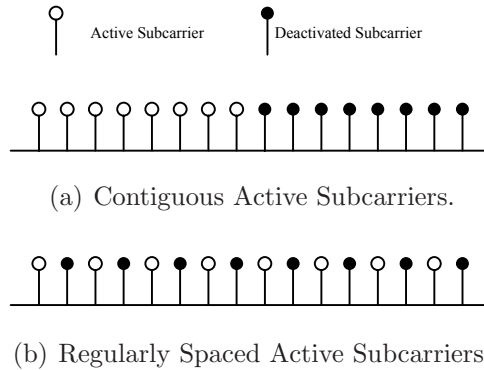
Figure 5.27. Subcarrier Distribution.

where m represents the subcarrier spacing. The NC-OFDM contains the copies of the signal equal to the number of zeroes[19]. For example, when there are $m-1$ deactivated subcarriers between any two consequtive active subcarriers, then the time-domain NC-OFDM signal contains m copies of the original OFDM time-domain signal. Therefore, only a portion of the time-domain signals, i.e. N/m, would be needed to estimate the PAPR of the signal. However, this also does not have any effect on the PAPR of the signal.

Randomly-spaced Active Subcarriers – When the number of active subcarriers is significantly smaller than the total number of subcarriers in NC-OFDM system, the common assumption of input symbols being i.i.d. is not valid. Moreover, the random locations of the nulled subcarriers (or zeros) can significantly alter the addition and subtraction of symbols relative to other active subcarrier configurations yielding different peak values for the same symbols modulated over the active subcarriers. Therefore, the CCDF of the PAPR for NC-OFDM signals would be different from OFDM.

---

[19]It is intuitively straightforward from the bufferfly structure of the IFFT block [92].

Maximum PAPR of an NC-OFDM Signal $-$ It is known that the PAPR of an MPSK OFDM signal is always less than or equal to N, where N is the total number of subcarriers [70]. Note that in OFDM, all of N subcarriers are active. Now, consider the NC-OFDM signal in Eq. (4.1) with p active subcarriers, where the input data symbols are chosen from an MPSK constellation such that $|A_k| = 1$. The peak power of the NC-OFDM signal is given by [70]:

$$
\begin{aligned}
\max_{0 \leq t \leq T} |s(t)|^2 &= \max_{0 \leq t \leq T} \left| \frac{1}{\sqrt{N}} \sum_{k=0}^{N-1} A_k e^{j2\pi kt/T} \right|^2 \\
&\leq \left(\frac{1}{\sqrt{N}} \sum_{k=0}^{N-1} \max |A_k| \right)^2 \\
&\leq \frac{p^2}{N}.
\end{aligned}
\tag{5.26}
$$

Using the Parseval's relationship the average power of the NC-OFDM signal is given by [98]:

$$
\begin{aligned}
E\{|s(t)|^2\} &= E \left\{ \left| \frac{1}{\sqrt{N}} \sum_{k=0}^{N-1} A_k e^{j2\pi kt/T} \right|^2 \right\} \\
&= \frac{1}{N} \sum_{k=0}^{N-1} \{E|A_k|^2\} \\
&= \frac{p}{N}.
\end{aligned}
\tag{5.27}
$$

Then, the PAPR of the NC-OFDM signal is given from Eq.(4.2) as follows:

$$
\begin{aligned}
\text{PAPR}(s(t)) &= \frac{\max\limits_{0 \leq t \leq T} |s(t)|^2}{E\{|s(t)|^2\}} \\
&\leq \frac{p^2/N}{p/N} \\
&\leq p.
\end{aligned}
\tag{5.28}
$$

Therefore, the maximum value of PAPR for the MPSK modulated NC-OFDM signal with p active subcarriers is equal to p, regardless of the total number of subcarriers N.

5.7.1.2 Design Requirements of PAPR Reduction Techniques for NC-OFDM Signal

The conventional PAPR reduction techniques for OFDM systems inherently assume a contiguous set of subcarriers. Therefore, PAPR reduction techniques proposed for OFDM systems would need to be adapted to a system employing NC-OFDM. In spectrum opportunistic systems, the active subcarriers are co-located with the occupied subcarriers. As a result, both intersymbol interference (ISI) and intercarrier interference (ICI) may cause distortion in the primary user transmissions. Therefore, time-domain-based or distortion-based techniques, such as clipping and filtering [72], and frequency domain-based techniques assuming contiguous subcarriers, such as coding [78], cannot be used for reducing PAPR of NC-OFDM signals. However, frequency-domain PAPR reduction techniques are better suited, since it is easier to sort out the nulled subcarriers avoiding any interference to existing user transmissions. The techniques, such as interleaving [112], SLM [79], and PTS [80], need to be aware of the locations of the active

subcarriers. Moreover, in a dynamic spectrum access network, the total number of active subcarriers and their locations might change continuously and the PAPR reduction techniques should be able to adapt to these changes.

5.7.2 Simulation Results

If the number of active subcarriers is equal to the total number of possible orthogonal subcarriers over a given bandwidth, NC-OFDM system is equivalent to the OFDM system. When the fraction of null carriers increases, the PAPR distribution starts to differ from the conventional PAPR distribution.

To study the effect of null carriers in the PAPR of an NC-OFDM signal, we consider 500,000 randomly generated QPSK symbols, modulate them over randomly placed active subcarriers co-located with different number of deactivated subcarriers, and calculate the PAPR of the NC-OFDM signal. In Fig. 5.28(a), we present the CCDF of PAPR with the fixed number of active subcarriers and different numbers of deactivated subcarriers. From the results, we observe that the probability of occurrence of high PAPR increases with the increase the total number of subcarriers, for a given number of active subcarriers. In Fig. 5.28(b), we show the CCDF of PAPR for various number of active subcarriers, while the total number of subcarriers are kept constant. The CCDF of PAPR shows the probability of getting high PAPR increases with the increase in the number of active subcarriers, even though the total number of subcarriers is kept constant.

The mean and standard deviation of the PAPR of an NC-OFDM signal with fixed number of active subcarriers is shown in Table 5.1. From the results, we observe that as the total number of the subcarriers increases, the value of the mean PAPR also increases, whereas the value of the standard deviation decreases, even
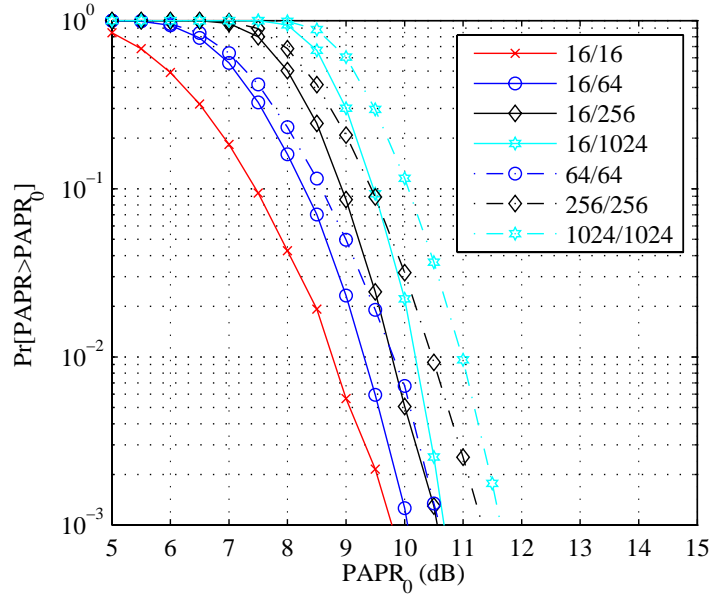
(a) Fixed number of active subcarriers.
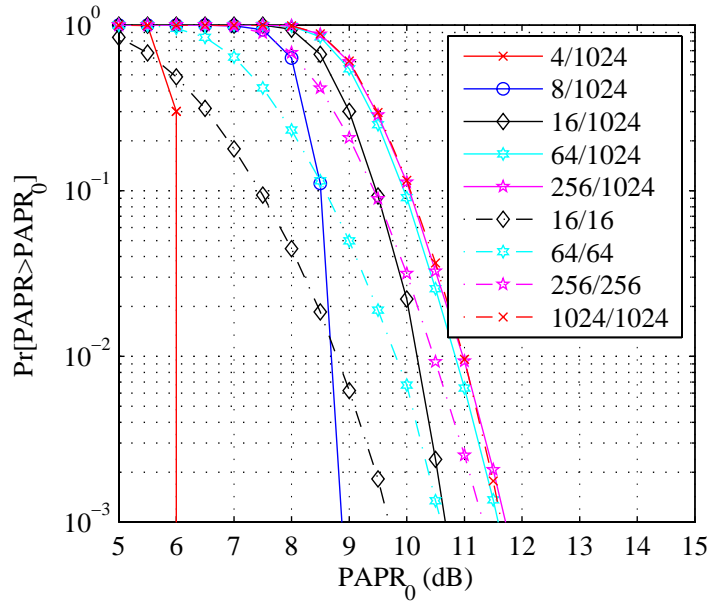
(b) Fixed number of total subcarriers.

Figure 5.28. CCDF of PAPR for random location distributions of active subcarriers, where c_a/c_t is ratio of the number of active subcarriers over the total number of subcarriers.

Table 5.1. Mean and standard deviation of the PAPR of an NC-OFDM signal*

	16/16	16/64	16/256	16/1024
mean (in dB)	7.8238	8.5624	9.0650	9.4260
std. dev.	1.043	0.8303	0.664	0.5350
worst-case PAPR	16	16	16	16

*c_a/c_t is ratio of the number of active subcarriers over the total number of subcarriers.

though the number of active subcarriers is kept constant. It is also observed that the highest value of PAPR is equal to the number of active subcarriers. Although the probability of occurrence of high PAPR depends upon the total number of subcarriers, the upper-bound in PAPR is determined by the total number of active subcarriers.

From simulation results, we demonstrated the upper-bound in PAPR is determined by the total number of active subcarriers. The CCDF of PAPR shows the higher probability of getting large PAPR values in NC-OFDM system with the increase in the total number of subcarriers for a fixed number of active subcarriers as well as the increase in the number of active subcarriers for a fixed total number of subcarriers, while compared to the conventional OFDM for the same information rate. Therefore, PAPR minimization is more important in NC-OFDM systems as compared to OFDM.

5.8 Chapter Summary

Large values of peak-to-average power ratio of OFDM signal is one of the major issues in its implementation. In this chapter, we proposed several PAPR reduction techniques as well as the statistical analysis of the PAPR for NC-OFDM

signals.

In Section 5.2, we proposed a practical phase updating algorithm for reducing the PAPR. The algorithm can achieve an adequate reduction in PAPR, while ensuring a manageable amount of overhead information. We also proposed a robust technique for grouping the phase adjustment over several subcarriers for improving the system throughput. Compared with other techniques, the proposed algorithm achieves a balance between PAPR reduction and reasonable transmission overhead.

In Section 5.3, we presented a novel algorithm for the reduction of PAPR. The algorithm adaptively selects the appropriate approach to achieve the largest possible decrease in PAPR, given the available PAPR reduction approaches. In this work, we employed two PAPR reduction approaches: (1) interleaving, and (2) subcarrier phase adjustment. The results show when the approaches are employed across a wide range of operating conditions, they only achieve substantial performance gains for a small subset of cases. However, "gear-shifting" between approaches achieves much better results across a wider range of scenarios.

In Section 5.4, we propose a novel subcarrier power adjustment algorithm for PAPR reduction that does satisfy spectrum regulation requirements. The proposed algorithm achieves large reduction in PAPR at the cost of slight degradation in aggregate BER performance of the system. The primary advantage of the proposed algorithm is that no overhead information needs to be transmitted to the receiver when the OFDM transceiver employs M-ary PSK modulation. Therefore, no throughput loss and no additional processing are required at the receiver side.

In Section 5.5, we proposed a novel non-iterative algorithm for utilizing NDB subcarriers to reduce the peak-to-average power ratio of an OFDM signal. The

number of NDB subcarriers can either be kept constant at a predefined value or the proposed algorithm determines the number of NDB subcarriers and symbols over these subcarriers to reduce PAPR to a large extent for both moderate to high PAPR values. The proposed adaptive algorithm ensures that unnecessary throughput reduction due to NDB subcarriers can be kept to a minimum required for PAPR reduction. Additionally, BER performance of the system is independent of the error in the NDB subcarriers, since they do not carry any information. So, the proposed PAPR reduction algorithm is robust towards error in the NDB subcarriers.

In Section 5.6, we present a comparative study of using various low correlation sequences for SLM-based PAPR minimization. With a large number of phase sequences, SLM and PTS techniques can provide improved PAPR reduction at the expense of additional complexity. In this section, we also proposed new algorithms for determining phase adjustment factors for SLM techniques. Based on the simulation results and analysis, we find restricted Schroeder phase sequences are less complex and easily implemented, since the phase adjustments can be made without any complex multiplications. Moreover, when the phase correction factors are restricted to 0 and π, the side information does not need to be transmitted to the receiver, while maintaining similar PAPR reduction as compared to the one achieved with restricted Schroeder phase sequences.

In Section 5.7, a statistical analysis of PAPR for NC-OFDM system has been presented. We demonstrated that the probability of obtaining high PAPR increases with the number of total subcarriers, even if the total number of active subcarriers is kept constant. Therefore, the importance of PAPR reduction techniques is much higher in NC-OFDM as compared to OFDM for the same data

rate, when the number of deactivated subcarriers is quite large.

In this chapter, we presented five novel algorithms for PAPR reduction for OFDM and NC-OFDM signals. Moreover, design requirements as well as PAPR characteristics of NC-OFDM signal are elaborated.

Chapter 6

An Efficient Implementation of NC-OFDM Transceivers for Cognitive Radios†

6.1 Introduction

In the implementation of an OFDM transceiver, the fast Fourier transform (FFT) algorithm is employed to make modulation and demodulation highly efficient in terms of hardware and computational complexity [30]. However, an NC-OFDM may have several subcarriers that are deactivated, i.e., zero-valued inputs. Thus, the hardware resources of the FFT are not fully being exploited. Therefore, a new approach is needed to efficiently implement the FFT when several subcarriers are deactivated.

It has been shown that for situations in which the relative number of zero-

valued inputs is quite large, significant time savings can be obtained by "pruning" the FFT algorithm[1] [135]. Several algorithms have been proposed in literature for enhancing the efficiency of the FFT algorithm based on decimation-in-time (DIT) and decimation-in-frequency (DIF) algorithms [136–143]. However, most of these algorithms are suitable only for systems with specific zero-input pattern distributions. Furthermore, algorithms that prune the FFT for any zero-input pattern do not yield an efficient implementation with respect to computational time [136].

In this chapter, we present an FFT pruning algorithm designed for NC-OFDM transceivers. The proposed algorithm can quickly design an efficient FFT implementation for any zero-input pattern. The performance of the proposed algorithm is compared with several other algorithms proposed in the literature with respect to mean execution time.

6.2 NC-OFDM Framework

A general schematic of an NC-OFDM transceiver is shown in Figure 2.9. For an overview of the NC-OFDM framework, please refer to Section 2.5.1.

6.3 FFT Pruning Technique

In a wide-band communication system, a large portion of frequency channels may be occupied by other transmissions, whether incumbent or other unlicensed users. As a result, these subcarriers are off-limits to our transceiver. Thus, to avoid

---

[1] *FFT pruning* refers to the procedure for improving the efficiency of the fast Fourier transform by removing operations on input values which are zeroes, and on output values which are not required [135].
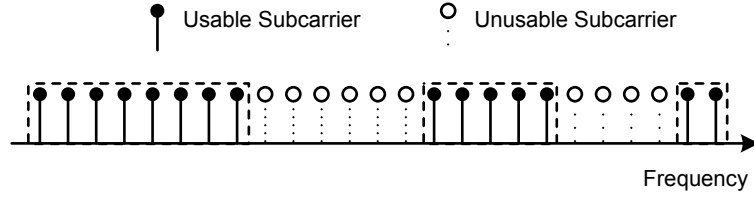
Figure 6.1. Subcarrier distribution over wideband spectrum

interfering with these other transmissions, the subcarrier within their vicinity are turned off, or *nulled*, as shown in Figure 6.1. For the FFT and IFFT blocks, these null subcarriers are represented as zero-valued inputs. For highly sparse available frequency spectrum, the number of zero-valued inputs in the FFT may be significant relative to the total number of the usable subcarriers. When the relative number of zero-valued inputs is quite large, significant time saving can be obtained by pruning the FFT algorithm.

For instance, an 8-point DIF FFT butterfly structure is shown in Figure 6.2, where a_i represents the ith input signal to the FFT block. Suppose the incumbent users are located at subcarriers a_1, a_5, a_7 and a_8. Therefore, input data over all these carrier must always be zero. For a conventional FFT algorithm, the total number of multiplications and additions would be $N \log_2 N$. However, with an FFT pruning algorithm, the unnecessary multiplications and addition operations at the stages b_1 and b_5 can be pruned as their values will always be zeroes. Moreover, multiplications and additions at nodes $b_3, b_4, b_7,$ and b_8 can be replaced with simple 'copy' operation, whereas addition operations in nodes $c_1, c_3, c_5,$ and c_7 can be pruned to save the FFT computation time. Therefore, the FFT computation time can be significantly improved with partial and complete pruning.

In wideband communication systems, the channel conditions and ISO varies over time. Thus, the FFT pruning algorithm should be able to design an efficient

151
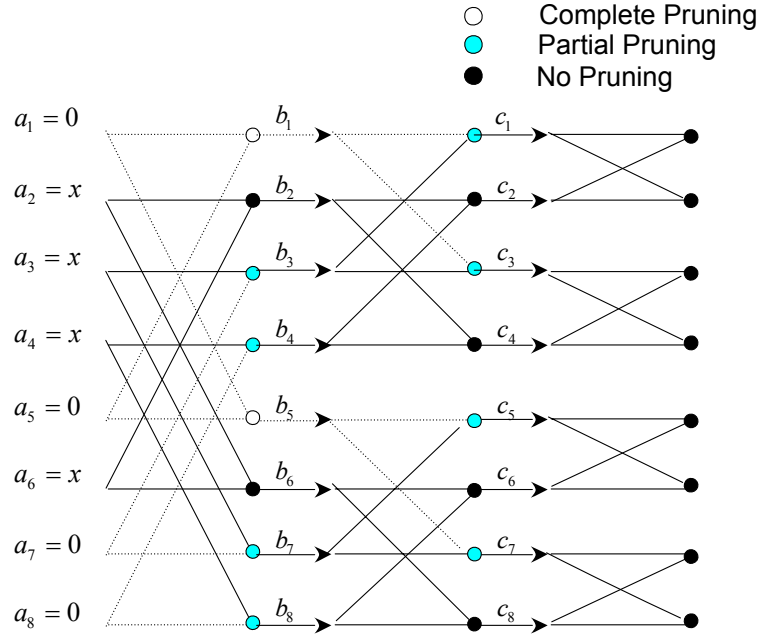
Figure 6.2. FFT butterfly structure. A value of '0' denotes a zero-valued subcarrier and 'x' denotes a data bearing subcarrier. The dotted lines represent the computations that can be pruned.

FFT implementation every time the channel condition and ISO changes.

6.3.1 General FFT Pruning Algorithm

Alves *et al.* proposed an FFT pruning algorithm that operates on any zero-valued input distribution [136]. Suppose we have a radix-2 FFT algorithm with N levels (2^N FFT points). A matrix M_i, with N columns and 2^N rows is generated using Algorithm 6.3. Each element of the matrix corresponds to a addition/multiplication node of the FFT flow graph. The node needs to be computed if the corresponding element in the matrix M_i is non-zero. On the other hand, if the element of the matrix is zero, the corresponding node does not need to be computed. For instance, the matrix M_i for the FFT butterfly structure in

Figure 6.2 would be:

$$M_i = \begin{pmatrix} 0 & 1 & 1 \\ 1 & 1 & 1 \\ 1 & 1 & 1 \\ 1 & 1 & 1 \\ 0 & 1 & 1 \\ 1 & 1 & 1 \\ 1 & 1 & 1 \\ 1 & 1 & 1 \end{pmatrix}.$$

To obtain the matrix M_i, a subcarrier input vector with 2^N elements, where each element of this vector correspond to each input element. If the input element is nonzero, the corresponding vector element will be unity, and if the input element is zero, the corresponding vector element will be zero. By using this input vector, we can compute the first column of the matrix M_i. In turn, by using the first column of the matrix M_i, second column of matrix M_i can be obtained, and so forth. The algorithm to obtain the matrix M_i is presented in Algorithm 6.3.

Note that the FFT pruning algorithm proposed by Alves *et al.* uses conditional statements [136]. However, it is known that time to execute the conditional statement often exceeds the savings obtained by the fewer operations [144]. Therefore, we propose a re-indexing algorithm and modified FFT pruning algorithm to avoid using the conditional statements and reduce FFT computation times.

6.4 Proposed Algorithm

To save execution time, the proposed algorithm builds upon the previous algorithm by avoiding the use of conditional statements. The proposed FFT pruning

153

function M_i=generateMi(m,ivector)

1: $n = 2^m$
2: $M_i = zeros(n, m)$
3: **for** $l = 1$ to m **do**
4:     $shift1 = 2^{(m-l)}$
5:     $shift2 = 2 \times shift1$
6:     **for** $j = 1$ to $shift1$ **do**
7:         **for** $k = shift2 : shift2 : n$ **do**
8:             $j1 = k - shift1 - j + 1$
9:             $j2 = j1 + shift1$
10:            $j1 = k - shift1 - j + 1$
11:            $j2 = j1 + shift1$
12:            **if** $l == 1$ **then**
13:                **if** $ivector(j1) == 1$ **then**
14:                    $M_i(j1, l) = 1$
15:                    $M_i(j2, l) = 1$
16:                **end if**
17:                **if** $ivector(j2) == 1$ **then**
18:                    $M_i(j2, l) = 1$
19:                    $M_i(j1, l) = 1$
20:                **end if**
21:            **else**
22:                **if** $M_i(j1, l-1) == 1$ **then**
23:                    $M_i(j1, l) = 1$
24:                    $M_i(j2, l) = 1$
25:                **end if**
26:                **if** $M_i(j2, l-1) == 1$ **then**
27:                    $M_i(j2, l) = 1$
28:                    $M_i(j1, l) = 1$
29:                **end if**
30:            **end if**
31:        **end for**
32:    **end for**
33: **end for**
34: **return** M_i

Figure 6.3. Generate M_i (proposed by Alves *et al.* [136])

algorithm is shown in Algorithm 6.4. The algorithm is based on Cooley-Tukey divide-and-conquer algorithm that uses in-place computation [145]. For a radix-2 FFT, Cooley-Tukey algorithm divides the problem size into two interleaved halves

with each recursive stage. This manner of computation requires the computations proportional to $N \log_2 N$, whereas the equivalent discrete Fourier transform (DFT) would require the computations proportional to N^2. In this work, the proposed algorithm operates in the similar manner. Additionally, the proposed algorithm prunes the unnecessary multiplication and addition operations at the nodes in the FFT flow graph, in order to reduce the execution time for the FFT computations.

First, the matrix M_i similar to the one in Section 6.3.1 is calculated, where each element of the matrix corresponds to a node of the FFT flow graph. Suppose we have a radix-2 algorithm with N levels (2^N FFT points). Then, the matrix M_i has N columns and 2^N rows. Second, information in the matrix M_i is processed to the matrix M_{index}, where indices and the total number of nonzero elements in each column of the matrix M are recorded. To obtain the matrix M_{index}, we employ Algorithm 6.5. The matrix M_{index} has N columns and $2^N + 1$ rows. For the example in Figure 6.2, the matrix M_{index} would be:

$$
M_{\text{index}} = \begin{pmatrix}
6 & 8 & 8 \\
2 & 1 & 1 \\
3 & 2 & 2 \\
4 & 3 & 3 \\
6 & 4 & 4 \\
7 & 5 & 5 \\
8 & 6 & 6 \\
0 & 7 & 7 \\
0 & 8 & 8
\end{pmatrix}.
$$

The first row of the matrix M_{index} tells the number of nodes and the column of

```
 1: m = 10
 2: n = 2^m
 3: i = √(−1)
 4: for l = 1 to m do
 5:     le = 2^(m+1−l)
 6:     le_2 = le/2
 7:     u = 1
 8:     w = cos(π/le_2) − sin(π/le_2) × i
 9:     for j = 1 to le_2 − M_index(1, l) do
10:         for ii = 1 to M_index(j + 2, l) − M_index(j + 1, l) − 1 do
11:             u = u × w
12:         end for
13:         for k = M_index(j + 2, l) to n do
14:             ip = k + le_2
15:             t = x(k) + x(ip)
16:             x(ip) = (x(k) − x(ip)) × u
17:             x(k) = t
18:             k = k + le
19:         end for
20:         u = u × w
21:     end for
22: end for
```

Figure 6.4.   Proposed FFT Pruning Algorithm

the matrix M_{index} provides the indices of the nodes that needs to be calculated in each FFT stage. Proposed FFT pruning algorithm in Algorithm 6.4 uses information provided by M_{index} to prune unnecessary computations at the corresponding nodes, hence reducing the execution time for the FFT computation.

6.4.1 Simulation Results

For the simulations, $N = 1024$ BPSK-modulated subcarriers were employed. Mean execution time for the FFT operations for the original Cooley-Tukey algorithm, the algorithm by Alves *et al.*, and the proposed algorithm were compared

---

function M_{index}=generateindex(M_i)

1: $[n,m]$=size(M) % n rows, m columns
2: y=zeros(n,m)
3: **for** $j = 1$ to m **do**
4:    te=find($M(:,j)$)
5:    $y(1{:}\text{length}(te),j) = te$
6: **end for**
7: $y = [sum(M,1); zeros(1,m); y]$
8: $j = [1 : m]$
9: $y(1,:) = (n - y(1,:))./2^j$
10: **return** $M_{\text{index}} = y$

Figure 6.5. Proposed M_{index} Calculator

for 10,000 random data inputs, with the range of sparseness factor[2] from $0 - 99\%$.

In Figure 6.6, the mean execution times for the three FFT algorithms are presented for the case of 1024-point FFT. We observe significant reduction in the mean execution time for calculating the FFT with the proposed algorithm as compared to the conventional Cooley-Tukey algorithm for the sparseness factor of 60% or higher. On the other hand, for a sparseness factor of less than 60%, the proposed algorithm performs slightly worse. Moreover, we find the time to execute the conditional statements exceeds the savings obtained by the FFT pruning. We observe reduction in the mean execution times of the proposed algorithm for calculating the 1024-point FFT with increase in the sparseness factor. However, the mean execution time of Cooley-Tukey algorithm and Alves *et al.* algorithm remain relatively constant all the time.

In Figure 6.7, the mean number of multiplications employed by 1024-point FFT are presented for three FFT algorithms. We observe that the reduction in the multiplication and addition operations due to FFT pruning. The reduction in

---

[2] *Sparseness factor* simply denotes the fraction of the zeroes in a given data set.

157

addition and multiplication operations with the proposed algorithm is same as that achieved by Alves *et al.* algorithm. On the other hand, the proposed algorithm avoids using conditional statements. Therefore, the proposed algorithm achieves reduction in FFT computation time.

6.5 Why use large single FFT instead of multiple smaller FFTs?

Even though the multiple smaller FFTs would yield smaller complexities, the main issue with the cognitive radios employed in DSA environment is reconfigurability. In case of using the multiple smaller FFT blocks, the complexity of computation would be smaller. However, each FFT block needs to be modulated in different bands with different center frequencies, which would require the multiple number of oscillators (or additional processing) in the RF transceiver. This would also add the complexity.

Every time the channel conditions change, the usable spectrum bands would change. This would consequently require the change in the center frequencies, which would require adaptive oscillators. In this case, the reconfigurability can be a serious challenge.

6.6 Chapter Summary

In this chapter, we present a general FFT pruning algorithm for use in NC-OFDM transceivers to reduce the computation time or the resources for computing FFT or IFFT. The proposed algorithm can accept any zero-valued input distribution and prune the FFT to yield an implementation that results in a faster
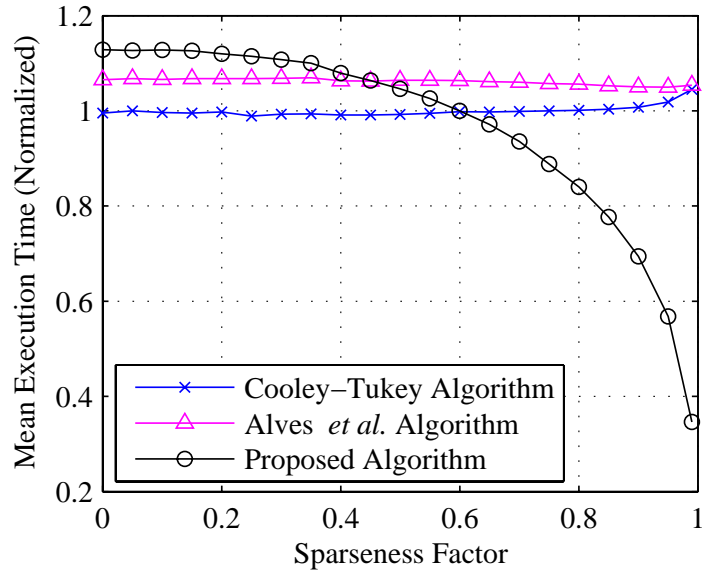
Figure 6.6. Mean execution times for 1024-point FFT employing the three FFT algorithms
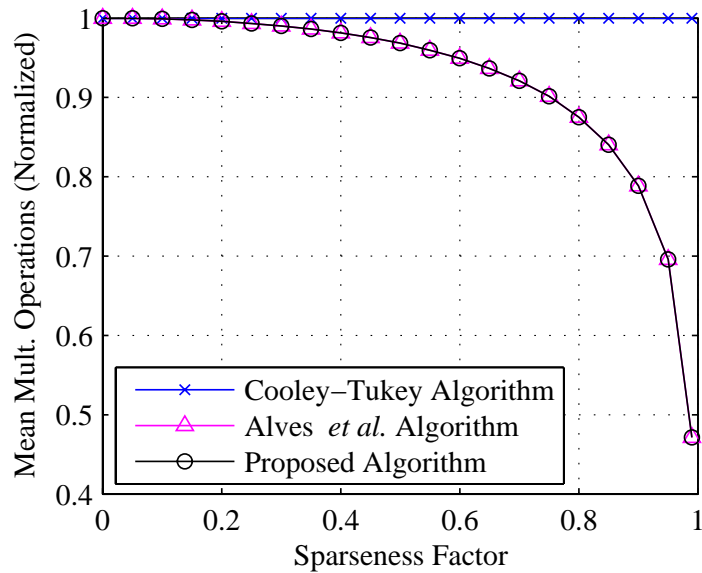
Figure 6.7. Mean number of addition and multiplication operations for different 1024-point FFT employing the three FFT algorithms

execution time. Given that the cognitive radio units employing NC-OFDM would need to quickly adapt to the changing operating environment, and that the hardware resources of small form factor cognitive radios are limited, such an algorithm

would be very beneficial.

Chapter 7

Conclusion

7.1 Research Achievements

Frequency spectrum is a limited resource. Most of the frequency spectrum has already been licensed. Moreover, with the regulations on put by the Government agencies and scarcity of the spectrum deems the importance of the communication which can utilize sparse frequency spectrum collectively for high data rate communications.

In this dissertation, a number of contributions have been made in the area of OFDM-based cognitive radios for DSA networks. The research achievements of this thesis are the following:

- A OFDM-based system framework for utilizing the non-contiguous subcarriers collectively, which is also termed as NC-OFDM, for high data rate transmissions is presented. The NC-OFDM technique can achieve the agility necessary for the secondary usage of a licensed frequency spectrum without interfering with the incumbent user transmissions. The performance of NC-OFDM technique is compared with an MC-CDMA technique which is

another popular multi-carrier technique.

- A detailed theoretical background, analysis, and characterization of PAPR properties as well as its theoretical bounds are presented. Moreover, an extensive survey and a taxonomy of PAPR reduction algorithms proposed in the literature are presented.

- Five novel algorithms for minimizing the PAPR value of an OFDM signal are presented. First, a subcarrier phase adjustment technique computes the subcarrier phase adjustment terms to minimize the PAPR value of an OFDM signal. Second, an adaptive-mode PAPR reduction algorithm chooses an interleaver based technique, phase adjustment technique, or combination thereof, to reduce the PAPR of an OFDM signal based on the current operating conditions. Third, the subcarrier power adjustment technique alters the subcarrier power levels obeying regulatory power requirements to minimize the PAPR values of an OFDM signal. Fourth, OFDM symbol design technique employs non-data bearing subcarriers to minimize PAPR values of an OFDM signal. A novel technique to compute the number and values of the non-data bearing subcarriers is presented. Fifth, a novel low correlation phase sequence technique can generate the phase adjustment factors, which can be as simple as flipping the sign of a symbol of the input sequence for an OFDM signal to minimize its PAPR value.

- Characteristics of PAPR for NC-OFDM signals are analyzed, which are different from that of an OFDM signal due to non-contiguous subcarriers. Moreover, the design requirements of PAPR reduction techniques for an NC-OFDM signal are outlined.

- an efficient implementation of NC-OFDM transceiver is proposed by using general FFT pruning algorithm for efficient modulation and demodulation of the NC-OFDM signal. The information about the deactivated subcarriers can be used to prune the FFT operations, thereby yielding an efficient FFT implementations for NC-OFDM transceivers.

The list of publications related to the work presented in this thesis is as follows:

Book Chapter

B1. R. Rajbanshi, A. M. Wyglinski, and G. J. Minden, *Cognitive Radio Communications Networks*. Springer-Verlag, 2007, ch. OFDM-Based Cognitive Radios for Dynamic Spectrum Access Networks.

B2. R. Rajbanshi, A. M. Wyglinski, and G. J. Minden, *Submitted to Encyclopedia on Wireless and Mobile Communications*. CRC Press, Dec. 2006, ch. Peak-to-Average Power Ratio Reduction of Multicarrier Transceivers.

Journal Papers

J1. G. J. Minden, J. B. Evans, L. Searl, D. DePardo, R. Rajbanshi, J. Guffey, Q. Chen, T. Newman, V. R. Petty, F. Weidling, M. Lehnherr, B. Cordill, D. Datla, B. Barker, and A. Agah, "An agile radio for wireless innovation," *IEEE Commun. Mag.*, May 2007.

J2. R. Rajbanshi, A. M. Wyglinski, and G. J. Minden, 'Peak-to-average power ratio reduction in OFDM transceivers," *Submitted to IEEE Commun. Mag.*, 2006.

Conference Papers

C1. R. Rajbanshi, Q. Chen, A. M. Wyglinski, J. B. Evans, and G. J. Minden, "Comparative study of frequency agile data transmission schemes for cognitive radio transceivers," in *Proc. of 2nd Annual International Wireless Internet Conference - Int. Wksp. on Technol. and Policy for Accessing Spectrum*, Boston, MA, USA, Aug. 2006.

C2. R. Rajbanshi, Q. Chen, A. M. Wyglinski, G. J. Minden, and J. B. Evans, "Quantitative comparison of agile modulation techniques for cognitive radio transceivers," in *Proc. IEEE Consumer Commun. and Networking Conf. - Wksp. on Cognitive Radio Networks*, Las Vegas, NV, USA, Jan. 2007.

C3. R. Rajbanshi, A. M. Wyglinski, and G. J. Minden, "An efficient implementation of NC-OFDM transceivers for cognitive radios," in *Proc. of 1st Int. Conf. on Cognitive Radio Oriented Wireless Networks and Commun.*, Mykonos, Greece, June 2006.

C4. R. Rajbanshi, A. M. Wyglinski, and G. J. Minden, "Adaptive mode peak-to-average power ratio reduction algorithm for OFDM-based cognitive radios," in *Proc. 64th IEEE Veh. Technol. Conf. - Fall*, Montreal, Quebec, Canada, Sept. 2006.

C5. R. Rajbanshi, A. M. Wyglinski, and G. J. Minden, "Subcarrier power adjustment technique for peak-to-average power ratio reduction of ofdm systems," in *Proc. IEEE Military Commun. Conf.*, Washington DC, USA, May 2006.

C6. R. Rajbanshi, A. M. Wyglinski, and G. J. Minden, "OFDM symbol design

for peak-to-average power ratio reduction employing non-data bearing sub-carriers," *In preparation for IEEE Commun. Lett.*, 2007.

C7. R. Rajbanshi, A. M. Wyglinski, and G. J. Minden, "Low correlation phase sequences for PAPR reduction in OFDM systems," *In preparation for IEEE Commun. Lett.*, 2007.

C8. R. Rajbanshi, A. M. Wyglinski, and G. J. Minden, "PAPR analysis for NC-OFDM signals," in *Accepted to appear at Proc. 66th IEEE Veh. Technol. Conf. - Fall*, 2007.

7.2 Future Work

There exists a number of topics that have resulted from this research that can be continued.

- In this dissertation, a performance of an NC-OFDM system is analyzed using MATLAB simulations. It would be interesting to develop a prototype of NC-OFDM transceiver in hardware and to evaluate real-time performance of NC-OFDM with spectrum measurements.

- Although the PAPR reduction algorithms proposed in this dissertation viz., subcarrier power adjustment, OFDM symbol design approach, and low correlation phase sequence approach, can be used with minor modifications for minimizing PAPR values of an NC-OFDM signal, it would be interesting to develop more sophisticated PAPR reduction algorithms which are aware of deactivated subcarriers in NC-OFDM transmissions.

- Although it has been shown that NC-OFDM transmissions do not interfere with other users given that the users are perfectly synchronized and the transmissions are perfectly band limited. It would be interesting to perform an interference analysis of NC-OFDM transmissions in multiuser environment with imperfect filters.

- We have proposed a general FFT pruning algorithm for use in NC-OFDM transceivers to reduce the computation time or the resources for computing FFT or IFFT. We demonstrated the performance improvement of the FFT procedure with our proposed FFT pruning technique using MATLAB simulations. It would be interesting to implement our proposed FFT pruning algorithms in hardware or other C/C++ implementations such as FFTW.

The distribution of zeros can significantly affect the computational efficiency of the pruned FFT algorithm. Therefore, instead of using all the available subcarriers, the subcarriers might be cleverly chosen so as to improve the efficiency of the FFT pruning algorithm. However, there would always exist a trade-off between the computational efficiency of the FFT pruning algorithm and the throughput of the NC-OFDM system. A dynamic subcarrier selection algorithm needs to be developed to meet the user requirements, optimize the performance based on computational complexity (or computation time) of the FFT algorithm, or increase throughput of the communication system.

- In this work, we assumed that both the receiver and the transmitter has perfect knowledge about the spectrum availability. However, reliable detection of the incumbent user transmissions over wide bandwidth in a very short

166

time is one of the several research challenges that need to be investigated for the developing the spectrum sensing function. OFDM-based techniques can be used for and efficient spectrum sensing and mining. Moreover, adaptive techniques for spectrum sensing can be developed.

References

[1] Spectrum Efficiency Working Group, "Report of the Spectrum Efficiency Working Group," Federal Communications Commission Spectrum Policy Task Force, Tech. Rep., Nov 2000.

[2] BBN Technologies, "The XG Vision, version 2.0," DARPA XG Program, Tech. Rep., Jan 2004.

[3] Federal Communications Commission, "Spectrum policy task force report," ET Docket No. 02-135, 2002.

[4] M. J. Marcus, "Unlicensed cognitive sharing of TV spectrum: The controversy at the federal communications commission," *IEEE Commun. Mag.*, vol. 43, no. 5, pp. 24–25, May 2005.

[5] Federal Communications Commission, "Unlicensed operation in the TV broadcast bands," ET Docket No. 04-186, 2004.

[6] J. Mitola III, *Cognitive Radio Architecture.* New Jersey, USA: A John Wiley and Sons, Inc., 2006.

[7] A. J. Viterbi, "Wireless digital communication: a view based on three lessons learned," *IEEE Commun. Mag.*, vol. 29, pp. 33–36, Nov. 1991.

[8] L. Hanzo, M. Munster, B. J. Choi, and T. Keller, *OFDM and MC-CDMA for Broadband Multi-user Communications, WLANs and Broadcasting.* IEEE Press, 2003.

[9] J. Mitola, III, "An integrated agent architecture for software defined radio," Ph.D. dissertation, Royal Institute of Technology (KTH), May 2000.

[10] Federal Communications Commission, "Spectrum policy task force report," ET Docket No. 02-135, 2002.

[11] "IEEE 802.22: Working group on wireless regional area networks," http://www.ieee802.org/22.

[12] C. Cordeiro, K. Challapali, D. Birru, and S. Shankar N, "Ieee 802.22: the first worldwide wireless standard based on cognitive radios," in *Proc. IEEE Int. Symp. New Frontiers Dynamic Spectr. Access Networks*, Baltimore, MD, USA, Nov. 2005.

[13] D. Cabric, I. D. O'Donnel, M. S.-W. chen, and R. W. Brodersen, "Spectrum sharing radios," *IEEE Circuits Syst. Mag.*, vol. 2, pp. 30–45, 2006.

[14] T. A. Weiss and F. K. Jondral, "Spectrum pooling: an innovative strategy for the enhancement of spectrum efficiency," *IEEE Commun. Mag.*, vol. 43, pp. 8 – 14, Mar. 2004.

[15] R. Rajbanshi, A. M. Wyglinski, and G. J. Minden, *Cognitive Radio Communications Networks.* Springer-Verlag, 2007, ch. OFDM-Based Cognitive Radios for Dynamic Spectrum Access Networks.

[16] J. Mitola, III, "Cognitive radio for flexible mobile multimedia communications," in *Proc. IEEE Int. Wksp. Mobile Multimedia Commun.*, vol. 1, San Diego, CA, USA, Nov. 1999, pp. 3–10.

[17] F. N. Hatfield and P. J. Weiser, "Property rights in spectrum: taking the next step," in *Proc. IEEE Int. Symp. New Frontiers Dynamic Spectr. Access Networks*, vol. 1, Baltimore, MD, USA, Nov. 2005, pp. 43–55.

[18] T. R. Newman, B. A. Barker, A. M. Wyglinski, A. Agah, J. B. Evans, and G. J. Minden, "Cognitive engine implementation for wireless multicarrier transceivers," *Wireless Commun. and Mobile Computing*, vol. 6, (in press) 2006.

[19] J. Zhao, H. Zheng, and G.-H. Yang, "Distributed coordination in dynamic spectrum allocation networks," in *Proc. IEEE Int. Symp. New Frontiers Dynamic Spectr. Access Networks*, vol. 1, Baltimore, MD, USA, Nov. 2005, pp. 259–268.

[20] T. W. Rondeau, B. Le, D. Maldonado, D. Scaperoth, and C. W. Bostian, "Cognitive radio formulation and implementation," in *Proc. of 1st Int. Conf. on Cognitive Radio Oriented Wireless Networks and Commun.*, Mykonos, Greece, June 2006.

[21] G. J. Minden, J. B. Evans, L. Searl, D. DePardo, R. Rajbanshi, J. Guffey, Q. Chen, T. Newman, V. R. Petty, F. Weidling, M. Lehnherr, B. Cordill, D. Datla, B. Barker, and A. Agah, "An agile radio for wireless innovation," *IEEE Commun. Mag.*, May 2007.

[22] J. A. C. Bingham, "Multicarrier modulation for data transmission: an idea whose time has come," *IEEE Commun. Mag.*, vol. 28, pp. 5–14, May 1990.

[23] B. R. Saltzberg, "Comparison of single-carrier and multitone digital modulation for ADSL applications," *IEEE Commun. Mag.*, vol. 36, pp. 114–121, Nov. 1998.

[24] L. J. Cimini Jr., "Analysis and simulation of a digital mobile channel using orthogonal frequency division multiplexing," *IEEE Trans. Commun.*, vol. 33, pp. 665 – 675, July 1985.

[25] R. Prasad, *OFDM for Wireless Communications Systems.* Artech House, Inc., 2004.

[26] J. A. C. Bingham, *ADSL, VDSL, and Multicarrier Modulation.* New York, USA: John Wiley and Sons Inc., 2000.

[27] Institute of Electronics and Electrical Engineers, "Wireless LAN medium access control (MAC) and physical layer (PHY) specifications: High speed physical layer in 5 GHz band," IEEE Standard 802.11a, Nov. 1999.

[28] ——, "Wireless LAN medium access control (MAC) and physical layer (PHY) specifications: Further higher-speed physical layer extension in 2.4 GHz band," IEEE Standard 802.11g, June 2003.

[29] ——, "Air interface for fixed broadband wireless access systems: Medium access control modifications and additional physical layer specifications for 2-11 GHz," IEEE Standard 802.16a, June 2004.

[30] S. B. Weinstein and P. M. Ebert, "Data transmission by frequency division multiplexing using the discretefourier transform," *IEEE Trans. Commun. Technol.*, vol. 19, pp. 628 – 634, Oct 1971.

[31] I. F. Akyildiz, W. Y. Lee, M. C. Vuran, and S. Mohanty, "NeXt generation/dynamic spectrum access/cognitive radio wireless networks: a survey," *Elsevier Computer Networks Journal*, vol. 50, no. 13, pp. 2127–2159, Sept. 2006.

[32] C. Raman, R. D. Yates, and N. B. Mandayam, "Scheduling variable rate links via a spectrum server," in *Proc. IEEE Int. Symp. New Frontiers Dynamic Spectr. Access Networks*, vol. 1, Baltimore, MD, USA, Nov. 2005, pp. 110–118.

[33] C. Peng, H. Zheng, and B. Y. Zhao, "Utilization and fairness in spectrum assignment for opportunistic spectrum access," *Mobile Networks and Applications*, vol. 11, pp. 555 – 576, Aug. 2006.

[34] M. M. Buddhikot, P. Kolodzy, S. Miller, K. Ryan, and J. Evans, "DIM-SUMnet: new directions in wireless networking using coordinated dynamic spectrum," in *Proc. IEEE International Symposium on a World of Wireless Mobile and Multimedia Networks*, Taormina, Italy, June 2005, pp. 78–85.

[35] V. Brik, E. Rozner, S. Banerjee, and P. Bahl, "DSAP: a protocol for coordinated spectrum access," in *Proc. IEEE Int. Symp. New Frontiers Dynamic Spectr. Access Networks*, vol. 1, Baltimore, MD, USA, Nov. 2005, pp. 611–614.

[36] L. Cao and H. Zheng, "Distributed spectrum allocation via local bargaining," in *Proc. IEEE Sensor and Ad Hoc Commun. and Networks*, Santa Clara, CA, USA, Sept. 2005, pp. 475–486.

[37] J. Huang, R. A. Berry, and M. L. Honig, "Spectrum sharing with distributed interference compensation," in *Proc. IEEE Int. Symp. New Frontiers Dynamic Spectr. Access Networks*, vol. 1, Baltimore, MD, USA, Nov. 2005, pp. 88–93.

[38] W. Krenik and A. Batra, "Cognitive radio techniques for wide area networks," in *42nd Design Automation Conf.*, Anaheim, CA, USA, June 2005, pp. 409–412.

[39] A. Ghasemi and E. S. Sousa, "Collaborative spectrum sensing for opportunistic access in fading environments," in *Proc. IEEE Int. Symp. New Frontiers Dynamic Spectr. Access Networks*, vol. 1, Baltimore, MD, USA, Nov. 2005, pp. 131–136.

[40] H. Zheng and L. Cao, "Device centric spectrum management," in *Proc. IEEE Int. Symp. New Frontiers Dynamic Spectr. Access Networks*, Baltimore, MD, USA, Sept. 2005, pp. 56–65.

[41] S. Sankaranarayanan, P. Papadimitratos, A. Mishra, and S. Hershey, "A bandwidth sharing approach to improve licensed spectrum utilization," in *Proc. IEEE Int. Symp. New Frontiers Dynamic Spectr. Access Networks*, vol. 1, Baltimore, MD, USA, Nov. 2005, pp. 611–614.

[42] Q. Zhao, L. Tong, and A. Swami, "Decentralized cognitive MAC for dynamic spectrum access," in *Proc. IEEE Int. Symp. New Frontiers Dynamic Spectr. Access Networks*, vol. 1, Baltimore, MD, USA, Nov. 2005, pp. 224–232.

[43] R. Etkin, A. Parekh, and D. Tse, "Spectrum sharing for unlicensed bands," in *Proc. IEEE Int. Symp. New Frontiers Dynamic Spectr. Access Networks*, vol. 1, Baltimore, MD, USA, Nov. 2005, pp. 251–258.

[44] M. Z. Win and R. A. Scholtz, "Impulse radio: How it works," *IEEE Commun. Lett.*, vol. 2, pp. 36–38, Feb. 1998.

[45] Federal Communications Commission, "FCC first report and order: Revision of part 15 of the commissions's rules regarding ultra-wideband transmission systems," ET Docket No. 98-153, Apr. 2002.

[46] K. S. Gilhousen, I. M. Jacobs, R. Padovani, A. J. Viterbi, L. A. Weaver Jr., and C. E. Wheatley III, "On the capacity of a cellular CDMA system," *IEEE Trans. Veh. Technol.*, vol. 40, pp. 303–312, May 1991.

[47] R. Menon, R. M. Buehrer, and J. H. Reed, "Outage probability based comparison of underlay and overlay spectrum sharing techniques," in *Proc. IEEE Int. Symp. New Frontiers Dynamic Spectr. Access Networks*, vol. 1, Baltimore, MD, USA, Nov. 2005, pp. 101–109.

[48] J. Wang, "Narrowband interference suppression in time hopping impulse radio," in *Proc. 60th IEEE Veh. Technol. Conf.*, vol. 3, Los Angeles, CA, USA, Sept. 2005, pp. 2138– 2142.

[49] C. Rose, S. Ulukus, and R. D. Yates, "Wireless systems and interference avoidance," *IEEE Trans. Wireless Commun.*, vol. 1, pp. 415–428, July 2002.

[50] S. Haykin, "Cognitive radio: Brain-empowered wireless communications," *IEEE J. Select. Areas Commun.*, vol. 23, no. 2, pp. 201–220, Feb. 2005.

[51] U. Berthold and F. K. Jondral, "Guidelines for designing OFDM overlay systems," in *Proc. IEEE Int. Symp. New Frontiers Dynamic Spectr. Access Networks*, vol. 1, Baltimore, MD, Nov. 2005, pp. 626–629.

[52] T. Weiss, J. Hillenbrand, A. Krohn, and F. Jondral, "Mutual interference in OFDM-based spectrum pooling systems," in *Proc. 59th IEEE Veh. Technol. Conf. - Spring*, vol. 4, Milan, Italy, May 2004, pp. 1873 – 1877.

[53] S. Kapoor and S. Nedic, "Interference suppression in DMT receivers using windowing," in *Proc. IEEE Int. Conf. Commun.*, vol. 2, New Orleans, LA, USA, June 2000, pp. 778 – 782.

[54] I. Cosovic, S. Brandes, and M. Schnell, "A technique for sidelobe suppression in OFDM systems," in *Proc. IEEE Global Telecommun. Conf.*, vol. 1, St. Louis, MO, USA, Nov. 2005, pp. 204–208.

[55] S. Brandes, I. Cosovic, and M. Schnell, "Sidelobe suppression in OFDM systems by insertion of cancellation carriers," in *Proc. 62st IEEE Veh. Technol. Conf. - Fall*, vol. 1, Dallas, TX, USA, Sept. 2005, pp. 152 – 156.

[56] H. Tang, "Some physical layer issues of wide-band cognitive radio systems," in *Proc. IEEE Int. Symp. New Frontiers Dynamic Spectr. Access Networks*, vol. 1, Baltimore, MD, USA, Nov. 2005, pp. 151–159.

[57] F. Weidling, D. Datla, V. Petty, P. Krishnan, and G. J. Minden, "A framework for RF spectrum measurements and analysis," in *Proc. IEEE Int.*

Symp. New Frontiers Dynamic Spectr. Access Networks, vol. 1, Baltimore, MD, USA, Nov. 2005, pp. 573–576.

[58] R. Rajbanshi, Q. Chen, A. M. Wyglinski, J. B. Evans, and G. J. Minden, "Comparative study of frequency agile data transmission schemes for cognitive radio transceivers," in *Proc. of 2nd Annual International Wireless Internet Conference - Int. Wksp. on Technol. and Policy for Accessing Spectrum*, Boston, MA, USA, Aug. 2006.

[59] R. Rajbanshi, Q. Chen, A. M. Wyglinski, G. J. Minden, and J. B. Evans, "Quantitative comparison of agile modulation techniques for cognitive radio transceivers," in *Proc. IEEE Consumer Commun. and Networking Conf. - Wksp. on Cognitive Radio Networks*, Las Vegas, NV, USA, Jan. 2007.

[60] J. D. Poston and W. D. Horne, "Discontiguous OFDM considerations for dynamic spectrum access in idle TV channels," in *Proc. IEEE Int. Symp. New Frontiers Dynamic Spectr. Access Networks*, vol. 1, Baltimore, MD, USA, Nov. 2005, pp. 607–610.

[61] B.-J. Choi, E.-L. Kuan, and L. Hanzo, "Crest-factor study of MC-CDMA and OFDM," in *Proc. 50th IEEE Veh. Technol. Conf. - Fall*, vol. 1, Amsterdam, The Netherlands, Sept. 1999, pp. 233 – 237.

[62] J. G. Proakis, *Digital Communications.* New York, NY: McGraw Hill, 2001.

[63] H. Sari, G. Karam, and I. Jeanclaude, "Transmission techniques for digital terrestrial TV broadcasting," *IEEE Commun. Mag.*, vol. 33, pp. 100–109, Feb. 1995.

[64] T. S. Rappaport, *Wireless Communications: Principles and Practice.* Upper Saddle River, NJ, USA: Prentice Hall, 1996.

[65] K. S. Shanmugan and A. M. Breipohl, *Random Signals: Detection, Estimation and Data Analysis.* USA: John Wiley & Sons, 1988.

[66] R. Rajbanshi, A. M. Wyglinski, and G. J. Minden, *Submitted to Encyclopedia on Wireless and Mobile Communications.* CRC Press, Dec. 2006, ch. Peak-to-Average Power Ratio Reduction of Multicarrier Transceivers.

[67] ——, "Peak-to-average power ratio reduction in OFDM transceivers," *Submitted to IEEE Commun. Mag.*, 2006.

[68] N. Y. Ermolova and P. Vainikainen, "On the relationship between peak factor of a multicarrier signal and aperiodic autocorrelation of the generating sequence," *IEEE Commun. Lett.*, vol. 7, pp. 107–108, Mar. 2003.

[69] C. Tellambura, "Upper bound on peak factor of N-multiple carriers," *Electron. Lett.*, vol. 33, pp. 1608–1609, Sept. 1997.

[70] J. Tellado, *Multicarrier modulation with low PAR: Applications to DSL and Wireless.* Massachusetts, USA: Kluwer Academic Publishers, 2000.

[71] X. Li and L. J. Cimini, "Effects of clipping and filtering on the performance of OFDM," *IEEE Commun. Lett.*, vol. 2, pp. 131–133, May 1998.

[72] J. Armstrong, "Peak-to-average power reduction for OFDM by repeated clipping and frequency domain filtering," *Electron. Lett.*, vol. 38, pp. 246–247, Feb. 2002.

[73] H. Chen and A. M. Haimovich, "Iterative estimation and cancellation of clipping noise for OFDM signals," *IEEE Commun. Lett.*, vol. 7, pp. 305–307, July 2003.

[74] T. A. Wilkison and A. E. Jones, "Minimization of the peak to mean envelope power ratio of multicarrier transmission schemes by block coding," in *Proc. 45th IEEE Veh. Technol. Conf.*, vol. 2, Chicago, IL, USA, July 1995, pp. 825 – 829.

[75] R. Van Nee, "OFDM codes for peak to average power reduction and error correction," in *Proc. IEEE Global Telecommun. Conf.*, vol. 1, London, UK, Nov. 1996, pp. 740 – 744.

[76] C. Tellambura, "A coding technique for reducing peak to average power ratio in OFDM," in *Proc. IEEE Global Telecommun. Conf.*, vol. 5, Sydney, Australia, Nov. 1998, pp. 2783 – 2787.

[77] Y. Zhang, A. Yongacoglu, J. Chouinard, and L. Zhang, "OFDM peak power reduction by subblock coding and its extended versions," in *Proc. 49th IEEE Veh. Technol. Conf. - Spring*, vol. 1, Houston, TX, USA, May 1999, pp. 695 – 699.

[78] H. Ahn, Y. M. Shin, and S. Im, "A block coding scheme for peak to average power ratio reduction in an orthogonal frequency division multiplexing system," in *Proc. 51st IEEE Veh. Technol. Conf. - Spring*, vol. 1, Tokyo, Japan, May 2000, pp. 56 – 60.

[79] R. W. Bauml, R. F. H. Fischer, and J. B. Huber, "Reducing the peak to average power ratio of multicarrier modulation by selective mapping," *Electron. Lett.*, vol. 32, pp. 2056 – 2057, Oct. 1996.

[80] S. H. Muller and J. B. Huber, "OFDM with reduced peak to average power ratio by optimum combination of partial transmit sequences," *Electron. Lett.*, vol. 33, pp. 368 – 369, Feb. 1997.

[81] H. Nikookar and K. S. Lidsheim, "Random phase updating algorithm for OFDM transmission with low PAPR," *IEEE Trans. Broadcast.*, vol. 48, no. 6, pp. 123 – 128, June 2002.

[82] P. Foomooljareon, W. A. C. Fernando, and K. M. Ahmed, "PAPR reduction of OFDM systems using input sequence envelope scaling," in *Proc. 57th IEEE Veh. Technol. Conf. - Spring*, vol. 2, Jeju, Korea, Apr. 2003, pp. 1243 – 1247.

[83] D. L. Jones, "Peak power reduction in OFDM and DMT via active channel modification," in *Proc. Asilomar Conf. Signals, Systems and Computers*, vol. 2, Pacific Grove, CA, Oct. 1999, pp. 1076–1079.

[84] B. S. Krongold and D. L. Jones, "PAR reduction in OFDM via active constellation extension," *IEEE Trans. Broadcast.*, vol. 49, pp. 258 – 268, Sept. 2003.

[85] B. S. Krongold, "New techniques for multicarrier communication systems," Ph.D. dissertation, University of Illinois at Urbana-Champaign, Urbana, Illinois, 2003.

[86] S. Sezginer and H. Sari, "Peak power reduction in OFDM systems using dynamic constellation shaping," in *Proc. of 13th European Signal Process. Conf.*, Antalya, Turkey, Sept. 2005.

[87] K. R. Panta and J. Armstrong, "Effects of clipping on the error performance of OFDM in frequency selective fading channels," *IEEE Trans. Wireless Commun.*, vol. 3, pp. 668–671, Mar. 2004.

[88] C. Tellambura, "Computation of the continuous time PAR of an OFDM signal with BPSK subcarriers," *IEEE Commun. Lett.*, vol. 5, no. 5, pp. 185–187, May 2001.

[89] H. Yu and G. Wei, "Computation of the continuous time PAR of an OFDM signal," in *Proc. IEEE Int. Conf. Acoust., Speech, Signal Process.*, vol. 2003, Hong Kong, Apr. 2003, pp. IV – 529–31.

[90] H. Ochiai and H. Imai, "On the distribution of the peak-to-average power ratio in OFDM signals," *IEEE Trans. Commun.*, vol. 49, pp. 282–289, Feb. 2001.

[91] R. J. Baxley and G. T. Zhou, "Power savings analysis of peak-to-average power ratio reduction in OFDM," *IEEE Trans. Consumer Electron.*, vol. 50, pp. 792–798, Aug. 2004.

[92] A. V. Oppenheim, R. W. Schafer, and J. R. Buck, *Discrete-time signal processing.* Upper Saddle River, NJ, USA: Pearson Education, Inc., 1999.

[93] R. Rajbanshi, A. M. Wyglinski, and G. J. Minden, "An efficient implementation of NC-OFDM transceivers for cognitive radios," in *Proc. of 1st*

Int. Conf. on Cognitive Radio Oriented Wireless Networks and Commun., Mykonos, Greece, June 2006.

[94] M. Friese, "Multitone signals with low crest factor," *IEEE Trans. Commun.*, vol. 45, pp. 1338–1344, Oct. 1997.

[95] S. Boyd, "Multitone signals with low crest factors," *IEEE Trans. Circuits Syst.*, vol. 33, pp. 1018–1022, Oct. 1986.

[96] M. R. Schroeder, "Synthesis of low-peak-factor signals and binary sequences with low correlation," *IEEE Trans. Inform. Theory*, vol. 16, pp. 85–59, Jan. 1970.

[97] S. Narahashi and T. Nojima, "New phasing scheme of N-multiple carriers for reducing peak-to-average power ratio," *Electron. Lett.*, vol. 30, pp. 1382–1383, Aug. 1994.

[98] A. Papoulis and S. U. Pillai, *Probability, Random Variables and Stochastic Processes.* New York: McGraw-Hill Inc., 2002.

[99] R. van Nee and A. de Wild, "Reducing the peak-to-average power ratio of OFDM," in *Proc. 48th IEEE Veh. Technol. Conf.*, Ottawa, Ontario, Canada, May 1998, pp. 2072–2076.

[100] S. Wei, D. L. Goeckel, and P. E. Kelly, "A modern extreme value theory approach to calculating the distribution of the peak-to-average power ratio in OFDM systems," in *Proc. IEEE Int. Conf. Commun.*, vol. 3, New York, NY, USA, Apr. 2002, pp. 1686– 1690.

[101] H. Yu, M. Chen, and G. Wei, "Distribution of PAR in DMT systems," *Electron. Lett.*, vol. 39, pp. 799 – 801, May 2003.

[102] H. Wang and B. Chen, "On the distribution of peak-to-average power ratio for non-circularly modulated OFDM signals," in *Proc. IEEE Global Telecommun. Conf.*, vol. 1, San Francisco, CA, USA, Dec. 2003, pp. 502 – 506.

[103] L. Wang and C. Tellambura, "A simplified clipping and filtering technique for PAR reduction in OFDM systems," *IEEE Signal Processing Lett.*, vol. 12, pp. 453–456, June 2005.

[104] S.-K. Deng and M.-C. Lin, "OFDM PAPR reduction using clipping with distortion control," in *Proc. IEEE Int. Conf. Commun.*, vol. 4, Seoul, Korea, May 2005, pp. 2563– 2567.

[105] S. C. Thompson, J. G. Proakis, and J. R. Zeidler, "The effectiveness of signal clipping for PAPR and total degradation reduction in OFDM systems," in *Proc. IEEE Global Telecommun. Conf.*, St. Louis, MO, USA, Nov. 2005, pp. 2807–2811.

[106] J. G. Proakis and M. Salehi, *Communication Systems Engineering.* Upper Saddle River, NJ, USA: Prentice Hall, 2002.

[107] X. Wang, T. Tjhung, and C. Ng, "Reduction of peak-to-average power ratio of OFDM system using a companding technique," *IEEE Trans. Broadcast.*, vol. 45, pp. 303 – 307, Sept. 1999.

[108] T. Jiang, Y. Yang, and Y. H. Song, "Exponential companding technique for PAPR reduction in OFDM systems," *IEEE Trans. Broadcast.*, vol. 51, pp. 244–248, June 2005.

[109] S. H. Han and J. H. Lee, "Peak-to-average power ratio reduction of an OFDM signal by signal set expansion," in *Proc. IEEE Int. Conf. Commun.*, vol. 2, Paris, France, June 2004, pp. 867–971.

[110] Y. Kou, L. Wu-Sheng, and A. Antoniou, "New peak-to-average power-ratio reduction algorithms for multicarrier communications," *IEEE Trans. Circuits Syst.*, vol. 51, pp. 1790 – 1800, Sept. 2004.

[111] P. van Eetvelt, G. wade, and M. Tomlinson, "Peak to average power reduction for OFDM schemes by selective scrambling," *Electron. Lett.*, vol. 32, pp. 1963–1964, Oct. 1996.

[112] A. D. S. Jayalath and C. Tellambura, "The use of interleaving to reduce the peak to average power ratio of an OFDM signal," in *Proc. IEEE Global Telecommun. Conf.*, vol. 1, San Francisco, CA, USA, Nov. 2000, pp. 82 – 86.

[113] S. C. Thompson, "Constant envelope OFDM phase modulation," Ph.D. dissertation, University of California, San Diego, CA, USA, 2005.

[114] S. H. Han and J. H. Lee, "An overview of peak-to-average power ratio reduction techniques for multicarrier transmission," *IEEE Trans. Wireless Commun.*, vol. 12, pp. 56 – 65, Apr. 2005.

[115] D. Wulich, "Definition of efficient PAPR in OFDM," *IEEE Commun. Lett.*, vol. 9, no. 9, pp. 832–834, Sept. 2005.

[116] M. Friese, "On the achievable information rate with peak-power-limited orthogonal frequency division multiplexing," *IEEE Trans. Inform. Theory*, vol. 46, pp. 2579–2587, Nov. 2000.

[117] H. Ochiai and H. Imai, "Performance analysis of deliberately clipped OFDM signals," *IEEE Trans. Commun.*, vol. 50, pp. 89–101, Jan. 2002.

[118] D. R. Gimlin and C. R. Patisaul, "On minimizing the peak-to-average power ratio for the sum of N sinusoids," *IEEE Trans. Commun.*, vol. 41, pp. 631–635, Apr. 1993.

[119] R. Rajbanshi, A. M. Wyglinski, and G. J. Minden, "Adaptive mode peak-to-average power ratio reduction algorithm for OFDM-based cognitive radios," in *Proc. 64th IEEE Veh. Technol. Conf. - Fall*, Montreal, Quebec, Canada, Sept. 2006.

[120] ——, "Subcarrier power adjustment technique for peak-to-average power ratio reduction of OFDM systems," in *Proc. IEEE Military Commun. Conf.*, Washington DC, USA, May 2006.

[121] A. M. Wyglinski, "Physical layer loading algorithms for indoor wireless multicarrier systems," Ph.D. dissertation, McGill University, Montreal, Quebec, Canada, Nov. 2004.

[122] H. Nikookar and R. Prasad, "Weighted OFDM for wireless multipath channels," *IEICE Trans. Commun.*, vol. E83-B, pp. 1864–1872, Aug. 2000.

[123] T. A. Thomas, "PAPR reduction via a fixed frequency-domain weighting across multiple OFDM bauds," in *Proc. IEEE Int. Conf. Acoust., Speech, Signal Process.*, Montreal, Quebec, Canada, May 2004, pp. 1081–1084.

[124] I. A. Tasadduq and R. K. Rao, "Weighted OFDM with block codes for wireless communication," in *Proc. IEEE Pacific Rim Conf on Comm., Computers and Signal Process.*, vol. 2, Victoria, BC, Canada, 2001, pp. 441–444.

[125] I. Kalet, "The multitone channel," *IEEE Trans. Commun.*, vol. 37, pp. 119–124, Feb. 1989.

[126] R. F. H. Fischer and J. B. Huber, "A new loading algorithm for discrete multitone transmission," in *Proc. IEEE Global Telecommun. Conf.*, vol. 1, London, UK, Nov. 1996, pp. 724–728.

[127] Federal Communications Commission, "Part 15 - radio frequency devices, subpart E - unlicenced national information infrastructure devices, section 403 - definitions," Code of Federal Regulations – FCC 47CFR15.403, Oct. 2000.

[128] R. Rajbanshi, A. M. Wyglinski, and G. J. Minden, "OFDM symbol design for peak-to-average power ratio reduction employing non-data bearing subcarriers," in *In preperation for IEEE Commun. Lett.*, 2007.

[129] H.-G. Ryu, J.-E. Lee, and J.-S. Park;, "Dummy sequence insertion (DSI) for PAPR reduction in the OFDM communication system," in *IEEE Trans. Consumer Electron.*, vol. 50, Feb. 2004, pp. 89–94.

[130] R. Rajbanshi, A. M. Wyglinski, and G. J. Minden, "Low correlation phase sequences for PAPR reduction in OFDM systems," *In preperation for IEEE Commun. Lett.*, 2007.

[131] A. D. S. Jayalath, C. Tellambura, and H. Wu, "Reduced complexity PTS and new phase sequences for SLM to reduce PAP of an OFDM signal," in

Proc. 51st IEEE Veh. Technol. Conf. - Spring, Tokyo, Japan, May 2000, pp. 1914–1917.

[132] L. J. Cimini Jr. and N. R. Sollenberger, "Peak-to-average power ratio reduction of an OFDM signal using partial transmit sequences," *IEEE Commun. Lett.*, vol. 4, no. 3, pp. 86–88, Mar. 2000.

[133] R. Rajbanshi, A. M. Wyglinski, and G. J. Minden, "PAPR analysis for NC-OFDM signals," in *Proc. 66th IEEE Veh. Technol. Conf. - Fall*, 2007.

[134] Y. H. You, I. T. Hwang, C. K. Song, and H. K. Song, "PAPR analysis for multi-band OFDM signals," *Electron. Lett.*, vol. 41, pp. 261–262, Mar. 2005.

[135] J. D. Markel, "FFT Pruning," *IEEE Trans. Audio Electroacoust.*, vol. 19, pp. 305 – 311, Dec. 1971.

[136] R. G. Alves, P. L. Osorio, and M. N. S. Swamy, "General FFT Pruning Algorithm," in *Proc. 43rd IEEE Midwest Symp. Circuits and Systems*, vol. 3, Aug. 2000, pp. 1192 – 1195.

[137] S. Holm, "FFT pruning applied to time domain interpolation and peak localization," in *Proc. IEEE Int. Conf. Acoust., Speech, Signal Process.*, vol. 35, Dec. 1987, pp. 1776 – 1778.

[138] Z. Hu and H. Wan, "A Novel Generic Fast Fourier Transform Pruning technique and Complexity Analysis," *IEEE Trans. Signal Processing*, vol. 53, pp. 274 – 282, Jan. 2005.

[139] L. P. Jaroslavski, "Comments on "FFT algorithm for both input and output pruning"," in *Proc. IEEE Int. Conf. Acoust., Speech, Signal Process.*, vol. 29, June 1981, pp. 448 – 449.

[140] J. Schoukens, R. Pintelon, and H. Van Hamme, "The interpolated fast Fourier transform: a comparative study," *IEEE Trans. Instrum. Meas.*, vol. 41, pp. 226 – 232, Apr. 1992.

[141] D. P. Skinner, "Pruning the Decimation in time FFT algorithm," in *Proc. IEEE Int. Conf. Acoust., Speech, Signal Process.*, vol. 24, Apr. 1976, pp. 193 – 194.

[142] T. V. Sreenivas and P. V. S. Rao, "High-resolution narrow band spectra by FFT pruning," in *Proc. IEEE Int. Conf. Acoust., Speech, Signal Process.*, vol. 28, Apr. 1980, pp. 254 – 257.

[143] T. V. Sreenivas and P. Rao, "FFT algorithm for both input and output Pruning," in *Proc. IEEE Int. Conf. Acoust., Speech, Signal Process.*, vol. 27, June 1979, pp. 291 – 292.

[144] H. V. Sorensen and C. S. Burrus, "Efficient computation of the DFT with only a subset of input or output points," *IEEE Trans. Signal Processing*, vol. 41, pp. 1184 – 1200, Mar. 1993.

[145] J. W. Cooley and J. W. Tukey, "An algorithm for the machine calculation of complex Fourier series," *Math. Computation*, vol. 19, pp. 297–301, Apr. 1965.